

INFORMATION TO USERS

This manuscript has been reproduced from the microfilm master. UMI films the text directly from the original or copy submitted. Thus, some thesis and dissertation copies are in typewriter face, while others may be from any type of computer printer.

The quality of this reproduction is dependent upon the quality of the copy submitted. Broken or indistinct print, colored or poor quality illustrations and photographs, print bleedthrough, substandard margins, and improper alignment can adversely affect reproduction.

In the unlikely event that the author did not send UMI a complete manuscript and there are missing pages, these will be noted. Also, if unauthorized copyright material had to be removed, a note will indicate the deletion.

Oversize materials (e.g., maps, drawings, charts) are reproduced by sectioning the original, beginning at the upper left-hand corner and continuing from left to right in equal sections with small overlaps.

Photographs included in the original manuscript have been reproduced xerographically in this copy. Higher quality 6" x 9" black and white photographic prints are available for any photographs or illustrations appearing in this copy for an additional charge. Contact UMI directly to order.

**Bell & Howell Information and Learning
300 North Zeeb Road, Ann Arbor, MI 48106-1346 USA
800-521-0600**

UMI[®]

**INFLUENCE OF PHYTOPLANKTON COMMUNITIES ON
RELATIONSHIPS BETWEEN OPTICAL PROPERTIES OF
COASTAL SURFACE WATERS**

by

Áurea Maria Ciotti

**Submitted in partial fulfillment of the requirements for the
degree of Doctor of Philosophy**

at

**Dalhousie University
Halifax, Nova Scotia
June, 1999**

© Copyright by Áurea Maria Ciotti, 1999



**National Library
of Canada**

**Acquisitions and
Bibliographic Services**

395 Wellington Street
Ottawa ON K1A 0N4
Canada

**Bibliothèque nationale
du Canada**

**Acquisitions et
services bibliographiques**

395, rue Wellington
Ottawa ON K1A 0N4
Canada

Your file Votre référence

Our file Notre référence

The author has granted a non-exclusive licence allowing the National Library of Canada to reproduce, loan, distribute or sell copies of this thesis in microform, paper or electronic formats.

The author retains ownership of the copyright in this thesis. Neither the thesis nor substantial extracts from it may be printed or otherwise reproduced without the author's permission.

L'auteur a accordé une licence non exclusive permettant à la Bibliothèque nationale du Canada de reproduire, prêter, distribuer ou vendre des copies de cette thèse sous la forme de microfiche/film, de reproduction sur papier ou sur format électronique.

L'auteur conserve la propriété du droit d'auteur qui protège cette thèse. Ni la thèse ni des extraits substantiels de celle-ci ne doivent être imprimés ou autrement reproduits sans son autorisation.

0-612-49252-4

Canada

DALHOUSIE UNIVERSITY

FACULTY OF GRADUATE STUDIES

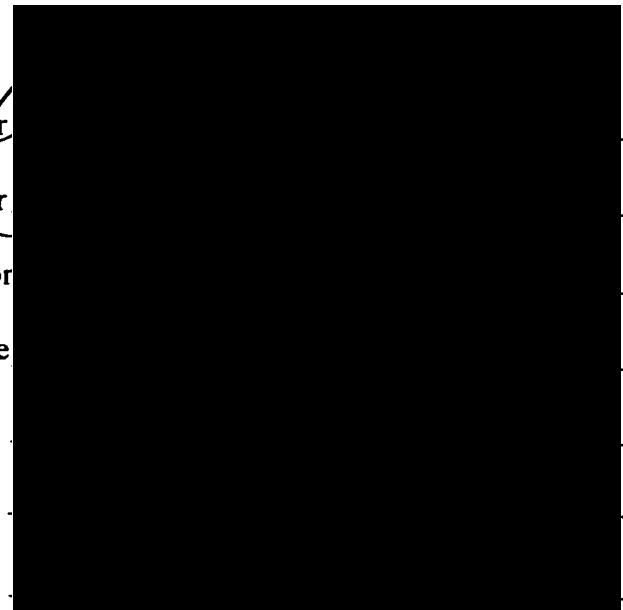
The undersigned hereby certify that they have read and recommend to the Faculty of Graduate Studies for acceptance a thesis entitled "Influence of Phytoplankton Communities on Relationships Between Optical Properties of Coastal Surface Waters"

by Áurea Maria Ciotti

in partial fulfillment of the requirements for the degree of Doctor of Philosophy.

Dated: June 25, 1999

External Examiner
Research Supervisor
Research Supervisor
Examining Committee



DALHOUSIE UNIVERSITY

Date: **June, 1999**

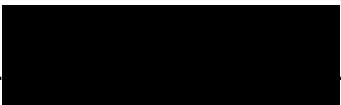
Author: **Áurea Maria Ciotti**

Title: **Influence of phytoplankton communities on relationships between optical properties of coastal surface waters**

Department: **Oceanography**

Degree: **Ph.D.** Convocation: **October** Year: **1999**

Permission is herewith granted to Dalhousie University to circulate and to have copied for non-commercial purposes, at its discretion, the above title upon request of individuals or institutions.

_____  _____

Signature of the Author

THE AUTHOR RESERVES OTHER PUBLICATION RIGHTS, AND NEITHER THE THESIS NOR EXTENSIVE EXTRACTS FROM IT MAY BE PRINTED OR OTHERWISE REPRODUCED WITHOUT THE AUTHOR'S WRITTEN PERMISSION.

THE AUTHOR ATTESTS THAT PERMISSION HAS BEEN OBTAINED FOR THE USE OF ANY COPYRIGHTED MATERIAL APPEARING IN THIS THESIS (OTHER THAN BRIEF EXCERPTS REQUIRING ONLY PROPER ACKNOWLEDGEMENT IN SCHOLARLY WRITING) AND THAT ALL SUCH USE IS CLEARLY ACKNOWLEDGED.

**To my Grandfather, João Antonio Moyano Lopes and his
best friend, Danilo Bessa Caminha.**

Acknowledgments

After seven years in Halifax, I have many people and situations to be thankful for. Every year was special, so this acknowledgment section will be organized in chronological order. Many important moments, however, started a long time ago.

First I would like to thank my father, João Baptista Ciotti, for one day waking me up in the middle of the night, when I was 4 years old. He wanted me to see the landing of Apollo 11. In his very unique way, on that night he made me believe I could do anything I wanted. He has been very supportive since.

I like to thank my grandfather, João Antonio Moyano Lopes, for clearly showing me when I was 11 years old, that phytoplankton do change the color of the ocean. I thought about being an oceanographer that day.

Many years later, I was starting my Masters degree. My supervisor then, Dr. Clarisse Odebrecht, had a great influence on my general attitude toward science that I will carry with me forever.

I thank one of my best friends, Carlos Freitas, who also happens to be my husband, for coming with me to Halifax, and for encouragement he gave me all these years. I also thank Carlos for making sure I could distinguish between science and life on many occasions.

We arrived from Brazil in January 1992. Along with the overall cultural changes, there was a difference of 50 degrees Celsius to get used to. In this process, the support of our friends Angel, Zeca and Monica was priceless. Muito obrigado!

I started with my field work in Bedford Basin immediately. I thank Marlon for trusting me to help coordinating this project and many others that followed. Thanks to Sherry Niven, for all the support during that first experiment; her help was crucial. My thanks are extended to all involved in this project, for their help and interesting discussions.

In the Summer of 1992, I had the great opportunity to be trained in the field and in the lab directly by Dr. John Cullen, who later become my co-supervisor. Needless to say, in one week I learned the equivalent of many years discovering things on my own. He is an amazing scientist and a great person. I am very proud to have been his student and I will probably brag about it for the rest of my life.

There was no luck my work was in good shape by the time I finished. I got myself a very good and demanding committee: Shubha Sathyendarnath, Paul Hill and Bill Miller, plus Marlon Lewis and John Cullen. Thank you for the many meetings and many hours of revisions and discussions. I also had the immense privilege of having Dr. Charles Yentsch as my external examiner. He has been my hero for many years, and his

contribution to bio-optical oceanography has been tremendous. He is a constant source of inspiration in my work.

In October of 1994 I had the opportunity of participating in a cruise off the Oregon coast and work directly with many people. I would like to thank Richard Davis (who became one of my best friends immediately) for all his assistance, and Collin Roesler and Terri Cucci for sharing a great data set with me. By this time I had also started working with Tammi Richardson and Gary Maillet in the lab. What can I say? Gary is just the best, and Tammi is great. We had a fantastic time working together. Betsy Webb was my buddy during the core courses. Both Tammi and Betsy taught me English, made me dinners and made both Carlos and me feel like we had a family around. A little while later, Geoff MacIntyre showed up in the lab and I haven't stop laughing since. Thanks also to J-P. Parkhill for bringing to the lab a totally new and entertaining environment.

In the beginning of 1996 Richard Davis decided to work at Dalhousie. The lab rapidly got organized, and we worked together in the Bering Sea and also in Bedford Basin. Besides his great help with my work and my transformation into an oceanographer (and the many Matlab tutorials and routines) Richard became more than a brother. Both Richard and Geoff helped me through very hard times. I love you both very much.

In 1997 I got two great new friends, Sophia Johannessen and Yannick Huot. They brought a refreshing and enthusiastic view of science, and I enjoyed, and I am sure will enjoy, many hours of conversation about science and life in general with them. They are brilliant (not to mention also extremely cute). I will miss you terribly.

They are many other people in the department I would like to thank. Dianne, Tammi and Pamela in the office, and Geri in our lab, were always extremely helpful. The professors for the courses and their patience with my English. I thank especially Keith Thompson for his help and interest in my work. Thanks also Gordana Lasin for her help during the cruise in the Bering Sea, and Wade Blanchard for statistical advice.

Thanks also to Grazyna, Vivian, Allison, Iain, Backy, Chirstine, Tracey and Penny for your friendship and support. To my log-distance friends Zuka, Ivan, Isa, Paulito and Dalva: thanks for the many emails and phone calls.

Both my family (Vovós, Mamma, Ciottão, Yoh, Nana, Vi, Plinio, Johann e Lu) and Carlos' (Mira, Chico, Cauto e Daniel) have been great sources of support, patience and love. Thanks for the many years coping with the long distance relationship, phone bills and air tickets.

Money was an important part of all of this. I was granted a 4.5 year scholarship by the Brazilian government (CNPq) and a 2 year Dalhousie Fellowship, and I was also supported by Carlos, Chico and my dad in the final months. Research expenses were covered by ONR and NSERC.

In my life

There are places I remember
All my life, though some have changed
Some forever not for better
Some have gone and some remain
All these places had their moments
With lovers and friends
I still can recall
Some are dead and some are living
In my life I've loved them all

But of all these friends and lovers
there is no one compares with you
And these memories lose their meaning
When I think of love as something new
Though I know I'll never lose affection
For people and things that went before
I know I'll often stop and think about them
In my life I love you more

Though I know I'll never lose affection
For people and things that went before
I know I'll often stop and think about them
In my life I love you more
In my life I love you more

Lennon and McCartney

"Rubber Soul", 1965

Table of Contents

Acknowledgments	v
List of Figures	xii
List of Tables.....	xxii
Abstract.....	xxv
List of Symbols	xxvi
Chapter 1: General Introduction.....	1
1.1 Ocean color and ecological processes in surface waters.....	1
1.2 Phytoplankton communities and trophic status	2
1.3 Optical properties of sea water constituents	4
1.3.1. Modeling optical properties of particles.....	5
1.3.1.1 Modeling optical properties of phytoplankton communities	7
1.4 Structure of the thesis research.....	8
Chapter 2: A semi-analytical model of the influence of phytoplankton community structure on the relationship between light attenuation and ocean color.....	11
2.1. Introduction	11
2.2 Background.....	13
2.2.1 Ratios of spectral radiance at the surface	13
2.2.2 Diffuse attenuation coefficient.....	15
2.3 Model structure and parameterization of IOPs.....	16
2.3.1 Total absorption	16
2.3.1.1 Parameterization of phytoplankton absorption	18
2.3.1.1.1 Packaging	19
2.3.1.1.2 Pigment composition	23
2.3.1.2 Parameterization of CDOM and detrital absorption.....	24
2.3.2 Total backscattering	28
2.3.2.1 Scattering by particles.....	29
2.3.2.2 Backscattering ratio	30

2.3.2.3 Wavelength dependence of backscattering.....	30
2.4 Implementation of the semi-analytical model	31
2.5 Bio-optical field data.....	33
2.6 Results and Discussion.....	35
2.6.1 Model versus established empirical relationships.....	35
2.6.1.1 Diffuse attenuation versus C	35
2.6.1.2 Retrieval of C from ocean color.....	37
2.6.1.3 Diffuse attenuation versus radiance ratio.....	37
2.6.2 Model versus independent bio-optical data	38
2.6.3 Sensitivity analysis.....	40
2.6.3.1 Packaging and pigment composition.....	40
2.6.3.2 Spectral dependence of total scattering	45
2.6.3.3 CDOM and detrital absorption.....	49
2.7 Summary and Conclusions.....	53
Chapter 3: Dominant cell size and its effects on the spectral shape of natural phytoplankton absorption spectra	56
3.1 Introduction	56
3.2 Background.....	58
3.3 Approach	60
3.4 Sampling design.....	63
3.5 Methods.....	63
3.6 Results.....	68
3.6.1 Hydrography and chlorophyll concentration in the different size ranges and main groups of organisms	69
3.6.1.1 Off the Oregon coast.....	69
3.6.1.2 Southern Bering Sea	75
3.6.1.3 Bedford Basin.....	81
3.6.1.3.1 Summer experiments	81
3.6.1.3.2 Time series from July to December 1996	85

3.6.2 Influence of the different communities on the spectral shape of phytoplankton absorption	87
3.6.2.1 Quantification of the effects of cell size	94
3.6.2.2 Estimation of a “size” parameter from the phytoplankton absorption coefficient	96
3.7. Discussion and Conclusions	98
Appendix 3.9A: Basis vectors.....	105
Appendix 3.9B: Linear regression subject to constraints.....	106
Chapter 4: Analyses of the influence of different cell sizes of phytoplankton on relationships between apparent optical properties	108
4.1 Introduction	108
4.2 Background.....	111
4.2.1 Reflectance and attenuation	112
4.2.2 Total backscattering	112
4.2.2.1 Minimizing the effects of total backscattering on reflectance ratios... 113	
4.2.3 Spectral shape of total absorption coefficient.....	116
4.3 Approach	117
4.4 Methods	117
4.4.1 Sampling design	117
4.4.2 Optical measurements	119
4.4.3 Water samples	121
4.4.4 Parameterization of the effects of cell size	122
4.4.5 Parameterization of the effects of CDOM and detritus	123
4.5 Results and Discussion.....	126
4.5.1 Main characteristics of the data sets.....	126
4.5.1.1 Observed $F_{<p>}$ and C	126
4.5.1.2 Observed $a_{\text{cdom+det}}(\lambda)$ and C.....	128
4.5.2 Remote sensing reflectance ratios and C.....	128
4.5.2.1 Influence of cell size on simple reflectance ratios	130
4.5.2.2 Influence of $a_{\text{cdom+det}}(\lambda)$ on simple reflectance ratios	132

4.5.3 Inflection ratios and C	133
4.5.3.1 Comparing effects of size and $a_{\text{cdom}+\text{det}}(\lambda)$	135
4.5.4 Retrieval of the size parameter from relationships between AOPS	140
4.5.4.1 Model approach.....	140
4.5.4.2 Comparison of the model approach with independent data.....	145
4.6 Summary and conclusions.....	148
Chapter 5: Summary, conclusions and future directions	151
5.1 Introduction	151
5.2. General conclusions and future work.....	153
References	159

List of Figures

- Figure 2.1** Parameterization of $K_d(490)$ and $L_u(443)/L_u(550)$ as functions of C (see Table 2.1 for symbols, and text for details). Absorption and backscatter, then attenuation and spectral reflectance, were predicted from C consistent with bio-optical relationships derived from theory (inverted triangle), laboratory studies (circle) and empirical relationships from the field (hexagons). Steps for deriving spectral absorption and spectral backscatter are described in the text.....17
- Figure 2.2** Steps for estimating the product of the cell diameter and the intracellular pigment concentration (dc_i) as a function of trophic status. A) Empirical relationship between $a_{ph}^*(675)$ and the product of cell diameter (d) and the intracellular concentration of pigments (c_i) for published data from cultures (references on legend). Ciotti and MacIntyre (unpub.) refers to the toxic dinoflagellate *Alexandrium tamarense* grown in K media in semi-continuous culture (see MacIntyre et al. (1997) for detail), and Ciotti and Parkhill (unpub.) refers to the coastal diatom *Thalassiosira pseudonana* in continuous culture. Table in the figure indicates equation form, parameter values and respective standard deviations, and r^2 . B) Empirical relationship between $a_{ph}^*(675)$ and C . Table indicates equation form, parameter values and respective standard deviations, and r^2 . C) Approximation for a relationship between the product dc_i and C . Error bars indicate 2 standard deviations.....22
- Figure 2.3** Best fit for derived values of a_{so1}^* versus C at the SeaWiFS wavebands. See Table 2.2 for equation form, parameter values and respective standard deviations, and r^227
- Figure 2.4** Comparison between empirical models and the parameterization of SAMOCAFOTS . A) Attenuation coefficient at 490 nm versus the empirical model by Morel (Morel, 1988). B) Radiance ratio of 490 to 550 nm

$(L_u(490)/L_u(550))$ which was calculated as in equation (2.26) with the relevant parameters modified from 443 to 490 nm (see text). Comparison with the CZCS algorithm for $C > 1 \text{ mg m}^{-3}$ (see Lewis and Cullen, 1991), and the more recent SeaWiFS algorithm (O'Reilly *et al.*, 1998). C) SAMOCAFOTS and empirical models relating $K_d(490)$ to $L_u(443)/L_u(550)$ derived by Austin and Petzold (1981), Aarup *et al.* (1996) and Mueller and Trees (1997). Note that empirical models were not extrapolated beyond the upper limit of $K_d(490)$ measured in each case.....36

Figure 2.5 Comparison of SAMOCAFOTS with independent data collected in a variety of coastal waters: off the Oregon coast in September 1994 (ORE94, see Ciotti *et al.* (1996)), in the Bering Sea in June of 1997 (WE97), and in Bedford Basin on several occasions: Summer of 1992 (BBS92), Summer of 1993 (BBS93) during a red tide event (in box), and also a time series from June to November of 1996 (BBTS96). Plot shows data from BBTS96 collected daily between 11:00 and 13:00 local time. Note that the radiance ratios measured during ORE94, BBS92 and BBS93 were between 443 and 555 nm and during BBTS96 were between 443 and 559 nm.....39

Figure 2.6 Absorption by detritus (particulate material after extraction with an organic solvent) plus CDOM and phytoplankton absorption at 443 nm during the weekly sampling in Bedford Basin in 1996 (BBST96) and during the Oregon cruise in September 1994 (ORE94). Lines represent an assumed linear relationship: the slope represents the fraction that is directly associated with phytoplankton and covaries with them (d_s) and the intercept represents a background value (D_0).41

Figure 2.7 Results of the sensitivity analysis of the effects of changes in packaging and pigment composition. Individual points represent fixed values of the product of cell diameter and intracellular concentration of pigments, dc_i (see legend).

Three fixed levels of $a_{sol}^*(\lambda)$ were used to represent high to low influence of accessory pigments, following the equations in Table 2.3 for C concentrations of 1 mg m^{-3} (A and D), 5 mg m^{-3} (B and E) and 20 mg m^{-3} (C and F). All the other parameters are a function of C , as in SAMOCAFOTS and SAMOCAFOTS high CDOM, respectively value (D_0)44

Figure 2.8 Analysis of the effects of changes in packaging for a fixed pigment composition (“Medium” accessory pigments, as in Figure 2.7B) and the relationships between : A) $L_u(443)/L_u(550)$ and C , and B) $K_d(490)$ and C . Individual points refer to fixed values of the product of cell diameter and intracellular concentration of pigments, dc_i (legend), and $a_{sol}^*(\lambda)$ computed as in the equations in Table 2.3 for C equal to 5 mg m^{-3} (“Medium” accessory pigments). Symbols indicate dc_i values in both graphs. Solid line is the general model.....46

Figure 2.9 Sensitivity of A) SAMOCAFOTS and B) SAMOCAFOTS high CDOM to the wavelength dependence of the particle scattering coefficient (γ), varying as described in the legend. More negative exponents are associated with the importance of smaller particles. All the other parameters (packaging, pigment composition and CDOM plus detrital absorption) are a function of C , as in SAMOCAFOTS. The empirical relationship by Austin and Petzold (1981) is plotted in A for comparison.48

Figure 2.10 Influence of an additional input of particles simulated by their attenuation coefficient at 660 nm, $b_{non-ph}(660)$. A and B) Increments of $b_{non-ph}(660)$, simulating the input of particles with backscattering ratio equal to 0.08, low absorption coefficient and dependency of λ^{-1} for the scattering coefficient, for SAMOCAFOTS and SAMOCAFOTS high CDOM, respectively. C and D) Same as A and B, only for input of particles with backscattering ratio of 0.01 and no spectral dependency for the scattering coefficient.....50

Figure 2.11 **A)** Sensitivity analysis of SAMOCAFOTS to changes in D_0 , the absorption by the background concentration of CDOM and detritus, representing ranges found from oligotrophic to estuarine waters. **B)** Sensitivity to d_s , the slope of the assumed linear relationship between phytoplankton and CDOM and detritus absorption, representing ranges found in a variety of coastal waters. **C and D)** Same as in **A** and **B**, only for the relationship between C and $L_u(490)/L_u(550)$ which was parameterized as in equation (2.26) with the relevant parameters modified from 443 to 490 nm.....52

Figure 2.12 Sensitivity of **A)** SAMOCAFOTS and **B)** SAMOCAFOTS high CDOM to changes in S , the slope of the decrease of CDOM plus detrital absorption with wavelength. Values of S represent ranges found in the literature and in the data base collected in this study.....54

Figure 3.1 Procedure followed to discriminate among different communities. Dominant cell size was attributed to the organism or group with the higher product of cell number and cell area.....62

Figure 3.2 Sampling areas and stations visited. **A)** Off the coast of Oregon state in September 1994. **B)** Bering Sea in 1996 and 1997. **C)** Bedford Basin on several occasions. See Table 3.1 for dates and measurements.....65

Figure 3.3 Selected vertical profiles of sigma-t (dotted line) and fluorescence in relative units (solid line) for the upper 60 meters during the cruise off the Oregon coast. **A)** Open ocean (surface chl < 0.3 mg m⁻³). **B)** Mid shelf (surface chl < 1 mg m⁻³). **C)** Coastal waters (surface chl > 10 mg m⁻³). Note that the fluorometer was off scale in the upper 15 m..71

Figure 3.4 Chlorophyll size-fractions (see Table 3.2) versus total chlorophyll during the cruise off Oregon in 1994. Samples are from surface (20 stations). Note that concentrations are in log scale. Lines are linear regressions on log-transformed

data, and are included to illustrate trends only. Coefficients of determination and fit parameters are not shown, as size fractions are not independent of total chlorophyll.....72

Figure 3.5 **A)** Phytoplankton absorption spectra measured in whole surface samples during the Oregon cruise. Spectra were normalized to the average phytoplankton absorption between 400 and 700 nm. Legend indicates the dominant chl size fractions (i.e., more than 50% when two size ranges were present or more than 40% when 3 or more size ranges were present). **B)** Phytoplankton absorption spectra measured directly for different size fractions collected on GF/F filters (see Figure 3.1 and Table 3.2). **C)** Comparison of absorption for size fractions using 1 μm and 2 μm filters.....74

Figure 3.6 Selected vertical profiles of sigma-t and fluorescence (relative units) for the upper 60 meters during the cruise in the Bering Sea in April 1996 (see Figure 3.2). **A)** Mid-shelf inside the 100 meters isobath (surface chl $<1 \text{ mg m}^{-3}$). **B)** Mid-shelf outside the 100 meters isobath (surface chl $>1 \text{ mg m}^{-3}$). **C)** Station by Unimak Pass (surface chl $>3 \text{ mg m}^{-3}$).....76

Figure 3.7 Chlorophyll size-fractions (see Table 3.2) versus total chlorophyll during the cruise in the Bering Sea in April 1996. Samples are from surface (12 stations). Note that the concentrations are in log scale. Lines are linear regressions on log-transformed data, and are included to illustrate trends only. Correlation coefficient and parameters are not shown, as size fractions are not independent of total chlorophyll..78

Figure 3.8 Shape of phytoplankton absorption spectra for surface samples collected in the southern Bering Sea. Spectra were normalized to the average phytoplankton absorption between 400 and 700 nm. **A)** April 1996. Legend indicates the dominant chlorophyll size range. **B)** June 1997.79

Figure 3.9 Three typical vertical profiles of sigma-t (dotted line) and beam attenuation minus attenuation by sea water, 0.367 m^{-1} (solid line), which was used as a proxy for total particle concentration during the intensive sampling in 1993 in Bedford Basin. Examples refer to August 18. Figures are identified with sampling time shown on the bottom of figures. At 9:33, a dense layer was detected at depth, related to large numbers of large dinoflagellates (mode of $32 \mu\text{m}$ in diameter) and surface chl ranged between 6 and 36 mg m^{-3} . At 14:38, the cells entrained in the surface due to wind mixing, and surface chl ranged between 27 and 135 mg m^{-3} . At 17:52 a well mixed upper layer was observed and surface chl ranged between 10 and 40 mg m^{-3}83

Figure 3.10 Chlorophyll size-fractions versus total chlorophyll during the Summer of 1996 in Bedford Basin. Data refer to samples from mixed layer ($n=21$). Note that concentrations are in log scale. Lines are linear regressions on log-transformed data, and are only illustrating the tendency..84

Figure 3.11 Spectral shape of phytoplankton absorption coefficient for whole water samples collected at the surface during the three intensive samplings in the summer in Bedford Basin. Legends indicate the communities characterized according to cell size and dominant group (see text). Lines are averages for the number of samples (n) indicated in the legend.....86

Figure 3.12 Weekly chl size-fractions (see Table 3.2) as proportions of total chl during the time series in 1996 in Bedford Basin, including the fall bloom. Samples from 1 and 3 meters, respectively, for each day.....88

Figure 3.13 Weekly river discharge (Sackville River, data from Environment Canada) and surface chlorophyll concentration during the Time Series in Bedford Basin in 1996 (July to December).....90

Figure 3.14 Spectral shape of phytoplankton absorption coefficient for surface samples collected in from July to November 1996 in Bedford Basin. Legends indicate the communities characterized according to size range and dominant group (see text). Lines are averages.....91

Figure 3.15 Spectral shape of phytoplankton absorption coefficient for whole-water surface samples collected in all experiments, according to cell size range of the dominant organism (see Figure 3.1). **A)** Picoplankton. **B)** Ultraplankton. **C)** Nanoplankton . **D)** Microplankton. **E)** Average for each cell size. Legends indicate the communities characterized in Table 3.3 and the cruises: ORE (off Oregon coast); BS96 (Bering Sea April 1996); BS97 (Bering Sea 1997), BBS92, BBS93 and BBS96 (intensive samplings in Bedford Basin in 1992, 1993 and 1996, respectively) and BBTS96 (time series in Bedford Basin from July to November 1996). See Table 3 for number of samples. CFD stands from chain-forming diatoms. Note changes in the scale on Y-axis.....92

Figure 3.16 Same as in Figure 3.14 except that phytoplankton absorption spectra were normalized by chl plus pheopigments. Note changes in the scale on Y-axis....95

Figure 3.17 Results of the multiple regression analyses for 301 wavelengths. **A)** Expected spectral shapes for phytoplankton absorption for each cell size fraction. **B)** Initial variance of the data set (16 different communities). **C)** Variability of the data explained by predefining cell size range of the dominant organism.....97

Figure 3.18 Three examples for recomposed normalized spectra of phytoplankton absorption using equation 3.4 and two basis vectors, representing the average for the smallest and largest cell sizes found in our data set. See Table 3.3 and 3.4 for details.....99

Figure 4.1 Inferred contributions of different size classes to phytoplankton absorption as a function of trophic status. SAMOCAFOTS estimates C -normalized phytoplankton absorption at 6 wavebands (see chapter 2). The set of wavebands at each C were decomposed using a linear combination of two spectra with 1 nm-resolution representing small and large cells, respectively, as described in chapter 3. The decomposition yields the size parameter $F_{<p>}$. **A)** Inferred spectra at each C using a linear combination of the two basis vectors and the estimated $F_{<p>}$ (see equation 4.6). Some spectra are not shown to facilitate visualization. **B)** Estimated $F_{<p>}$ at each C124

Figure 4.2 Inferred contributions of different size classes to phytoplankton absorption (i.e., values of $F_{<p>}$ computed from measured phytoplankton absorption spectra) as a function of trophic status in the different data sets (see legend) compared to “expected” values as a function of C estimated with SAMOCAFOTS (solid line). Points above the line correspond to spectra characteristic of cells smaller than predicted by the model.....127

Figure 4.3 Relationship between measurements of absorption by CDOM and detritus at 443 nm versus C in the different data sets (see legends) compared to values estimated by the model (solid lines). **A)** Data from the Bering Sea cruises and estimates from SAMOCAFOTS and **B)** Data from Bedford Basin and estimates from SAMOCAFOTS high CDOM.....129

Figure 4.4 Relationships between $R_t(490)/R_t(555)$ and C from all cruises. **A)** Solid line shows results of the semi-analytical model SAMOCAFOTS describing the central trend of the decrease in $F_{<p>}$ with C , in which small cells dominate at low C and large cells dominate at high C . Small dashed line represents SAMOCAFOTS with $F_{<p>}=1$ (dominance of small cells). Large dashed line represents SAMOCAFOTS with $F_{<p>}=0$ (dominance of large cells). An independent data set (SeaBAM validation data set, courtesy of Dr. C. McClain)

is included for comparison. **B)** Same as **A** only for data collected in Bedford Basin in several occasions compared to SAMOCAFOTS high CDOM. Note change in scales.....131

Figure 4.5 Same as Figure 4.4, only the model runs refers to changes in the total value of absorption by CDOM plus detritus of 1/4 of SAMOCAFOTS (small dashed line) and 4 times of SAMOCAFOTS (large dashed line). **A)** Data from the different cruises excluding Bedford Basin (see legend). The SeaBAM empirical relationship (O'Reilly et al., 1998) is plotted for comparison. **B)** Bedford Basin data only.....134

Figure 4.6 Sensitivity analysis of the influence of changes in dominant cell size and $a_{\text{cdom+det}}(\lambda)$ on relationships between $R_t(443)R_t(555)/R_t(490)^2$ versus C . **A)** Solid lines are results of the semi-analytical model SAMOCAFOTS with its general formulation. Dashed lines represent SAMOCAFOTS run with fixed values of $F_{<p>}$ (see legend). **B)** Same as **A** but the model runs refer to changes in the total value of absorption by CDOM plus detritus of 1/4 (small dashed line) and 4 times (large dashed line) of that predicted by SAMOCAFOTS. **C** and **D)** Same as **A** and **B**, but for SAMOCAFOTS high CDOM.....136

Figure 4.7 Relationships between $R_t(443)R_t(555)/R_t(490)^2$ versus C from cruises excluding the ones in Bedford Basin (see legend). Solid line are result of the semi-analytical model SAMOCAFOTS, showing the central trend of the decrease in $F_{<p>}$ with C , in which small cells dominate at low C and large cells dominate at high C . Small dashed line represents SAMOCAFOTS with $F_{<p>}=1$ (dominance of small cells). Large dashed line represents SAMOCAFOTS with $F_{<p>}=0$ (dominance of large cells).137

Figure 4.8 Summary of the influence of changes in phytoplankton absorption attributed to changes in cell size range ($F_{<p>}$) and changes in CDOM plus detrital

absorption on reflectance ratios. **A)** Relationship between $R_r(490)/R_r(555)$ and C . **B)** Relationship between $R_r(443)R_r(555)/R_r(490)^2$ and C139

Figure 4.9 Relationships between vertical attenuation coefficient and remote sensing reflectance ratios. Solid lines are results of the general formulation of the semi-analytical model; dotted lines represent model results with dominance of small cells; large-dashed lines represent model results with dominance of big cells; model results are presented for values of absorption CDOM plus detritus of 1/4 (diamonds) and 4 times (x) of that predicted by SAMOCAFOTS.....143

Figure 4.10 Nomograms for retrieving $F_{<p>}$ from relationships between vertical attenuation coefficient at 555 nm and remote sensing reflectance ratio of 490 to 555 nm. Lines represent model runs of SAMOCAFOTS **A)** and SAMOCAFOTS high CDOM **B)** with fixed values of $F_{<p>}$ as designated in the lines. Data are plotted for comparison (see legend for cruises). Note scale changes.....144

Figure 4.11 Retrieved $F_{<p>}$ from the nomogram of Figure 4.11 versus observed $F_{<p>}$ computed from surface samples of phytoplankton absorption (see legend for cruises).....146

Figure 4.12 **A)** Nomogram for retrieving $F_{<p>}$ from relationships between vertical attenuation coefficient at 555 nm and remote sensing inflection reflectance ratio using 443, 490 and 555 nm (equation 4.5). Lines represent model runs of SAMOCAFOTS with fixed values of $F_{<p>}$ as designated in the lines. Data from BS97 is plotted for comparison. **B)** Retrieved $F_{<p>}$ from the nomogram in **A** versus observed $F_{<p>}$ computed from surface samples of phytoplankton absorption during BS97.....149

List of Tables

Table 2.1 Parameters and correlation coefficient (r^2) values for the empirical relationships generated from the field data set of $a_{ph}^*(\lambda)$ and C . Phytoplankton absorption spectra were averaged, consistent with the spectral response of the SeaWiFS ocean color sensor (about 20 nm wavebands centered on the wavelength designated). The data are a compilation of spectra with 2-nm resolution (Bricaud *et al.*, 1995) and the phytoplankton absorption data (1-nm resolution) collected off the Oregon coast (Ciotti *et al.*, 1996) and in a coastal embayment (Bedford Basin, N.S., Canada). C is chlorophyll a plus pheopigment concentration. The parameter values designated ns means not significant; na means not available; sd are the standard deviations for each parameter.....25

Table 2.2 Parameters and r^2 values for the relationships generated for $a_{sol}^*(\lambda)$ and C . This value was used in combination with equations (2.14) and (2.15) to solve for $a_{sol}^*(\lambda)$ for each C . The parameter values in the table describe the best fit for $a_{sol}^*(\lambda)$ and C . Standard deviations (sd) for each parameter are indicated.....26

Table 2.3 List of cruises with respective location, dates and optical measurements at the surface.....34

Table 2.4 Values for the parameters and variables used in the sensitivity analysis. These values replaced the relationships with C in the general model. The parameter γ refers to the exponent of the relationship between particle scattering and wavelength.....42

Table 3.1 Location, dates, and measurements in each cruise.64

- Table 3.2** Physical separation of samples into 4 size fractions for chlorophyll *a* and particulate absorption, as determined by differential filtration. Filtrates from 20, 5 and 2 μm Poretics® polycarbonate filters, filtered either by gravity or very low pressure, were concentrated onto GF/F filters. The concentration of each size class was determined following the second column.....70
- Table 3.3** Summary of the distinct communities of phytoplankton characterized in the combined data sets. Name describes cell size range (P is pico; U is ultra; N is nano and M is micro) and species or groups of the dominant organism. N.S. is number of samples, na means not available. For details on cruises, refer to Table 3.1.....93
- Table 3.4** Results from a linear decomposition of the phytoplankton absorption spectra for the different communities (see Table 3.3) using a linear regression subjected to constraints (see Appendix 3.9B). $F_{<p>}$ is the factor estimated and varies from 1 to 0 for small and big cell sizes, respectively, and r^2 is the coefficient of determination between observed and estimated spectrum. The linear regression uses two basis vectors representing the minimum and maximum cell size found in our data set (see text and Appendix 3.9A). For reference, maximum $a_{\text{ph}}^*(\lambda)$ at the red peak (and respective wavelength) are presented, so $a_{\text{ph}}^*(\lambda)$ curves can be reconstructed for each community..... 101
- Table 4.1** Expected values of $b_b(\lambda_1)/b_b(\lambda_2)$ when the proportion of backscattering by particles at 555 nm, $b_{\text{ph}+\text{det}}(555)$, is varied (first column). This range represents the approximate values predicted by the semi-analytical model SAMOCAFOTS (i.e., from around 3 when C is 0.5 mg m^{-3} to 25 when C is 30 mg m^{-3} , see chapter 2). Backscatter by water, $b_{\text{b}_w}(\lambda)$, follows a power function with wavelength; the slope is -4.65 , corresponding to a $b_{\text{b}_w}(490)/b_{\text{b}_w}(555)$ of 1.631 and $b_{\text{b}_w}(443)/b_{\text{b}_w}(555)$ of 2.579. Backscattering by particles also

follows a power function with wavelength: the value of γ indicates the slope.....114

Table 4.2 Location, dates, measurements and instruments used in each cruise. TSRB: Tethered spectral radiometer buoy, TACCS: Tethered attenuation coefficient chain sensor, SPMS: SeaWifs profiling multichannel radiometer, OCI-200: Ocean color radiometer with irradiance sensors, OCTS: Ocean color and temperature sensor. All instruments from Satlantic, Inc.118

Table 4.3 Results for the decomposition of $a_{ph}^*(\lambda)$ computed for 6 wavebands (412, 443, 490, 510, 555 and 670 nm) using the semi-analytical model for the given range of C (see text). Decomposition is a result of a linear combination of two extreme $a_{ph}^*(\lambda)$, representing small and big cells, using a linear regression subjected to constraints (see text). The regression yields the factor $F_{<p>}$. For comparison, coefficients of determination (r^2) and slopes are presented for the regressions using both basis vectors and using each vector separately. Analysis was performed for 6 wavebands only.....125

Abstract

The effects of different communities of phytoplankton on optical properties of surface waters in the coastal ocean were examined. Data from large data sets were used to develop semi-analytical expressions describing quantitatively how idealized phytoplankton assemblages could affect apparent optical properties (AOPs), such as diffuse attenuation and surface reflectance. Spectral absorption by idealized phytoplankton assemblages was simulated by varying the parameters governing pigment packaging and accessory pigments as a function of trophic status represented by the concentration of chlorophyll plus pheopigments ($C \text{ mg m}^{-3}$). Backscattering and absorption by other optically active components were also parameterized as functions of C . The model reproduced central trends in apparent optical properties with C and agreed to within 20% of empirical models that relate diffuse attenuation to radiance ratios within a range of C between 0.5 and 30 mg m^{-3} . Sensitivity analyses and independent data suggested that changes in phytoplankton community structure account in part for observed deviations from the central trends. Variability in the spectral shape of the absorption coefficient in distinct communities of phytoplankton in surface waters was related to two major ecological factors: cell size and taxonomic composition. It was found that when the cell size range of the dominant organism is known, approximately 80% of the variability in spectral shape of the phytoplankton absorption could be explained. More than 95% of the variability in all observed spectra was accounted for when phytoplankton absorption was parameterized using two constant spectral shapes and a size parameter. This new parameterization was integrated in the former model, so that AOPs could be estimated for specifying cell sizes of phytoplankton dominating the community. Forward modeling was used to select relationships between diffuse attenuation and ratios of surface reflectance with minimum influence of backscattering and CDOM plus detrital absorption. This approach provided a tool to observe and monitor changes in the nature of a phytoplankton community (i.e., dominant cell size) using optical measurements only. Although refinement in the model is still required, the results suggested that mechanistic approaches to interpreting bio-optical data are feasible and can provide simple parameters relating optical signatures to ecological features of phytoplankton.

List of Symbols

AOPs	apparent optical properties.
$a(\lambda)$	total absorption coefficient, m^{-1} .
$a_{\text{cdom}}(\lambda)$	absorption coefficient due to CDOM, m^{-1} .
$a_{\text{cdom+det}}(\lambda)$	absorption coefficient due to combined effects of CDOM and detritus, m^{-1} .
$a_{\text{ph}}(\lambda)$	absorption coefficient for phytoplankton, m^{-1} .
$a_{\text{w}}(\lambda)$	absorption coefficient for pure water, m^{-1} .
$a_{\text{ph}}^*(\lambda)$	phytoplankton specific absorption coefficient, $\text{m}^2 \text{mgChl}^{-1}$.
$\langle a_{\text{ph}} \rangle$	average phytoplankton absorption between 400 and 700 nm, m^{-1} .
$a_{\text{sol}}^*(\lambda)$	pigment cellular solution specific absorption coefficient, $\text{m}^2 \text{mgChl}^{-1}$.
$b(\lambda)$	total scattering coefficient, m^{-1} .
$b_{\text{b}}(\lambda)$	total backscattering coefficient, m^{-1} .
$b_{\text{f}}(\lambda)$	total forward scattering coefficient, m^{-1} .
$b_{\text{ph+det}}(\lambda)$	scattering coefficient for particles, m^{-1} .
$b_{\text{non-ph}}(\lambda)$	scattering coefficient for additional inorganic particles, m^{-1} .
$b_{\text{b}_{\text{ph+det}}}(\lambda)$	backscattering coefficient for particles, m^{-1} .
$b_{\text{b}_{\text{non-ph}}}(\lambda)$	backscattering coefficient for additional inorganic particles, m^{-1} .
$b_{\text{b}_{\text{w}}}(\lambda)$	backscattering coefficient for water, m^{-1} .
$\tilde{b}_{\text{b}_{\text{ph+det}}}(\lambda)$	backscattering ratio for the particle assemblage, dimensionless.
$\beta(\lambda)$	volume scattering function, $\text{m}^{-1} \cdot \text{sr}^{-1}$.
$c(\lambda)$	total attenuation coefficient, m^{-1} .
chl	chlorophyll <i>a</i> concentration measured fluorometrically, mg m^{-3} .
<i>C</i>	chlorophyll <i>a</i> plus pheopigment concentration, mg m^{-3} .
c_i	intracellular pigment concentration, mg m^{-3} .
<i>d</i>	equivalent spherical diameter, m.
dc_i	product of <i>d</i> and c_i , mg m^{-2} .

D_o	intercept of the linear relationship between $a_{ph}(\lambda)$ and $a_{c_{dom+det}}$ at 443 nm, m^{-1} .
d_s	slope of the linear relationship between $a_{ph}(\lambda)$ and $a_{c_{dom+det}}$ at 443 nm, dimensionless.
$E_u(\lambda), E_d(\lambda)$	upwelling and downwelling irradiance at the sea surface, $W m^{-2} nm^{-1}$.
$E_d(\lambda, 0^+)$	downwelling irradiance in the air, $W m^{-2} nm^{-1}$.
$E_{o_d}(\lambda)$	downwelling scalar irradiance, $W m^{-2} nm^{-1}$.
$f(\lambda)$	parameter that relates reflectance to the ratio between backscattering and absorption, dimensionless.
$F_{<p>}$	size parameter.
IOPs	inherent optical properties.
$K_{d_w}(\lambda)$	diffuse attenuation coefficient by water, m^{-1} .
$K_d(\lambda)$	diffuse attenuation coefficient for downwelling irradiance, m^{-1} .
$L_u(\lambda)$	upwelling radiance, $W m^{-2} nm^{-1} sr^{-1}$.
$L_{u-tsrb}(\lambda)$	upwelling radiance measured at 0.45 m, $W m^{-2} nm^{-1} sr^{-1}$.
λ	wavelength, nm.
M	factor representing a ratio of $E_d(\lambda)$.
γ	spectral dependency of $b_{ph+det}(\lambda)$, dimensionless.
$\gamma_{non-ph}(\lambda)$	spectral dependency of $b_{non-ph}(\lambda)$, dimensionless.
$\rho'(\lambda)$	particle optical thickness, dimensionless.
$Q(\lambda)$	ratio of upwelling irradiance to upwelling nadir radiance, sr.
$Q_a(\lambda)$	efficiency coefficient for absorption, dimensionless.
$Q_a^*(\lambda)$	packaging effect coefficient, dimensionless.
RSC	estimated C from radiance ratio algorithms, $mg m^{-3}$.
$R(\lambda)$	irradiance reflectance, dimensionless.
$R_r(\lambda)$	remote sensing reflectance, dimensionless.
S	slope of the exponential decrease of $a_{c_{dom-det}}$ with wavelength, nm^{-1} .
$\bar{\mu}_d$	average cosine for downwelling irradiance, dimensionless.

Chapter 1

General Introduction

1.1 Ocean color and ecological processes in surface waters

Primary productivity and the way it is transferred to the higher trophic levels is strongly influenced by the structure of phytoplankton communities (see review by Kiørboe, 1993), which in turn becomes a desirable quantity to know for the general understanding and quantification of biogeochemical processes in the ocean. Early ecological studies describing phytoplankton communities involved taxonomic surveys, which are not only time consuming but also difficult to quantify, as phytoplankton comprise thousands of different species classified according to their size, shape, external structures, pigment composition and mobility (see Sournia *et al.*, 1991; Tomas, 1997). It is therefore important to develop simpler ways to observe and monitor changes in the nature of phytoplankton communities. A number of different approaches have been developed, mainly related to the description of pigment composition as a taxonomic indicator. Pigmentation is characterized with fluorescence signatures (Yentsch and Phinney, 1985) using flow cytometric analyses (e.g., Li, 1995) or *in situ* instruments (Cowles *et al.*, 1993), and also quantified by High Performance Liquid Chromatography (HPLC) methods (e.g., Letelier *et al.*, 1993; Johnsen *et al.*, 1994b). Although automated, these methods still require extensive field sampling, which limits their spatial and

temporal resolution.

The appearance of remote sensing optical instruments provided the opportunity to observe biological variability synoptically over large spatial scales (Hovis *et al.*, 1980). *In situ* optical instruments provide continuous and autonomous measurements. Much progress has been made since the original works relating ocean color to phytoplankton abundance (Clarke *et al.*, 1970): new types of *in situ* instruments are steadily appearing and being improved, and satellite sensors, both deployed (e.g., SeaWiFS) and planned, should be more reliable and have better spectral resolution than the original Coastal Zone Color Scanner. Nonetheless, the extent to which our understanding of phytoplankton variability will improve with better instrumentation relies first on understanding the measurements. In particular, it is important to understand how different communities of phytoplankton influence ocean color. Then, mechanistic approaches and ecological interpretation can be applied to the optical data. The central goal of this thesis is to develop an approach for an ecological interpretation of optical variability in surface coastal waters. Specifically, this thesis will explore how phytoplankton cell size can influence relationships between optical properties, and if combinations of optical measurements can provide a simple approach for detecting changes in dominant phytoplankton cell size. This research is direct toward synoptic or real time observations of changes in phytoplankton size structure, and as a consequence, the description of physiological and ecological characteristics of phytoplankton assemblages directly related to cell size.

1.2 Phytoplankton communities and trophic status

The local phytoplankton assemblage in any body of water is determined by environmental conditions, physiological features of the different groups, (Margalef, 1978; Kiørboe, 1993) and ecological interactions between the trophic levels (see review by Banse, 1982; Harris, 1986). Phytoplankters, being drifters, have evolved a number of physiological and morphological adaptations for the different scales of water motion to

which they are subjected (see Estrada and Berdalet, 1997), so that the diverse populations present at a given moment reflect their ability to maximise nutrient uptake and light utilization.

This coupling between physical environment and phytoplankton community structure is reflected in general and well-established trends of species composition along a trophic gradient. When nutrients are scarce (i.e., oligotrophic environments), phytoplankton biomass is dominated by small prokaryotic cells (Chisholm *et al.*, 1988; Olson *et al.*, 1990). Cells growing in low nutrient conditions tend to have a higher concentration of accessory pigments (including photoprotective pigments) than when nutrients are abundant (Prézelin and Matlick, 1983; Sosik and Mitchell, 1991; Geider *et al.*, 1993; Stuart *et al.*, 1998). Physical processes that supply nutrients to the euphotic zone (e.g., vertical mixing, upwelling) will allow larger cells to proliferate, complementing the ubiquitous small-sized groups (Malone, 1980; Yentsch and Phinney, 1989; Chisholm, 1992). A considerable time lag in the numerical response of predators allows larger cells to bloom (Banse, 1982; Thingstad and Sakshaug, 1990; Kiørboe, 1993; Riegman *et al.*, 1993; Carr, 1998).

Light utilisation by phytoplankton depends on cell size and internal pigments (chlorophylls carotenoids and phycobiliproteins Rowan, 1989; Jeffrey and Vesk, 1997). The common pigment to all groups is chlorophyll *a* (divinyl chlorophyll *a* in prochlorophytes) and because the measurement of this pigment is relatively simple, chlorophyll *a* has been used as a measure of phytoplankton abundance since the early 1950's (Richards and Thompson, 1952). It is thus not surprising that the study of phytoplankton variability using ocean color has been done with relationships between ocean color and "phytoplankton pigment," that is, chlorophyll plus phaeophytin (Gordon and Morel, 1983; Aiken *et al.*, 1995; O'Reilly *et al.*, 1998). The main disadvantage of such relationships derives from the fact that chlorophyll *a* is an imprecise description of phytoplankton biomass (Cullen, 1982), because the ratio of chlorophyll *a* to carbon varies with both species composition and their physiological state (see Taylor *et al.*, 1997 and

references therein). Thus, processes directly related to phytoplankton biomass (i.e., growth rate, carbon flux, nitrogen flux) should not be parameterized as functions of chlorophyll *a* alone when either species composition changes or the physiological state of the species are altered.

Nonetheless, any gradient of phytoplankton abundance (i.e., chlorophyll gradient) will intrinsically contain changes in species composition which will be manifested in their optical characteristics. A common feature in any trophic gradient is the increase in size of the phytoplankton as chlorophyll concentration increases, which at first approximation increases the degree of packaging of pigments (Duysens, 1956; Bricaud *et al.*, 1983; Yentsch and Phinney, 1989) and decreases the relative importance of accessory pigments with respect to chlorophyll *a* (Geider and Osborne, 1986; Agusti, 1991; Sosik and Mitchell, 1991; Geider *et al.*, 1993; Claustre, 1994; Richardson *et al.*, 1996; Stuart *et al.*, 1998). On the other hand, the increase in biomass also corresponds to changes in taxonomic groups, with distinct accessory pigments that could be used to distinguish them (Bidigare *et al.*, 1988; Hoepffner and Sathyendranath, 1991; Millie *et al.*, 1993). The detection of distinct pigments using optical measurements will be a function of how important their signals are and of the spectral resolution of the instruments used (e.g., Johnsen *et al.*, 1994b; Sathyendranath *et al.*, 1994).

1.3 Optical properties of sea water constituents

Light that reaches surface waters is absorbed, scattered or transmitted to greater depths. The theory that quantifies absorption ($a(\lambda)$) and scattering ($b(\lambda)$) assumes a parallel “light beam” passing through a very thin layer of sea water. The attenuation coefficient ($c(\lambda)$) is the sum of the absorption and scattering coefficients, and the volume scattering function ($\beta(\lambda)$) characterizes the angular distribution of the scattered flux. For ocean color applications it is pertinent to separate scattering into forward scattering ($b_f(\lambda)$) and backscattering ($b_b(\lambda)$) coefficients. The properties described above are inherent

optical properties (IOPs, Preisendorfer, 1961) because their effects depend exclusively on the components in the water.

Inherent optical properties have two main characteristics: the effects of the different components are additive, and there is a linear relationship between effect and concentration of each component. In sea water, optical constituents can be divided into four categories: water itself, colored dissolved organic matter (CDOM), phytoplankton, and other organic and inorganic particles (Kirk, 1994b). Generally, in open ocean waters, the main contributors to optical variability are living organisms. The scattering and absorption coefficients for sea water are well known and vary little (Morel and Smith, 1974; Buiteveld *et al.*, 1994; Mobley, 1994; Pope and Fry, 1997). Scattering by CDOM is generally considered negligible (Mobley, 1994). Within the visible range (i.e. 400 to 700 nm), CDOM, detritus and heterotrophic organisms absorb light with a spectrum following an exponential decay with increasing wavelength (Kirk, 1976; Bricaud *et al.*, 1981; Nelson and Robertson, 1993). Phytoplankters are the main absorbers of light due to their photosynthetic pigments, but heterotrophic components such as flagellates and ciliates (Morel and Ahn, 1991), bacteria (Morel and Ahn, 1990; Ulloa *et al.*, 1992; Nelson and Robertson, 1993) and other heterotrophic organisms (e.g., Balch and Haxo, 1984) can also contribute significantly to light attenuation (Stramski and Kiefer, 1991). Generalizations are difficult for the absorption and scattering properties of living and non-living particles, however, because they are mainly controlled by particle size and respective refractive index (Bohren and Hoffman, 1983), as will be shown below.

1.3.1 Modeling optical properties of particles

Optical properties of particles with sizes that are similar to or somewhat larger than the wavelengths of interest (which is the case of phytoplankton in the visible range), generally follow Mie theory (Mie, 1908). Mie theory assumes that the particles are spherical and homogeneous, and that their size (i.e., cross sectional area) and refractive indices (real and imaginary parts) are known. Mie calculations have been used to estimate

optical properties in monospecific cultures of phytoplankton (Morel and Bricaud, 1981; Bricaud *et al.*, 1983; Bricaud and Morel, 1986). The theoretical formulations were then tested with measurements of absorption, scattering and attenuation coefficients (Bricaud and Morel, 1988) for a number of phytoplankton species showing different degrees of deviation from the assumptions of spherical shape and homogeneous internal composition. A good agreement between measurements and modeled coefficients was found in almost all the cases (Bricaud and Morel, 1988). Because phytoplankton are considered “soft” particles (i.e., their refractive index in relation to that of sea water is close to 1), the absorption and scattering (but not backscattering) efficiency coefficients, can be derived from much simpler expressions, the van de Hulst’s anomalous diffraction approximation (van de Hulst, 1957).

The estimation of IOPs from single cell type to a population of these cells depends upon knowing their size distribution (see Morel, 1991; Stramski and Kiefer, 1991). The extrapolation for a whole community (i.e., an assemblage of many populations) will depend not only on knowing the particle size distributions (living and non-living) but also on the indices of refraction for each size category (Mobley and Stramski, 1997; Stramski and Mobley, 1997). In most oceanic waters, the particle size distributions are unimodal, skewed toward smaller size classes (Chisholm, 1992 and references therein). For convenience, they are generally modeled as a Junge-type size distributions, a power-function of size, in which a lower limit of cell size is assumed (Morel, 1991; Mobley, 1994). In eutrophic areas, however, one or more additional modes in the size distributions may appear due to contribution of larger cells (Malone, 1980; Yentsch and Phinney, 1989; Chisholm, 1992). Indices of refraction, on the other hand, are more complicated to generalize. The index of refraction is a complex number: its real part is related to scattering properties, while its imaginary part is related to the absorption characteristics of the particles. Thus, the index of refraction of phytoplankton cells is determined by internal and external composition. Because most of the phytoplankton are “soft” optical particles, intracellular composition controls their

refractive index (Bricaud and Morel, 1988; Stramski *et al.*, 1995), which in turn is a primary result of their physiology regulating pigment concentration and composition. In addition, their backscattering efficiencies will be rather small (Bricaud *et al.*, 1983; Stramski and Kiefer, 1991; Ahn *et al.*, 1992), so they are relatively unimportant for backscattering in the ocean. As a consequence, the contribution of phytoplankton to the optical properties in the ocean derives primarily from their absorption coefficient. Coccolithophores which have strongly-scattering calcareous plates are an exception; their index of refraction is controlled also by their extracellular composition (Balch *et al.*, 1996). Nonetheless, backscattering tends to covary with phytoplankton abundance, which has been suggested to be a result of the influence of phytoplankton on the shape of the size distribution of the entire particle assemblage (see Ulloa *et al.*, 1994).

1.3.1.1 Modeling optical properties of phytoplankton communities

When different communities of phytoplankton are present, their influence on optical properties will be differentiated by changes in spectral absorption, which is mainly regulated by accessory pigments and the “packaging” of pigments within cells (Morel and Bricaud, 1981; Bricaud *et al.*, 1983; Sathyendranath *et al.*, 1987; Yentsch and Phinney, 1989; Babin *et al.*, 1993; Nelson and Robertson, 1993; Bricaud *et al.*, 1995; Sosik and Mitchell, 1995; Lutz *et al.*, 1996; Stuart *et al.*, 1998). However, both changes in pigmentation and packaging must be large enough to overwhelm the contribution of other optically active components.

Measurements such as ocean color or diffuse attenuation coefficient are defined as apparent optical properties (AOPS, Preisendorfer, 1961) because their formulations take into account the structure of the light field, which in turn depends not only on the optical characteristics of the main optically active components, but also on the geometrical distribution of the solar radiation. Nonetheless, AOPs can be approximated to IOPs reasonably well (Morel and Prieur, 1977), so that the same principle is applicable: different communities of phytoplankton will affect AOPs by changes in their

spectral absorption (i.e. packaging and pigment composition). Logically, phytoplankton abundance plays an essential role determining the AOPs in surface waters, and as mentioned before (see section 1.2), expected changes in packaging and pigment composition will occur along a trophic gradient. Therefore, different communities of phytoplankton are only anticipated to produce significant departures from the expected changes in AOPS for a given range of phytoplankton abundance (i.e., trophic status) when their bulk absorption coefficient also differs significantly from the expected or central trend of changes in packaging and pigment composition.

1.4 Structure of the thesis research

This thesis examines the influence of different communities of phytoplankton on inherent optical properties. The emphasis is on the effects of different communities of phytoplankton on the bulk absorption coefficient, and the consequences of these influences on the relationships between AOPs. The contributions by CDOM and scattering are also considered. The central goals are:

- 1) to understand how different communities can affect AOPs;
- 2) to quantify this influence;
- 3) to propose approaches that allow ecological interpretation of optical data (e.g., relationships between AOPs) by the retrieval of parameters that are related to changes in phytoplankton community structure.

This thesis is structured as three independent reports (chapters 2, 3 and 4) with a general introduction (chapter 1) and conclusion (chapter 5). This has resulted in some degree of repetition in the introduction and background sections of the different chapters.

Chapter 2 presents the theoretical framework describing relationships between IOPs and AOPs. Semi-analytical formulations of the optical properties of the different components of sea water at the surface are parameterized as functions of trophic status, which is represented by the concentration of chlorophyll plus pheopigments (C , mg m^{-3}). The equations describing the optical properties of all optically active components as

functions of C were developed using basic principles of bio-optics to reconcile well recognized relationships between optical properties and C with ecologically interpretable shifts in phytoplankton communities. The equations for phytoplankton absorption represent the central trend on changes in packaging and pigment composition as a function of C , consistent with trends in large data sets from the field and laboratory. The general formulation of the model, although very simple, reproduced well empirical relationships between AOPs and also relationships between AOPs and C . By changing packaging and pigment composition within ranges observed in field and laboratory data, a sensitivity analysis suggested that predictable departures from established relationships between AOPs can be expected when assemblages differ from the central trend in the degree of pigment packaging and accessory pigmentation.

Chapter 3 compares size-fractionated chlorophyll concentration and absorption spectra of phytoplankton for a wide variety of natural communities. Communities were characterized according to dominant cell size and taxon. It was found that by specifying only the cell size range of the dominant organism, more than 80% of the variability in the spectral shape of the phytoplankton absorption coefficient could be explained by the strong covariation between size of dominant organism and several factors, such as pigment packaging and composition. The results suggested that phytoplankton absorption could be parameterized using two spectra representing the spectral shape of the phytoplankton absorption coefficient for the smallest and biggest cells found in our data set, and one size parameter. Consequently, we can quantify the effects of changes in phytoplankton cell size, independent of trophic status, using bio-optical, semi-analytical approaches. In addition, the potential retrieval of a size parameter for phytoplankton communities may have important applications for using optical data in biogeochemical models.

Chapter 4 incorporates the parameterization of phytoplankton absorption described in Chapter 3 in the semi-analytical model described in Chapter 2. With the use of forward modeling, the influence of phytoplankton assemblages on relationships

between AOPs along a trophic gradient was quantified for hypothetical cases of dominance of small and big cells. It was found that cell size indeed played an important role in determining relationships between AOPs and also between AOPs and C , especially at high C . However, changes in colored organic dissolved matter and detrital absorption will produce variability in these relationships that is comparable to that associated with cell size at C below $1\text{-}2\text{ mg m}^{-3}$. A series of model simulations was used to select a combination of AOPs measurements for the retrieval of the size parameter, which can be used to follow changes in size structure of phytoplankton assemblages using optical methods. The retrieval of the size parameter suggested by the sensitivity analysis of the model was tested with independent data sets. It was found, however, that the retrieval of the size parameter had a systematic bias that was probably related to the parameterization and assumptions of the model.

Finally, the most relevant findings of the thesis are summarized in chapter 5. It is concluded that changes in phytoplankton community structure influence the bulk absorption coefficient of phytoplankton, and that these changes can be mainly related to the cell size range of the dominant organism. If no significant changes in backscattering are assumed when different communities of phytoplankton are present, profound changes in relationships between AOPs and trophic status can be expected when the cell size range of phytoplankton is aberrant. The relevance of this work, therefore, is the establishment of a simple set of relationships of bio-optical properties as functions of trophic status that are consistent with ecological features of changes in phytoplankton community structure. These relationships can be used to quantify the effects of distinct phytoplankton assemblages on the optical properties of coastal surface waters.

Chapter 2

A semi-analytical model of the influence of phytoplankton community structure on the relationship between light attenuation and ocean color

2.1. Introduction

Understanding the factors controlling the attenuation of solar energy in the ocean is of central importance in oceanography, as attenuation influences photosynthetic rates (e.g., Platt *et al.*, 1988), photochemistry (e.g., Miller, 1994) and upper ocean thermal dynamics (e.g., Lewis *et al.*, 1990). Robust empirical relationships derived from regressions of attenuation on ocean color measurements (Austin and Petzold, 1981; Aarup *et al.*, 1996; Mueller and Trees, 1997) make feasible the use of ocean color drifters and remotely sensed observations to estimate attenuation in surface waters. The robust relationship between ocean color and attenuation reflects fundamental physical and biological bases that deserve further investigation. Explicit representation of the terms in these relationships allows a transition from an empirical approach for prediction to a more rigorous analytical foundation (Gordon *et al.*, 1988) which permits the quantitative exploration of the role of various dissolved and particulate components on its variability.

This is achieved by parameterizing the optical properties that govern both attenuation and ocean color, that is, absorption and scattering.

In most oceanic situations, the attenuation of light is strongly affected by biogenic particles, such as phytoplankton. In coastal waters the parameterization of both absorption and scattering is complicated by the presence of inorganic particles and colored dissolved organic matter (CDOM), and by variability in species composition of phytoplankton. The approach of this chapter is to develop a model that explains the central tendency for both absorption and backscattering coefficients to vary with chlorophyll, in terms of ecologically interpretable shifts in phytoplankton communities from oligotrophic to eutrophic environments (Yentsch and Phinney, 1989). The basis of the parameterization was a large data set that comprised optical measurements from both field and laboratory investigations; the influences of pigment packaging and changes in pigment composition on phytoplankton absorption were considered independently. The influence of detrital and CDOM optical properties were also included in the model.

The resulting model, therefore, reconciles a wide range of known relationships between optical properties and trophic status, along with theoretical relationships and data from field and laboratory, so that the optical consequences of changes in phytoplankton community structure can be assessed. The model explains a large fraction of the variability in relationships between ocean color and diffuse attenuation, as well as most of the variability in a relationship between ocean color and bulk chlorophyll concentration using remote sensing techniques (i.e., radiance ratios). The semi-analytical nature of the model will permit us to examine several types of residual variation about the central tendency, associated with changes in cell size (pigment packaging) and in pigment composition, as well as with detritus and CDOM. Analysis of this residual variability allows assessment of the influence of local phytoplankton communities on optical relationships in coastal waters. In turn, the model has the potential for use in the interpretation of deviations in

optical relationships in terms of phytoplankton community structure, and hence, in ecological dynamics in coastal waters.

2.2 Background

Both attenuation coefficient and radiance ratios are so-called apparent optical properties (AOPs) which depend on both the optical properties of the water and its constituents, and the geometrical distribution of the radiance field (Preisendorfer, 1961). A parameterization of the relationship between attenuation and upwelling radiance ratios from first principles requires that this relationship be described using inherent optical properties (IOPs) only, which are independent of the radiance field. It is noteworthy that comparisons between two AOPs will be influenced by changes in the geometrical distribution of the radiance. Nevertheless, because the attenuation coefficient, which can be treated as a quasi-inherent optical property (Preisendorfer, 1961), is being compared to ratios of upwelling radiance, for which the parameters describing the geometric distribution of radiance largely cancel out (see below), the effects of changes in the light field in the comparisons presented in this chapter are expected to be small.

2.2.1 Ratios of spectral radiance at the surface

Surface irradiance reflectance ($R(\lambda)$, dimensionless) is defined as the ratio of upwelling to downwelling irradiance just below the surface. Relationships between $R(\lambda)$ and IOPs are well known (see Gordon et al. (1988) and references therein).

$$R(\lambda) = \frac{E_u(\lambda)}{E_d(\lambda)} = \frac{Q(\lambda)L_u(\lambda)}{E_d(\lambda)} \approx f(\lambda) \frac{b_b(\lambda)}{a(\lambda) + b_b(\lambda)}, \quad (2.1)$$

where $E_u(\lambda)$ and $E_d(\lambda)$ are the upwelling and downwelling spectral irradiances ($\text{W m}^{-2} \text{nm}^{-1}$), $L_u(\lambda)$ is the upwelling radiance ($\text{W m}^{-2} \text{nm}^{-1} \text{sr}^{-1}$), $Q(\lambda)$ is the ratio of the upwelling irradiance to the nadir upwelling radiance (sr), $f(\lambda)$ is a parameter that depends on the geometrical distribution of the light field (dimensionless), $a(\lambda)$ is the total absorption

coefficient (m^{-1}), and $b_b(\lambda)$ is the total backscattering coefficient (m^{-1}). It is important to note that while both $f(\lambda)$ and $Q(\lambda)$ vary primarily with changes in the local radiance distribution, they are also functions of the water constituents (e.g. Morel and Gentili, 1996).

Given two wavelengths, λ_1 and λ_2 , their radiance ratio can be expressed as

$$\frac{L_u(\lambda_1)}{L_u(\lambda_2)} = \frac{f(\lambda_1)b_b(\lambda_1)E_d(\lambda_1)}{Q(\lambda_1)(a(\lambda_1) + b_b(\lambda_1))} \cdot \frac{Q(\lambda_2)(a(\lambda_2) + b_b(\lambda_2))}{f(\lambda_2)b_b(\lambda_2)E_d(\lambda_2)}. \quad (2.2)$$

For consistency with previous work, and with no loss of generality, two specific wavelengths were chosen, 443 and 550 nm. Equation (2.2) can be further simplified if it is assumed that $b_b \ll a$ (Morel and Prieur, 1977; Gordon *et al.*, 1988):

$$\frac{L_u(443)}{L_u(550)} = \frac{f(443)/Q(443)}{f(550)/Q(550)} \cdot \frac{E_d(443)b_b(443)a(550)}{E_d(550)b_b(550)a(443)}. \quad (2.3)$$

This assumption will not be valid in highly turbid environments, which are outside the scope of this paper (but see Kirk, 1994a). The first two terms in (2.3) can be grouped, so that

$$\frac{f(443)/Q(443)}{f(550)/Q(550)} \cdot \frac{E_d(443)}{E_d(550)} = M. \quad (2.4)$$

The value of M can, in principle, be computed by assuming a spectral shape for $E_d(\lambda)$ and estimating the spectral dependence of $f(\lambda)/Q(\lambda)$. The spectral shape of $E_d(\lambda)$ can be measured easily, or computed using a clear sky model in which the inputs are atmospheric conditions, solar angle and surface albedo (Gregg and Carder, 1990). For a variety of parameters within the expected ranges for the experiments, several runs of the clear sky model by Gregg and Carder (1990) generated values of $E_d(443)/E_d(550)$ between 0.92 and 0.98, with a median value of 0.95. Both $f(\lambda)$ and $Q(\lambda)$ are functions of the geometrical distribution of radiance and of the IOPs, as mentioned before. However, for Case 1 waters with chlorophyll concentrations below 3 mg m^{-3} , Monte Carlo simulations (Morel and

Gentili, 1993) have shown that the relationship between $f(443)/Q(443)$ and $f(550)/Q(550)$ obeys a one-to-one ratio with an error of $\pm 3.5\%$. It will be assumed that this one-to-one ratio is valid in the parameterization described in this chapter, but increasing variability is expected as chlorophyll increases (Morel and Gentili, 1996). For simplicity, M will be initially considered to be equal to 0.95, representing an “expected” value of $E_d(443)/E_d(550)$, so that (2.3) becomes:

$$\frac{L_a(443)}{L_a(550)} = 0.95 \frac{b_b(443)a(550)}{b_b(550)a(443)}. \quad (2.5)$$

Throughout this chapter, 550 nm will be referred as to the green waveband, even when field data are for slightly different wavelengths (see Table 2.3). As will be shown later, both optical and biological data are in reality weighted by the various wavelength responses of the sensors, and in the green region gradients with respect to wavelength are small. Thus, at a first approximation, the differences among the instruments used and modeled relationships can be ignored.

2.2.2 Diffuse attenuation coefficient

The diffuse vertical attenuation coefficient, $K_d(\lambda)$, can be also described as a function of IOPs (e.g., Gordon *et al.*, 1975; Sathyendranath and Platt, 1988):

$$K_d(\lambda) = \frac{a(\lambda) + b_b(\lambda)}{\bar{\mu}_d(\lambda)}, \quad (2.6)$$

where $\bar{\mu}_d(\lambda)$ is the average cosine for downwelling irradiance, defined as the ratio of $E_d(\lambda)$ to $E_0(\lambda)$, the downwelling scalar irradiance. The value of $\bar{\mu}_d$ is influenced by the angular distribution of the incident radiance, changing with solar angle and with the proportions of diffuse to direct light (Bukata *et al.*, 1995). The average cosine is also a function of the ratio between the scattering and absorption coefficients (b/a) for a given solar angle (Kirk, 1994b and references therein); it will therefore change with different particle assemblages. Assuming fixed solar angles between vertically incident and 45° , and b/a ranging from 2

to 15 (coastal waters) in the visible, $\bar{\mu}_d$ varies from approximately 0.75 to 0.65 (Kirk, 1994b). Thus, a constant value of 0.7 will be assumed for $\bar{\mu}_d$. This assumption may not hold for waters with very small b/a (low particles and high CDOM concentration), but because this chapter refers mainly to coastal waters, this assumption will be considered valid for the situations analyzed in this chapter. In fact, for a time series of measurements collected in Bedford Basin (described below), the relationship between $K_d(\lambda)$ in the blue and green regions and total absorption coefficient (not shown) was linear ($r^2=0.79$) with a slope of 0.713 (± 0.035) consistent with the assumed value for $\bar{\mu}_d$.

2.3 Model structure and parameterization of IOPs

Equations (2.5) and (2.6) show that the IOPs necessary to reproduce the relationship between $K_d(490)$ and $L_u(443)/L_u(550)$ are the total absorption coefficients ($a(\lambda)$, m^{-1}) and the total backscattering coefficients ($b_b(\lambda)$, m^{-1}) at 443, 490 and 550 nm. The constituents that govern the variability in IOPs are generally divided into four groups (Kirk, 1994b): water (w), phytoplankton (ph), CDOM, and particles other than phytoplankton, hereafter referred to as detritus (det). In the following sections, the parameterization of these IOPs with trophic status will be described, representing each by the local concentration of chlorophyll plus pheopigments (C , $mg\ m^{-3}$). Pheopigments are assumed to be unimportant, as the analysis is focused on surface waters, where the lifetime of pheopigments is short (SooHoo and Kiefer, 1982). A schematic representation of the steps for the development of the model is presented in Figure 2.1.

2.3.1 Total absorption

IOPs are additive, so that, following the abbreviations described above:

$$a(\lambda) = a_w(\lambda) + a_{ph}(\lambda) + a_{cdom}(\lambda) + a_{det}(\lambda). \quad (2.7)$$

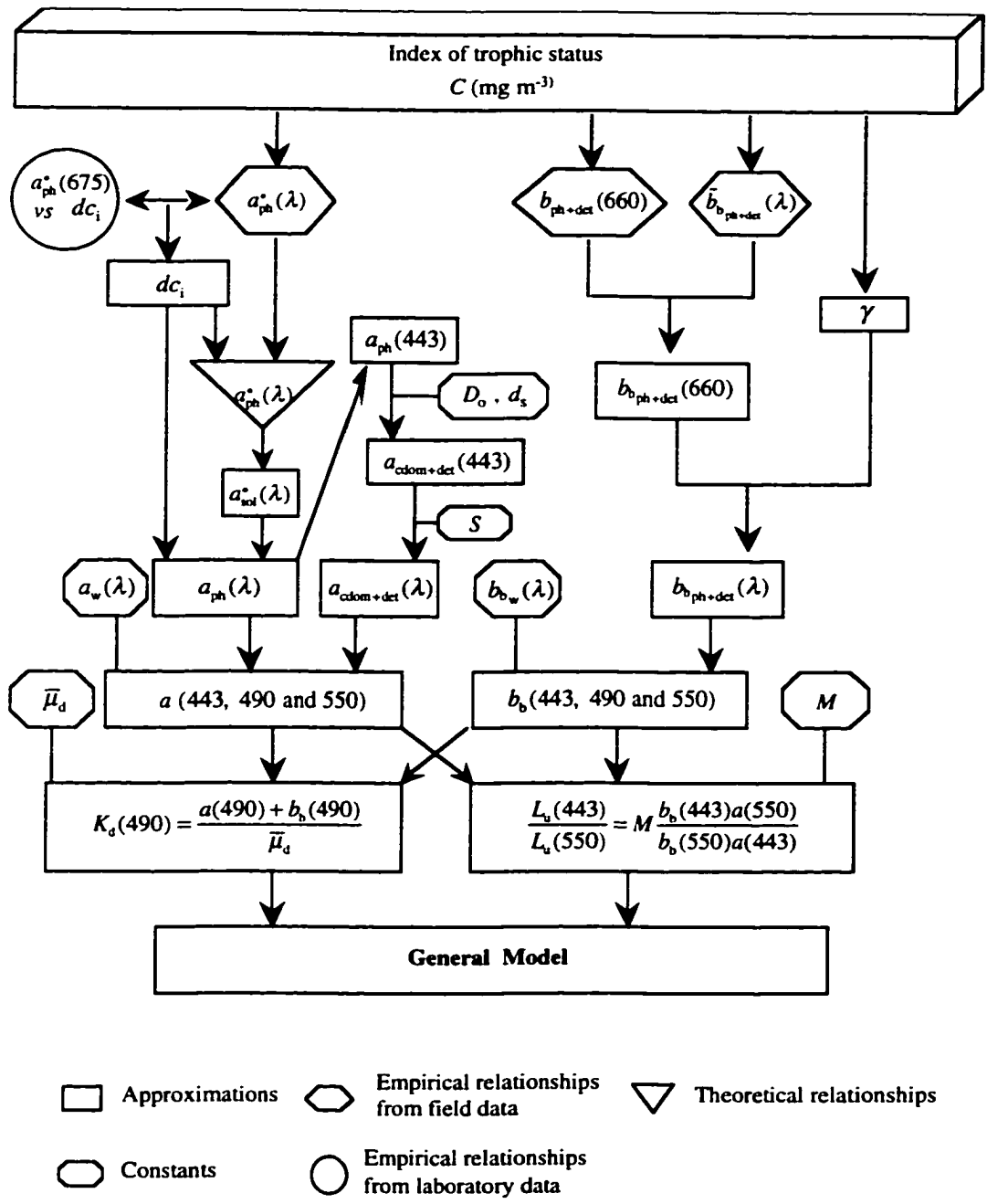


Figure 2.1 Parameterization of $K_d(490)$ and $L_u(443)/L_u(550)$ as functions of C (see Table 2.1 for symbols, and text for details). Absorption and backscatter, then attenuation and spectral reflectance, were predicted from C consistent with bio-optical relationships derived from theory (inverted triangle), laboratory studies (circle) and empirical relationships from the field (hexagons). Steps for deriving spectral absorption and spectral backscatter are described in the text.

The absorption coefficients for sea water are assumed to be constant and equal to those for pure water (Pope and Fry, 1997). The other components will be parameterized as a function of C , as described below.

2.3.1.1 Parameterization of phytoplankton absorption

Phytoplankton absorption is usually represented as

$$a_{\text{ph}}(\lambda) = C a_{\text{ph}}^*(\lambda), \quad (2.8)$$

where $a_{\text{ph}}^*(\lambda)$ ($\text{m}^2 \text{ mg Chl}^{-1}$) is the chlorophyll-specific absorption coefficient of phytoplankton. Changes in cell size and in the composition and degree of packaging of pigments influence $a_{\text{ph}}^*(\lambda)$ (Morel and Bricaud, 1981; Bricaud *et al.*, 1983; Sathyendranath *et al.*, 1987; Yentsch and Phinney, 1989; Babin *et al.*, 1993; Nelson and Robertson, 1993; Bricaud *et al.*, 1995; Sosik and Mitchell, 1995; Stuart *et al.*, 1998). Thus, $a_{\text{ph}}^*(\lambda)$ is not constant and has been parameterized as a function of C by assuming diverse forms for the relationship between $a_{\text{ph}}(\lambda)$ and C (see discussion in Lutz *et al.* (1996)).

When analyzed in the context of trophic status, changes in both spectral shape and amplitude of $a_{\text{ph}}^*(\lambda)$ are associated with changes in community structure. An extensive set of data is now available for $a_{\text{ph}}^*(\lambda)$ covering C from 0.02 to 25 mg m^{-3} (Bricaud *et al.*, 1995). The near-surface portion of this data was used (A. Bricaud pers. com., 1997) along with data collected off the Oregon coast (Ciotti *et al.*, 1996) and in a coastal embayment (Bedford Basin, N.S., Canada) to develop an approximation for packaging and pigment composition, each as a function of C . Only data from the first optical depth were used to minimize the effects of photoacclimation on $a_{\text{ph}}^*(\lambda)$ (Mitchell, 1992). These data correspond to particulate absorption, corrected for the absorption by detritus and normalized by the concentration of chlorophyll plus pheopigments. The optical depth (for

490 nm) was estimated from C following *Morel* (1988) when direct measurements of $K_d(490)$ were not available.

2.3.1.1.1 Packaging

The packaging effect (*Kirk*, 1994b) comes from the intracellular self-shading which lowers $a_{ph}^*(\lambda)$ and flattens the absorption spectra (*Duysens*, 1956). It is well known that $a_{ph}^*(\lambda)$ decreases as C increases as a result of increasing packaging (see *Bricaud et al.* (1995) and references therein), which is mainly controlled by the cell size, or diameter (d), and the intracellular concentration of pigments, c_i (*Bricaud and Morel*, 1986; *Sathyendranath et al.*, 1987). In what follows, approximation for the product of the diameter and the intracellular pigment concentration (dc_i) as a function of C will be developed. Ideally, dc_i should be parameterized versus C following first principles of physiological ecology and cell optics, using a characterization of changes in phytoplankton communities as C increases (cf. *Yentsch and Phinney*, 1989). In this chapter, the approach by *Yentsch and Phinney* (1989) was simplified by representing whole communities with an average dc_i that varies as a function of C . These average cells have the mean optical properties of the entire community (but see *Campbell* (1995) for a quantitative analysis of this assumption for phytoplankton absorption).

Once whole phytoplankton communities are characterized as average cells, their optical properties can be estimated within the framework of the anomalous diffraction approximation (*van de Hulst*, 1957) if it is assumed that these average cells are randomly distributed with respect to the light field, and that they behave as homogeneous spherical particles (*Morel and Bricaud*, 1986). The efficiency factor for absorption ($Q_a(\lambda)$; dimensionless) for a single phytoplankton cell, that is, the ratio of absorbed to impinged energy on the geometrical cross section of the cell, can be estimated as:

$$Q_a(\lambda) = 1 + \frac{2e^{(-\rho'(\lambda))}}{\rho'(\lambda)} + 2 \frac{e^{(-\rho'(\lambda))} - 1}{\rho'(\lambda)^2}, \quad (2.9)$$

where $\rho'(\lambda)$ is the dimensionless optical thickness of the particle. This is defined as the product of three quantities: the specific absorption coefficient of the cellular material as in solution ($a_{sol}^*(\lambda)$; $\text{m}^2 \text{mgChl}^{-1}$), the intracellular concentration of this material (c_i ; mg m^{-3}) and the cell diameter (d ; m), i.e.,

$$\rho'(\lambda) = a_{sol}^*(\lambda)dc_i. \quad (2.10)$$

Note that the only quantity that varies spectrally in (2.10) is $a_{sol}^*(\lambda)$.

This theoretical absorption efficiency can now be related to the variability in $a_{ph}^*(\lambda)$ observed in the field. To isolate the effect of the packaging (expressed as dc_i) on $a_{ph}^*(\lambda)$ from the effect of accessory pigments (hereafter referred to as “pigment composition”), one can look at a wavelength where the absorption by accessory pigments is not important. At 675 nm, phytoplankton absorption is due almost exclusively to chlorophyll *a* (Bidigare *et al.*, 1990) so a constant value for $a_{sol}^*(675)$, independent of pigment composition, can be assumed.

A coefficient representing the degree of pigment packaging is determined as follows:

$$Q_a^*(\lambda) = \frac{a_{ph}^*(\lambda)}{a_{sol}^*(\lambda)} = \frac{3}{2} \cdot \frac{Q_a(\lambda)}{a_{sol}^*(\lambda)dc_i}, \quad (2.11)$$

where the ratio 3/2 is the geometrical factor for a sphere (see Morel, 1994). Equations (2.9) and (2.10) are used to obtain $Q_a(\lambda)$ for calculating $Q_a^*(675)$ from $a_{sol}^*(675)$ and dc_i (i.e., $\rho'(675)$). The computation can be, however, greatly simplified. Solving the theoretical equation (2.11) for a range of $\rho'(675)$ normally found in phytoplankton (0.005 to around 6; (Agusti, 1991)) and fitting the results to an exponential function, $Q_a^*(675)$ can be described almost exactly ($n=1200$; $R^2=0.999$) with the function $Q_a^*(675) = m_1 + m_2 \cdot (\exp(-m_3 \cdot \rho'(675)))$, where m_i are coefficients.

Because $a_{sol}^*(675)$ is assumed constant in equation (2.11), the same functional form should describe the relationship between $a_{ph}^*(675)$ and dc_i . For a wide range of

phytoplankton species grown in laboratory using diverse culturing methods (Figure 2.2A), the relationship is

$$a_{\text{ph}}^*(675) = 0.00767 + 0.0227e^{(-0.0376dc_i)} \quad (2.12)$$

Thus, equation (2.12) is an approximation to the theory. This same exponential form was applied to derive a purely empirical expression for $a_{\text{ph}}^*(675)$ as a function of C (Figure 2.2B), using a compilation of phytoplankton absorption data collected in this study (i.e. particulate corrected for detrital absorption) and the data from *Bricaud et al.* (1995)

$$a_{\text{ph}}^*(675) = 0.0110 + 0.0158e^{(-0.311C)} \quad (2.13)$$

The relationship between dc_i and C was obtained by solving equations (2.12) and (2.13) for dc_i (Figure 2.2C):

$$dc_i = -26.59 \ln(0.147 + 0.696e^{(-0.311C)}) \quad (2.14)$$

The result, at a given C , is dc_i for an average cell that represents the entire phytoplankton community. It is important to stress that equation (2.14) is at best an approximation of the central tendency of both field and laboratory data sets used here. Thus, combining equations (2.9), (2.10) and (2.11):

$$a_{\text{ph}}^*(\lambda) = \frac{3}{2dc_i} \left(1 + \frac{2e^{-a_{\text{sol}}^*(\lambda)dc_i}}{a_{\text{sol}}^*(\lambda)dc_i} + \frac{2(e^{-a_{\text{sol}}^*(\lambda)dc_i} - 1)}{(a_{\text{sol}}^*(\lambda)dc_i)^2} \right) \quad (2.15)$$

The goal in generating this approximation was to allow the parameterization of phytoplankton absorption with two terms: one dominated by packaging and one dominated by changes in accessory pigments so that different types of communities could be tested in the sensitivity analysis. Although the compiled data were extensive, the use of this equation is limited to the assumptions that were made, the data set used, and to the models chosen for the curve fits. Error bars in Figure 2.2C represent two standard

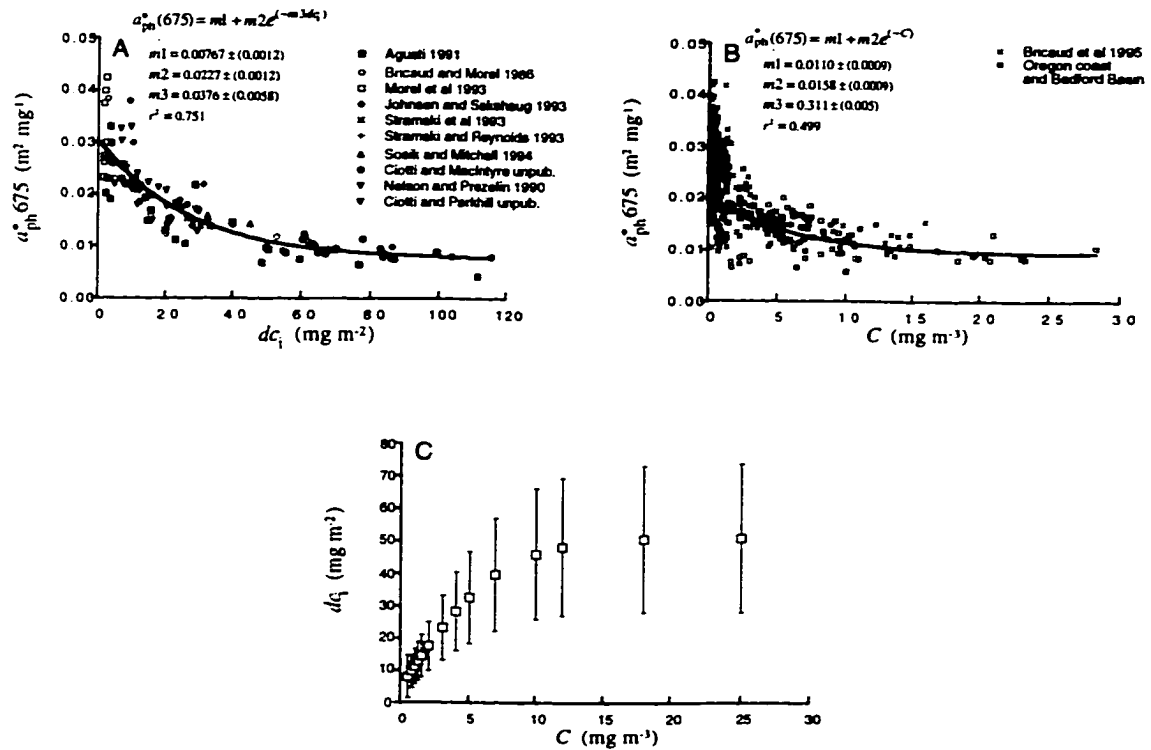


Figure 2.2 Steps for estimating the product of the cell diameter and the intracellular pigment concentration (dc_i) as a function of trophic status. **A**) Empirical relationship between $a_{ph}^*(675)$ and the product of cell diameter (d) and the intracellular concentration of pigments (c_i) for published data from cultures (references on legend). Ciotti and MacIntyre (unpub.) refers to the toxic dinoflagellate *Alexandrium tamarense* grown in K media in semi-continuous culture (see MacIntyre et al. (1997) for detail), and Ciotti and Parkhill (unpub.) refers to the coastal diatom *Thalassiosira pseudonana* in continuous culture. Table in the figure indicates equation form, parameter values and respective standard deviations, and r^2 . **B**) Empirical relationship between $a_{ph}^*(675)$ and C . Table indicates equation form, parameter values and respective standard deviations, and r^2 . **C**) Approximation for a relationship between the product dc_i and C . Error bars indicate 2 standard deviations.

deviations, computed using the Delta method, an approximation to a Taylor series (Bishop *et al.*, 1975). In this method, the variance is computed as the product of a matrix containing the variance and covariance terms of each fit and a vector containing the first derivatives of equation (2.14) evaluated at each C with respect to each of the six fitted parameters.

2.3.1.1.2 Pigment composition

At wavelengths other than 675 nm, the absorption by accessory pigments cannot be neglected. The spectral dependence of a_{sol}^* for the main accessory pigments of phytoplankton, as well as for chlorophyll a , has been described (Bidigare *et al.*, 1990; Hoepffner and Sathyendranath, 1991; Johnsen *et al.*, 1994b). However, the ratio of accessory pigments to chlorophyll a is expected to change with trophic status (Claustre, 1994), thus modifying $a_{\text{sol}}^*(\lambda)$. Briefly, as the trophic status changes from eutrophic to oligotrophic (i.e., as C decreases), the mass ratio of accessory pigments to chlorophyll a increases (Gieskes *et al.*, 1988; Claustre, 1994), and in turn $a_{\text{sol}}^*(\lambda)$ will increase in the blue-green portion of the spectrum.

Because the form by which $a_{\text{sol}}^*(\lambda)$ changes as a function of C is not known *a priori*, five steps were followed to derive an approximation (see also Figure 2.1):

- a) Empirical relationships between $a_{\text{ph}}^*(\lambda)$ and C for seven wavebands were derived using compiled data from the field, with C ranging from 0.03 to 32 mg m⁻³ (Table 2.1). The data for each waveband were averaged to be consistent with the spectral response of the SeaWiFS ocean color satellite and with the optical instruments used in this data set, which were designed to match SeaWiFS (Cullen *et al.*, 1994).
- b) For each of the seven wavebands, $a_{\text{ph}}^*(\lambda)$ was computed at 17 values of C (from 0.5 to 50 mg m⁻³) using the empirical relationships derived in (a).
- c) For the same 17 values of C , dc_i was calculated with equation (2.14).
- d) For each waveband and value of C , dc_i was substituted into equation (2.15) and (2.15) and $a_{\text{ph}}^*(\lambda)$ from (b).

e) The final relationships between $a_{\text{sol}}^*(\lambda)$ and C were generated by least-squares techniques (Figure 2.3, see equation form, parameters and r^2 in Table 2.2). These curves represent the “residual” variation of $a_{\text{ph}}^*(\lambda)$ versus C , after taking empirically determined changes in packaging into account.

It is important to stress once more that these equations are approximations valid only for the range of C used (i.e., 0.5 to 30 mg m⁻³).

2.3.1.2 Parameterization of CDOM and detrital absorption

Within the visible range (400 to 700 nm), CDOM absorption can be parameterized as

$$a_{\text{cdom}}(\lambda) = a_{\text{cdom}}(\lambda_0)e^{[S(\lambda-\lambda_0)]}, \quad (2.16)$$

where S (nm⁻¹) is the slope of the exponential decrease with wavelength and $a_{\text{cdom}}(\lambda_0)$ is the absorption coefficient for CDOM at one reference wavelength, usually between 400 and 440 nm (Bricaud *et al.*, 1981). The slope S generally varies from -0.017 to -0.0115 nm⁻¹ (Carder *et al.*, 1989; but see Green and Blough, 1994) with a mean of -0.015 nm⁻¹ for a variety of waters. Absorption by “detritus,” follows the same spectral shape as CDOM absorption from 400 to 600 nm (Bukata *et al.*, 1995) with comparatively smaller slopes (Roesler *et al.*, 1989). Because the blue and green regions of the spectrum are the main focuses, in the general model, both absorption coefficients will be combined in a single term, $a_{\text{cdom+det}}(\lambda)$ (see Roesler and Perry, 1995).

Different environments will have different sources of the detritus and CDOM (e.g., rivers versus autochthonous production), so a simple parameterization of $a_{\text{cdom+det}}(\lambda)$ with C is difficult. Nevertheless, an assumed linear relationship between detritus and phytoplankton absorption can explain particular situations (see Eppley *et al.*, 1977). Although the linear relationships presented by Eppley *et al.* (1977) were derived for phytoplankton and detrital carbon only, it will be assumed that the same type of relationship can be expected between phytoplankton absorption and a term combining

Table 2.1 Parameters and correlation coefficient (r^2) values for the empirical relationships generated from the field data set of $a_{ph}^*(\lambda)$ and C . Phytoplankton absorption spectra were averaged, consistent with the spectral response of the SeaWiFS ocean color sensor (about 20 nm wavebands centered on the wavelength designated). The data are a compilation of spectra with 2-nm resolution (Bricaud *et al.*, 1995) and the phytoplankton absorption data (1-nm resolution) collected off the Oregon coast (Ciotti *et al.*, 1996) and in a coastal embayment (Bedford Basin, N.S., Canada). C is chlorophyll a plus pheopigment concentration. The parameter values designated *ns* means not significant; *na* means not available; *sd* are the standard deviations for each parameter.

$$a_{ph}^*(\lambda) = m_1 + m_2e^{(-m_3C)} + m_4e^{(-m_5C)}$$

Parameter	Wavelength (nm)					
	412	443	490	510	555	670
m1	0.012	0.013	0.010	0.008	0.004	0.008
sd m1	0.002	0.003	0.002	0.002	0.001	0.001
m2	0.039	0.076	0.050	0.015	0.005	0.011
sd m2	0.004	0.004	0.003	0.002	0.001	0.001
m3	3.123	2.987	2.984	0.202	0.132	0.256
sd m3	0.555	0.033	0.377	0.067	0.041	0.045
m4	0.018	0.026	0.020	0.027	ns	ns
sd m4	0.003	0.004	0.003	0.002	na	na
m5	0.308	0.214	0.232	2.979	ns	ns
sd m5	0.122	0.080	0.081	0.478	na	na
r^2	0.745	0.824	0.810	0.749	0.260	0.446

Table 2.2 Parameters and r^2 values for the relationships generated for $a_{\text{sol}}^*(\lambda)$ and C . This value was used in combination with equations (2.14) and (2.15) to solve for $a_{\text{sol}}^*(\lambda)$ for each C . The parameter values in the table describe the best fit for $a_{\text{sol}}^*(\lambda)$ and C . Standard deviations (sd) for each parameter are indicated.

$$a_{\text{sol}}^*(\lambda) = m1C^{-m2}$$

Parameter	Wavelength (nm)					
	412	443	490	510	555	670
m1	0.0300	0.0460	0.0329	0.0245	0.0070	0.0178
sd m1	0.0007	0.0004	0.0005	0.0003	0.0001	0.0003
m2	0.2007	0.2525	0.2996	0.2781	0.0070	0.0178
sd m2	0.0149	0.0068	0.0115	0.0083	0.0069	0.0087
r^2	0.937	0.990	0.982	0.989	0.953	0.965

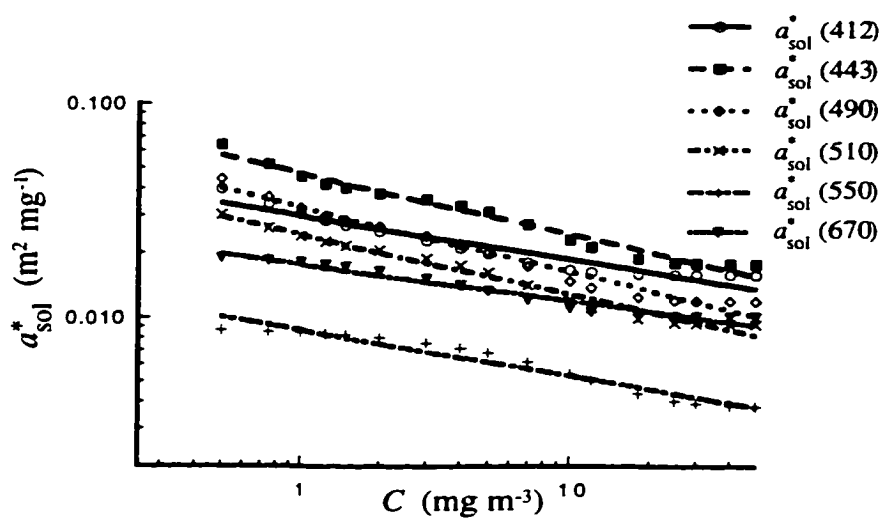


Figure 2.3 Best fit for derived values of a_{sol}^* versus C at the SeaWiFS wavebands. See Table 2.2 for equation form, parameter values and respective standard deviations, and r^2 .

detrital and CDOM absorption. The slope of this line represents the fraction that is directly associated or covaries with phytoplankton; the intercept represents a background value. Using 443 nm as a reference wavelength, $a_{\text{cdom+det}}(\lambda)$ is expressed as follows:

$$a_{\text{cdom+det}}(443) = D_o + d_s a_{\text{ph}}(443), \quad (2.17)$$

where D_o (m^{-1}) represents a background absorption that is not correlated with $a_{\text{ph}}(443)$, and d_s (dimensionless) is the slope of a linear relationship between $a_{\text{ph}}(443)$ and $a_{\text{cdom+det}}(\lambda)$. This type of relationship was observed in the data collected off the Oregon coast, however it may not hold in environments in which CDOM and/or detrital inputs and pools are highly variable. Once $a_{\text{cdom+de}}(443)$ is computed, the other wavelengths are estimated with equation (2.16) by assuming a value for S .

2.3.2 Total backscattering

Because backscattering by CDOM can be neglected (Mobley, 1994), the total backscattering coefficient can be partitioned into three components :

$$b_b(\lambda) = b_{b_w}(\lambda) + b_{b_{\text{det}}}(\lambda) + b_{b_{\text{ph}}}(\lambda). \quad (2.18)$$

Backscattering by sea water is assumed to be constant and the particulate components ($b_{b_i}(\lambda)$, m^{-1}) can be parameterized as follows (Gordon *et al.*, 1988; Sathyendranath and Platt, 1988):

$$b_{b_i}(\lambda) = \tilde{b}_{b_i}(\lambda) b_i(\lambda), \quad (2.19)$$

where $b_i(\lambda)$ is the scattering coefficient by each component (i) and $\tilde{b}_{b_i}(\lambda)$ (dimensionless) is the correspondent backscattering ratio, which is a function of the particle size and the real and imaginary parts of the refractive index (Morel and Bricaud, 1986).

The contribution of phytoplankton to the total backscattering coefficient is very small (Stramski and Kiefer, 1991 and references therein) because phytoplankton are generally large compared to the visible wavelengths and their relative index is similar to

that of sea water. Their backscattering ratios ($\tilde{b}_{b_{\text{ph+det}}}(\lambda)$) vary from around 0.0001 to 0.004 (Morel and Bricaud, 1981). The source of most of the backscattering in the ocean is unknown, and has been attributed to submicron inorganic particles and heterotrophic bacteria (Morel and Ahn, 1991; Stramski and Kiefer, 1991; Ulloa *et al.*, 1994) and more recently to bubbles (Stramski, 1994; Zhang *et al.*, 1998). Because of that, empirical relationships between backscattering and C account for backscattering of the whole particle assemblage (which in the terminology of this chapter would be $b_{b_{\text{ph+det}}}$) (Gordon *et al.*, 1983; Gordon *et al.*, 1988; Morel, 1988; Ulloa *et al.*, 1994). Thus,

$$b_b(\lambda) = b_{b_w}(\lambda) + \tilde{b}_{b_{\text{ph+det}}}(\lambda)b_{\text{ph+det}}(\lambda). \quad (2.20)$$

The parameterization of scattering and backscattering ratio by particles will be presented, accounting for the influence of particle assemblages on the backscattering coefficient, and the spectral shape of backscatter. It is stressed that all these relationships with C are purely empirical and, because of the low contribution of phytoplankton to the bulk backscattering, they likely reflect the relationship of backscattering to factors that covary with phytoplankton changes, rather than the direct influence of phytoplankton.

2.3.2.1 Scattering by particles

Empirical relationships between $b_{\text{ph+det}}(\lambda)$ and C are derived from measurements made predominantly in blue waters at a single wavelength, using data from transmissometers (i.e., at 660 nm) after correction for absorption by water. The most widely used relationship is the one proposed by Morel (1988), recently revisited by Loisel and Morel (1998). The new analyses were partitioned into upper (mixed) and deep layers, and new data were included, expanding the range of C previously published. The mixed-layer equation presented by Loisel and Morel (1998) showed a good agreement with the transmissometer data (after correcting for water and particulate absorption at 660 nm) and

with chlorophyll data collected during the Oregon cruise and during a Spring Bloom experiment in Bedford Basin in 1993; thus, it will be used to parameterize $b_{\text{ph+det}}(660)$.

$$b_{\text{ph+det}}(660) = 0.347C^{0.766}. \quad (2.21)$$

2.3.2.2 Backscattering ratio

Existing relationships for $\tilde{b}_{\text{b}_{\text{ph+det}}}(\lambda)$ as a function of C (Gordon *et al.*, 1988; Morel, 1988) were established from estimated values which accounted for the expected decrease in $\tilde{b}_{\text{b}_{\text{ph+det}}}(\lambda)$ as C increases, due to the increasing contribution of larger particles with low backscattering efficiency (Morel and Bricaud, 1981). Implicit in the selection of a particular $\tilde{b}_{\text{b}_{\text{ph+det}}}(\lambda)$, however, is an assumed size distribution for the whole particle assemblage. Ulloa *et al.* (1994) using Mie computations, showed that if the size distribution of particles with the same refractive index is modeled as a power-law (or a Junge-type distribution), $\tilde{b}_{\text{b}_{\text{ph+det}}}(\lambda)$ is independent of wavelength, and its magnitude depends strongly on the exponent which describes the slope of the size distribution: waters with a more negative exponent (i.e., smaller sizes are more important) will have a higher $\tilde{b}_{\text{b}_{\text{ph+det}}}(\lambda)$. Using inverse modeling of observed reflectance spectra, they derived an expression of $\tilde{b}_{\text{b}_{\text{ph+det}}}(\lambda)$ versus C consistent with empirical relationships presented by Gordon (1988) and Morel (1988). Thus, it is assumed that $\tilde{b}_{\text{b}_{\text{ph+det}}}(\lambda)$ is independent of wavelength and dependent on C following (Gordon *et al.*, 1988):

$$\tilde{b}_{\text{b}_{\text{ph+det}}}(\lambda) = 0.013481 - 0.00651 \log_{10}(C). \quad (2.22)$$

2.3.2.3 Wavelength dependence of backscattering

Given that $\tilde{b}_{\text{b}_{\text{ph+det}}}(\lambda)$ is assumed to be wavelength-independent, the spectral shape of particle backscattering will follow that of the particle scattering coefficient. Aiken *et al.* (1995) assumed that the wavelength dependence of $b_{\text{ph+det}}(\lambda)$ was approximately λ^{-1} . It has been shown, however, that from oligotrophic to eutrophic waters, the spectral dependence

of particle scattering changes. In oligotrophic waters, the total scattering coefficient has been shown to follow both λ^{-2} (Sathyendranath *et al.*, 1989) and λ^{-1} (Gordon *et al.*, 1988; Mobley, 1994), consistent with the dominance of small particles. In eutrophic environments, the total scattering has been shown not to vary much with wavelength (Gordon *et al.*, 1988; Morel, 1988), related to the addition of bigger particles with flatter scattering spectra. To account for this change with trophic status, it will be assumed that the scattering coefficient follows λ^{-2} when C is low ($0.05 \text{ mg}\cdot\text{m}^{-3}$) and λ^0 when C is high ($20 \text{ mg}\cdot\text{m}^{-3}$) and that the exponent decreases logarithmically with C (Gordon *et al.*, 1988). Accordingly,

$$b_b(\lambda) = b_{b_w}(\lambda) + \tilde{b}_{b_{ph+det}} b_{b_{ph+det}} \left(\frac{660}{\lambda}\right)^\gamma, \quad (2.23)$$

where γ decreases from 2 to 0 following a logarithmic function of C :

$$\gamma = 1 - 0.768 \log_{10}(C). \quad (2.24)$$

2.4 Implementation of the semi-analytical model

Given the parameterizations above, both $K_d(490)$ and $L_u(443)/L_u(550)$ can now be calculated as functions of trophic status. The approach is summarized in Figure 2.1, and the equations are given in section 3. $K_d(490)$ is given by:

$$K_d(490)_k = \frac{a_{ph}(490)_k + e^{(-47.5)}(D_o + d_s a_{ph}(443)_k) + a_w(490)}{\bar{\mu}_d}, \quad (2.25)$$

and $L_u(443)/L_u(550)$ is given by:

$$\left(\frac{L_u(443)}{L_u(550)}\right)_k = 0.95 \left[\frac{(b_{b_w}(443) + b_{b_{ph+det}}(660)_k 1.49^{\gamma_k})}{(b_{b_w}(550) + b_{b_{ph+det}}(660)_k 1.2^{\gamma_k})} \times \frac{(a_{ph}(550)_k + e^{(-107.5)}(D_o + d_s a_{ph}(443)_k) + a_w(550))}{D_o + a_{ph}(443)_k(1 + d_s) + a_w(443)} \right], \quad (2.26)$$

where γ designates the spectral dependence of the particle scattering and k represents the evaluation of each term for a given C value. In these equations:

$$\bar{\mu}_d = 0.7 \text{ (see section 2.2);}$$

$$S = -0.015 \text{ (nm}^{-1}\text{, see section 3.1.2);}$$

$$D_o = 0.02 \text{ (m}^{-1}\text{, simulating an oligotrophic } a_{\text{cdom+det}} \text{ background (Kirk, 1994b);}$$

$$d_s = 0.3 \text{ (following Bricaud and Stramski (1990));}$$

Assuming that this general model has the same form as empirically derived relationships (Austin and Petzold, 1981; Aarup *et al.*, 1996; Mueller and Trees, 1997):

$$\ln(K_d(490) - K_{d_w}(490)) = A_0 + A_1 \ln(L_u(443) / L_u(550)), \quad (2.27)$$

where $K_{d_w}(490)$ is the attenuation coefficient of pure water at 490 nm. The parameters A_0 and A_1 can be estimated statistically for predictive purposes given solutions of equations (2.25) and (2.26) over a range of C . For different environments and/or different assumptions, the parameters and relationships with C are expected to differ, as will be shown later. Nevertheless, the basic principles will hold and new relationships can be derived accordingly. Hereafter, this general model will be referred to as the Semi-analytical Model of Ocean Color and Attenuation as a Function of Trophic Status (SAMOCAFOTS). The model predicts absorption and backscatter in the ocean, and hence attenuation and spectral reflectance, as a function of surface chlorophyll, consistent with well described bio-optical relationships derived from theory, laboratory research and measurements in the field. Therefore, it reconciles a broad range of known relationships between phytoplankton community structure, optical properties of surface waters, and trophic status of surface waters.

It is acknowledged that modeling optical properties as functions of chlorophyll concentration can introduce many limitations, mainly regarding the imprecise relationship between chlorophyll and phytoplankton biomass (Cullen, 1982). Nonetheless, chlorophyll is the single most evident descriptor of phytoplankton abundance, and understanding how different communities influence optical properties is an important starting point to a better

interpretation of bio-optical models. The results of the sensitivity analysis (see below) reveal how different communities influence optical properties at a given chlorophyll concentration.

The validation of the semi-analytical model is done through comparisons with empirical relationships between diffuse attenuation at 490 nm, $K_d(490)$, and ratios of upwelling radiance of 443 to 550 nm, $L_u(443)/L_u(550)$. These particular wavelengths were selected due to the availability of several empirical relationships (e.g., Austin and Petzold, 1981; Aarup *et al.*, 1996; Mueller and Trees, 1997) and a large independent data set. By adjusting a few parameters (see below), the model can easily include other wavelengths.

2.5 Bio-optical field data

Bio-optical data at the surface were collected during a number of cruises (Table 2.3). For sampling details during the Bedford Basin Summer experiments (BBS92 and 93) and the cruise off Oregon (ORE94) refer to Cullen *et al.* (1994) and Ciotti *et al.* (1996), respectively. Chlorophyll (fluorometric) as well as particulate (filter pad method) and dissolved absorption were measured as described by Ciotti *et al.* (1996). Data from the 1996 time series in Bedford Basin (BBTS96) were collected every 10 minutes with a Tethered Attenuation Coefficient Chain Sensor (TACCS), which was moored in Bedford Basin from July to November. This instrument is a radiometer buoy measuring spectral upwelling radiance ($L_u(\lambda)$, $\mu\text{W cm}^{-2} \text{ nm}^{-1} \text{ sr}^{-1}$) in 7 wavebands at a depth of 0.45 m, and a chain containing four $E_d(490)$ sensors, positioned at 2, 4, 8 and 16 m, with another 30 cm above the surface. Surface (upper 2 m) $K_d(490)$ was computed using estimated $E_d(490)$ just below the surface (i.e. $E_d(490)$ in the air corrected for Fresnel reflectance (see Mobley, 1994) assuming wind speed equal to zero) and the $E_d(490)$ sensor from 2 meters. Because $L_u(\lambda)$ sensors are located at a depth of 0.45 m, $L_u(443)$ and $L_u(550)$ were propagated to just below the surface using the empirically determined spectral model of Austin and Petzold (1986) for $K_d(\lambda)$ as a function of $K_d(490)$. Independent $K_d(\lambda)$ data were obtained throughout the experiment confirming the appropriateness of this model for Bedford Basin

Table 2.3 List of cruises with respective location, dates and optical measurements at the surface.

Cruise	Location	Dates	Optical properties measured near-surface
ORE94	off the Oregon coast	September 1994	$L_u(443)$, $L_u(555)$, $K_d(490)$
WE97	Bering Sea	April 1997	$L_u(443)$, $L_u(555)$, $K_d(490)$
BBS92	Bedford Basin	August 1992	$L_u(443)$, $L_u(555)$, $K_d(490)$
BBS93	Bedford Basin during a red tide	August 1993	$L_u(443)$, $L_u(555)$, $K_d(490)$
BBTS96	Bedford Basin	June to November 1996	$L_u(443)$, $L_u(559)$, $K_d(490)$

during the study period.

During the WE97 cruise (Table 2.3), a radiometer buoy measuring radiance reflectance ($L_u(\lambda)$ and $E_d(\lambda)$ in 13 wavebands) and a profiling radiometer measuring $E_i(\lambda)$ in the same wavebands were used. Sampling design and data processing were similar to those used during the ORE94 cruise, but because the radiance sensors were very close to the surface, $L_u(\lambda)$ was not corrected for attenuation.

2.6 Results and Discussion

2.6.1 Model versus established empirical relationships

In this section, the parameterization of $K_d(490)$ and $L_u(490)/L_u(550)$ are compared with established empirical relationships.

2.6.1.1 Diffuse attenuation versus C

For $K_d(490)$ as a function of C , the relationship described by Morel (1988) was used (Figure 2.4A). The parameterization of $K_d(490)$, which is based on data from laboratory and field, agreed to within 20% of the empirical relationship based on direct measurements, varying from overestimating by 20% at 0.5 mg m^{-3} to underestimating by 15% at 10 mg m^{-3} ; above 10 mg m^{-3} , the model values remained 15% less than the empirical relationship. These results suggest some small inconsistencies in the parameterization of absorption by phytoplankton and/or by detritus plus CDOM. Although the visual comparison of model and empirical data in Figure 2.4A makes it tempting to infer that the parameterization underestimates total absorption (see equation (2.6)), the disagreement could also be a result of the form of the equation chosen to represent the field data, and also from keeping a constant value for the average cosine (see section 2.2). Nonetheless, considering all the assumptions made and the variability in the field data, the agreement is good: the semi-analytical expressions for IOPs, derived from basic bio-optical principles and relationships, reproduced well a statistically-derived relationship

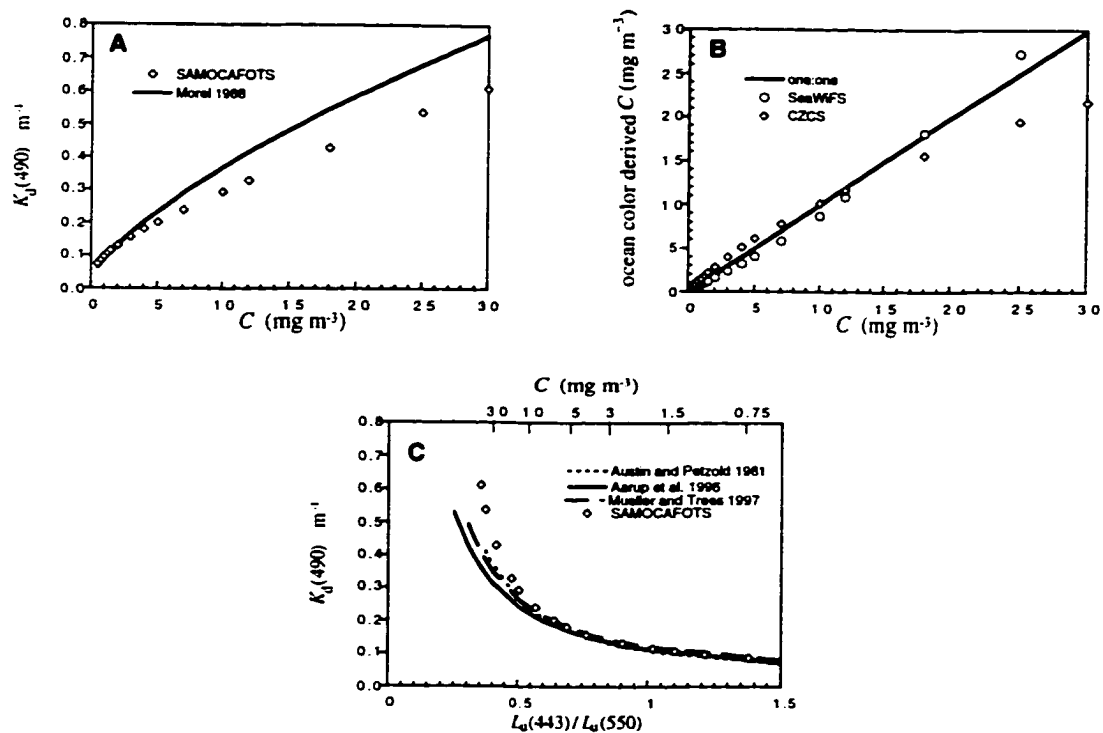


Figure 2.4 Comparison between empirical models and the parameterization of SAMOCAFOTS. **A)** Attenuation coefficient at 490 nm versus the empirical model by Morel (Morel, 1988). **B)** Radiance ratio of 490 to 550 nm ($L_u(490)/L_u(550)$) which was calculated as in equation (2.26) with the relevant parameters modified from 443 to 490 nm (see text). Comparison with the CZCS algorithm for $C > 1 \text{ mg m}^{-3}$ (see Lewis and Cullen, 1991), and the more recent SeaWiFS algorithm (O'Reilly *et al.*, 1998). **C)** SAMOCAFOTS and empirical models relating $K_d(490)$ to $L_u(443)/L_u(550)$ derived by Austin and Petzold (1981), Aarup *et al.* (1996) and Mueller and Trees (1997). Note that empirical models were not extrapolated beyond the upper limit of $K_d(490)$ measured in each case.

between AOPs.

2.6.1.2 Retrieval of C from ocean color

The comparison between the parameterization of reflectance ratios and empirical data was done for relationships between C and $L_u(490)/L_u(550)$, computed as in equation (2.26) and modifying relevant parameters from 443 to 490 nm. In coastal waters, 490 nm has been shown to work better than 443 nm (e.g., Aiken *et al.* (1995) and references therein) and the new global algorithms for retrieving C from ocean color are now based on $L_u(490)/L_u(550)$. For a range of C , the general model was used to compute $L_u(490)/L_u(550)$, which could be related to remotely sensed C (RSC) using published algorithms (Figure 2.4B). Two empirical RSC models were used: the CZCS algorithm for $RSC > 1 \text{ mg m}^{-3}$ (see Lewis and Cullen (1991), but note that the original algorithm was established for 500 and 560 nm) and the more recent SeaWiFS algorithm (O'Reilly *et al.*, 1998). Both empirical algorithms were derived with a very limited number of data points at high C , so comparisons at high C are meaningless. This analysis (Figure 2.4B) resulted in a good agreement (within 20%) between C used to compute $L_u(490)/L_u(550)$ and the retrieved RSC (inversion of $L_u(490)/L_u(550)$) using the SeaWiFS algorithm for C from 0.5 to 30 mg m^{-3} . Using the CZCS algorithm to retrieve RSC, the agreement was lower overall, and the retrieved C agreed within 20% only with input C from 5 to 18 mg m^{-3} . These comparisons also demonstrate how the semi-analytical expressions for IOPs derived from basic bio-optical principles can reconcile relationships between AOPs and C .

2.6.1.3 Diffuse attenuation versus radiance ratio

Empirical models relating $K_d(490)$ to $L_u(490)/L_u(550)$ (Austin and Petzold, 1981; Aarup *et al.*, 1996; Mueller and Trees, 1997) and the results derived by SAMOCAFOTS are shown in Figure 2.4C. The agreement between the model and the empirical relationships, and the agreement among the empirical relationships, is good for C up to 10 mg m^{-3} . Divergence among the different empirical models is noticeable in green waters

($L_u(443)/L_u(550) < 0.5$), reflecting the bio-optical differences among data sets, differences in sample size, and the ranges of $K_d(490)$ and $L_u(443)/L_u(550)$ included in each. SAMOCAFOTS also diverges from the empirical relationships when $L_u(443)/L_u(550) < 0.5$, that is, $C > 12 \text{ mg m}^{-3}$ with more influence of CDOM (see below). However, the fact that a good agreement was possible without adjusting any of the parameters suggests that the simplifications and assumptions made in deriving the semi-analytical model are valid at least for C between 0.5 and about 15 mg m^{-3} .

2.6.2 Model versus independent bio-optical data

The semi-analytical model can now be compared with independent optical measurements of $L_u(443)/L_u(550)$ and $K_d(490)$ (Figure 2.5). For $L_u(443)/L_u(550)$ from 0.5 to about 1.5, the general model explained most (above 90%) of the variability in $K_d(490)$ found in the field data. Note that the data from the Bering Sea cruise in 1997 tended to remain below the line defined by the general model. For radiance ratios below 0.5, however, it is clear that no single relationship can explain the dispersion of the data, especially those derived from Bedford Basin. These data suggest that a family of curves can be derived and show also a group of outliers associated with a red tide event during BBS93 (Cullen *et al.*, 1994).

The most obvious differences among the data collected in Bedford Basin and the other data sets are related to the higher influence of CDOM and detritus in Bedford Basin. From absorption data collected weekly in Bedford Basin in 1996 (Figure 2.6; data from the Oregon cruise is plotted for comparison) it can be observed that the parameters describing CDOM plus detrital absorption (D_o and d_s) differed from the original parameterization, although the slope, S , was in average close to -0.015. Thus, to encompass more properly the range of conditions in Bedford Basin, a second curve was constructed by using the same parameter values as in SAMOCAFOTS, except that D_o and d_s were set to 0.4 m^{-1} and 0.4 , respectively. The C range was also extended to 50 mg m^{-3} . Hereafter this relationship will be referred to as SAMOCAFOTS high CDOM.

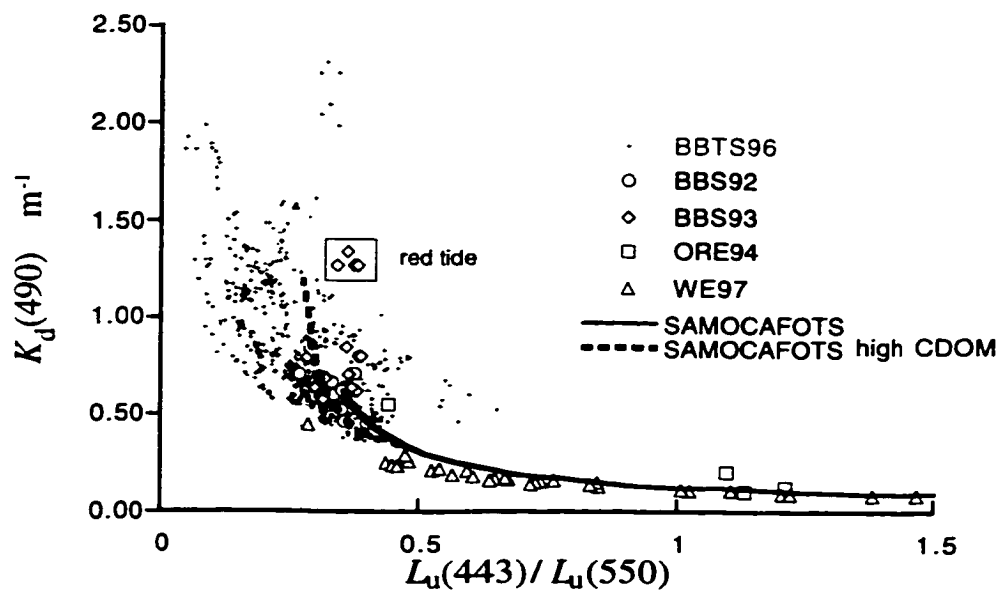


Figure 2.5 Comparison of SAMOCAFOTS with independent data collected in a variety of coastal waters: off the Oregon coast in September 1994 (ORE94, see Ciotti *et al.* (1996)), in the Bering Sea in June of 1997 (WE97), and in Bedford Basin on several occasions: Summer of 1992 (BBS92), Summer of 1993 (BBS93) during a red tide event (in box), and also a time series from June to November of 1996 (BBTS96). Plot shows data from BBTS96 collected daily between 11:00 and 13:00 local time. Note that the radiance ratios measured during ORE94, BBS92 and BBS93 were between 443 and 555 nm and during BBTS96 were between 443 and 559 nm.

Although SAMOCAFOTS high CDOM can explain some of the variability of the high $K_d(490)$ data as a function of C , the sources of the residuals about this mean relationship remain to be examined. In what follows, an analysis was developed to examine the independent influences of: (a) packaging (dc_i) and pigment composition ($a_{sol}^*(\lambda)$), (b) the dependence of the scattering coefficient on wavelength, and (c) the effects of CDOM and detrital absorption ($a_{cdom+det}(\lambda)$).

2.6.3 Sensitivity analysis

Relationships between $K_d(490)$ and $L_u(443)/L_u(550)$ were constructed using a range of fixed values for individual input parameters that were functions of C in SAMOCAFOTS (see Table 2.4). As mentioned above, the goal of this analysis was to identify the sources of the residual variability, including the effects of changes in phytoplankton community structure on this relationship.

2.6.3.1 Packaging and Pigment Composition

The idealized parameterization of phytoplankton absorption in the model accounted for changes in community structure as C increased, which was consistent with empirical relationships between $a_{ph}^*(\lambda)$ and C . Packaging and pigment composition were treated separately so that the effects of different cell sizes with distinct pigment composition could be analyzed.

In order to simulate the effects of pigment packaging, curves of $K_d(490)$ versus $L_u(443)/L_u(550)$ were reconstructed using the SAMOCAFOTS parameterizations but substituting constant dc_i for all C values (Table 2.4). The influence of different pigment composition was analyzed in a similar manner: the terms of $a_{sol}^*(\lambda)$ which varied with C (Table 2.2) were replaced with fixed values. Because three wavelengths are involved, $a_{sol}^*(443)$, $a_{sol}^*(490)$ and $a_{sol}^*(550)$ were computed for three concentrations of C (1, 5 and 20 mg m^{-3}), representing high, middle and low accessory pigmentation, respectively

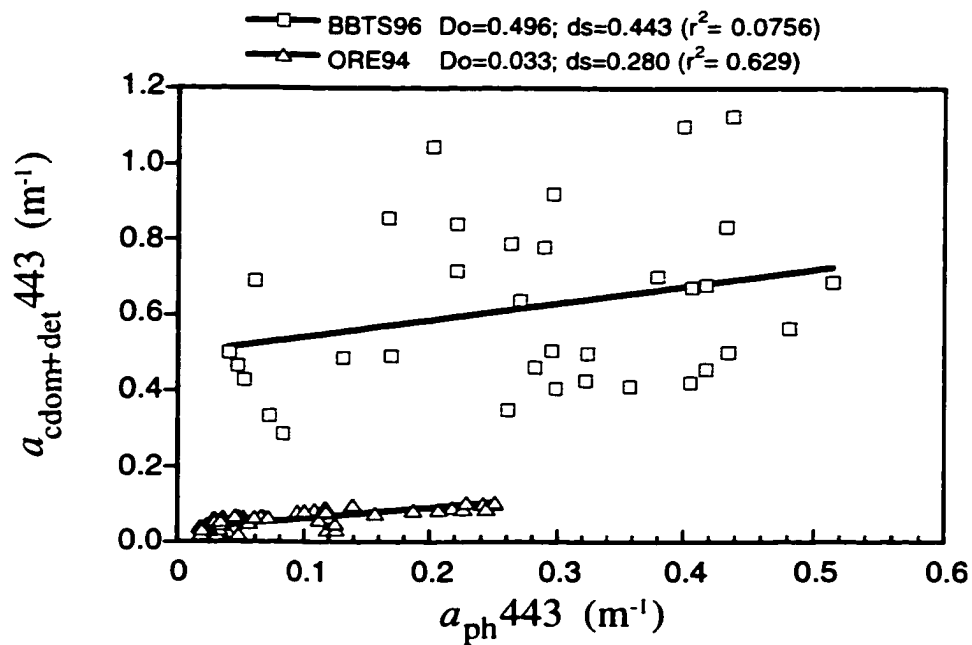


Figure 2.6 Absorption by detritus (particulate material after extraction with an organic solvent) plus CDOM and phytoplankton absorption at 443 nm during the weekly sampling in Bedford Basin in 1996 (BBST96) and during the Oregon cruise in September 1994 (ORE94). Lines represent an assumed linear relationship: the slope represents the fraction that is directly associated with phytoplankton and covaries with them (d_s) and the intercept represents a background value (D_o).

Table 2.4 Values for the parameters and variables used in the sensitivity analysis. These values replaced the relationships with C in the general model. The parameter γ refers to the exponent of the relationship between particle scattering and wavelength.

Input variables	Values
$C; \text{mg m}^{-3}$	0.5, 0.75, 1, 1.25, 1.5, 2, 3, 4, 5, 7, 10, 12, 18, 25 and 30 plus 40 and 50 for SAMOCAFOTS high CDOM
$a_{\text{sol}}^*(\lambda); \text{m}^2 \text{mgChl}^{-1}$	corresponding to equations in Table 2.2
$dc_i; \text{mg m}^2$	10, 20, 40, 60, 80, 100 and 120
γ	2, 1, 0 and -0.5
$D_0; \text{m}^{-1}$	0.0, 0.03, 0.06, 0.1, 0.2, 0.3 and 0.5
d_s	0.0, 0.1, 0.3, 0.5 and 0.8
$S; \text{nm}^{-1}$	-0.010, -0.012, -0.016, -0.018, -0.020 and -0.025

(Claustre, 1994). The goal was to keep the proportions among the three wavelengths consistent with field observations.

Both packaging and pigment composition strongly affected the shapes of the curves (Figure 2.7). Some of the combinations of parameter values resulted in reconstructed curves that were close to the general models (and consequently, close to the empirical models). However, no single combination was able to reproduce these models completely for the given ranges of C . The general trend in the model was in accordance with expected changes in phytoplankton composition as C increases can be seen in Figure 2.7: as cell size, hence dc_i , increases (Malone, 1980; Yentsch and Phinney, 1989; Chisholm, 1992), the ratio (mass to mass) of accessory pigments to chlorophyll a decreases (Claustre, 1994), thus decreasing $a_{sol}^*(\lambda)$. The combinations of fixed parameters created an “envelope” around the general relationship. Not surprisingly, the most significant deviations were observed when phytoplankton communities were composed of cells that were “opposed” to the normal trend, that is, small and less pigmented cells dominating at high C , or bigger cells that were heavily pigmented. These are possible occurrences in coastal and estuarine waters, for example, blooms of *Skeletonema costatum* (cells with low dc_i , (see Morel and Bricaud, 1986), or blooms of dinoflagellates (e.g. *Alexandrium tamarense* in laboratory experiments show dc_i values from 55 to 116 mg m⁻²).

Deviations occur in both $K_d(490)$ and $L_u(443)/L_u(550)$ as functions of C (see examples for “medium” accessory pigments in Figure 2.8). For a given C , bigger cells show higher reflectance ratios and smaller attenuation than the general tendency (SAMOCAFOTS). The two effects combined make the relationship between $K_d(490)$ and $L_u(443)/L_u(550)$ deviate to the upper part of the “envelope” observed around the expected central tendency. Conversely, dominance of small and “pale” cells push the relationship to the lower part of the envelope. The same trends were observed in the sensitivity analysis using SAMOCAFOTS high CDOM (Figures 2.7D, E and F).

Some of the deviations observed in the data set (Figure 2.5) can indeed be related to the “size” of the dominant organism. During the red tide event (BBS93), when large

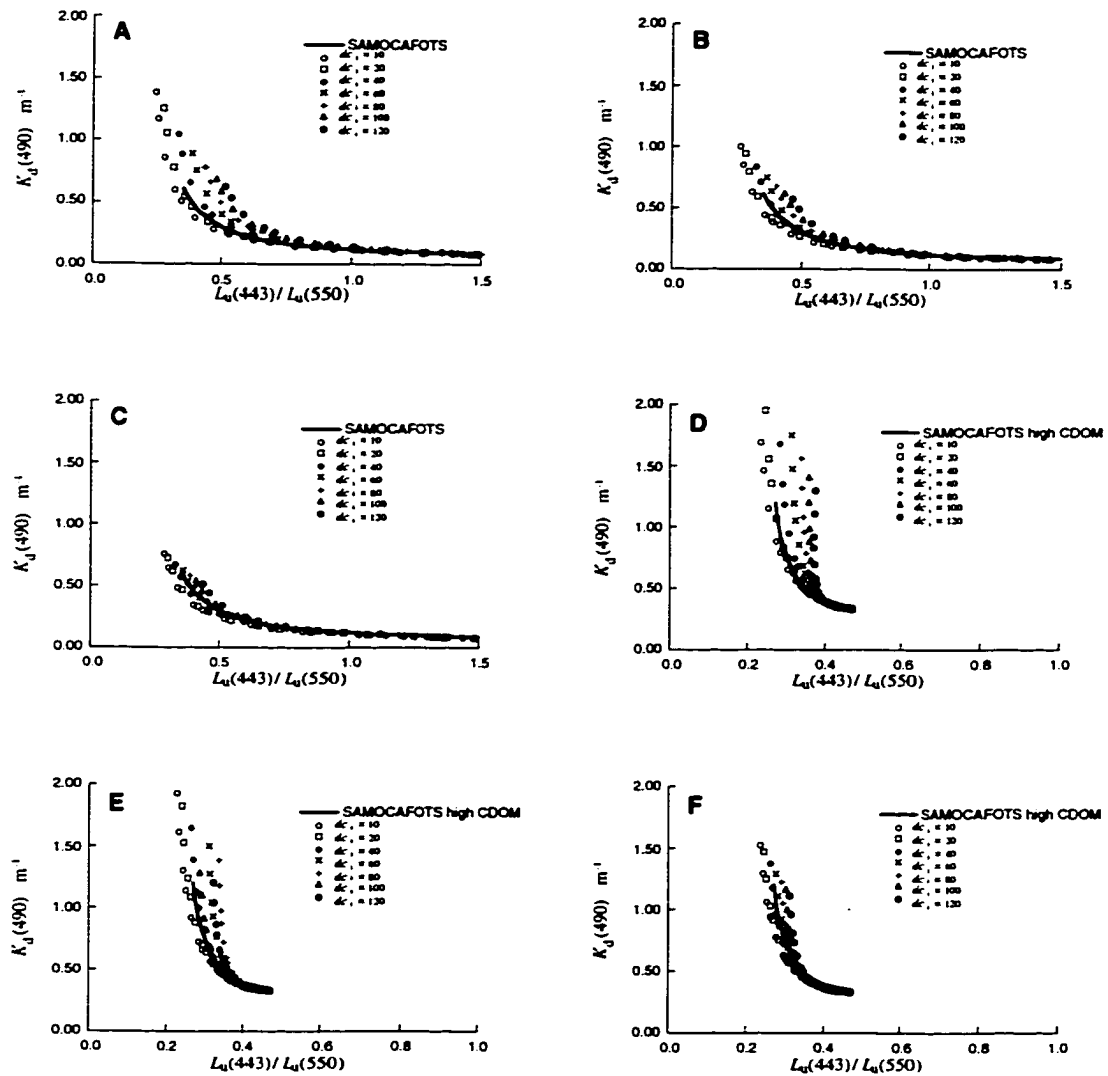


Figure 2.7 Results of the sensitivity analysis of the effects of changes in packaging and pigment composition. Individual points represent fixed values of the product of cell diameter and intracellular concentration of pigments, dc_i (see legend). Three fixed levels of $a_{\text{sol}}^*(\lambda)$ were used to represent high to low influence of accessory pigments, following the equations in Table 2.3 for C concentrations of 1 mg m^{-3} (A and D), 5 mg m^{-3} (B and E) and 20 mg m^{-3} (C and F). All the other parameters are a function of C, as in SAMOCAFOTS and SAMOCAFOTS high CDOM, respectively value (D_0).

dinoflagellates (*Gonyaulax digitale* and *Dinophysis spp.*) were at depth and the surface community was composed of small flagellates, the observations approached the general relationships. When the dinoflagellate cells were at the surface, the observations clearly deviated to the upper portion of the “envelope.” During the cruise in the Bering Sea in 1997, observations clustered to the lower portion at high C . These samples were dominated by colonies of *Phaeocystis sp.* (Cullen et al., unpub. data), containing small cells.

Thus, as a first approximation, deviations from the general relationship between $K_d(490)$ and $L_u(443)/L_u(550)$ could be used as a way to detect and characterize blooms optically. This might only work at a regional level, because the establishment of precise general relationships relies on knowledge of how the several parameters covary with C (equations (2.25) and (2.26)).

2.6.3.2 Spectral dependence of total scattering

As discussed in section 3.2, the particle backscattering coefficient can generally be represented by an inverse-wavelength dependent spectrum (see Mobley, 1994). In SAMOCAFOTS, its exponent (γ) followed an assumed logarithmic relationship with C , going from λ^{-2} at low C grading to λ^0 at high C , representing the importance of small and large particles, respectively. The sensitivity of SAMOCAFOTS to γ was, thus, established by substituting its relationship with C with fixed values from -2 to 0.5 (Figure 2.9). The effect of changes in γ appears small for the more commonly reported exponents of -1 to 0, becoming increasingly important as C increases (Figure 2.9A). The effect is larger when the absorption by CDOM plus detritus is important (Figure 2.9B).

The apparent change of the exponent from -2 or -1 to 0 is a “mean” observation (Gordon *et al.*, 1988; Morel, 1988; Sathyendranath *et al.*, 1989). Comparison of SAMOCAFOTS with the Austin and Petzold (1981) empirical relationship at high $K_d(490)$ (Figure 2.9A) suggests that the exponent could exceed 0 in eutrophic waters. Further investigation of the relationships between particle backscattering and C in these waters is required, especially given that laboratory experiments with large phytoplankton

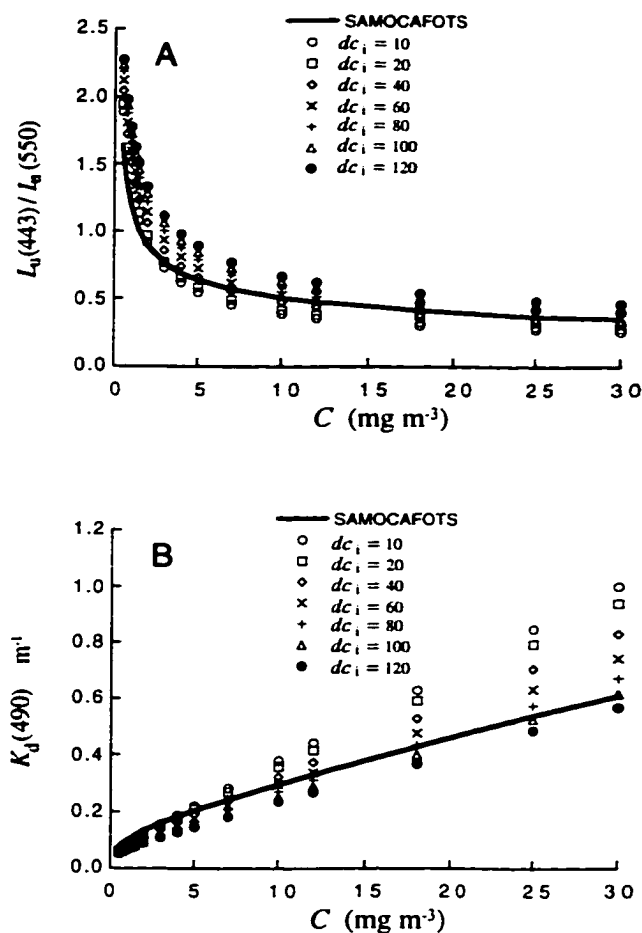


Figure 2.8 Analysis of the effects of changes in packaging for a fixed pigment composition (“Medium” accessory pigments, as in Figure 2.7B) and the relationships between : **A)** $L_u(443)/L_u(550)$ and C , and **B)** $K_d(490)$ and C . Individual points refer to fixed values of the product of cell diameter and intracellular concentration of pigments, dc_i (legend), and $\alpha_{\text{sol}}^*(\lambda)$ computed as in the equations in Table 2.3 for C equal to 5 mg m^{-3} (“Medium” accessory pigments). Symbols indicate dc_i values in both graphs. Solid line is the general model.

species have shown spectral features of b_b that do not necessarily conform to a simple relationship with wavelength (Stramski and Kiefer, 1991). This will probably be the case when blooms occur, because one particular group dominates the optical properties (e.g., Subramaniam and Carpenter, 1994). If a bloom of bigger cells (high packaging) had a large influence on the total scattering coefficient or on the backscattering ratio (Ahn *et al.*, 1992), it would result in positive exponents. In this case, the effect could counteract the effect of packaging on the deviations in the relationship between $K_d(490)$ and $L_u(443)/L_u(550)$. Thus, it will probably be necessary to measure directly both absorption and scattering signatures for pertinent groups of phytoplankton in the field during blooms.

This analysis also suggests that input of different sizes of inorganic and organic material can strongly affect the relationship between $K_d(490)$ and $L_u(443)/L_u(550)$. The inclusion of such particles, in addition to particle assemblage parameterized in SAMOCAFOTS can be easily done by the addition of an extra term in equation (2.23), such that:

$$b_b(\lambda) = b_{b_w}(\lambda) + \bar{b}_{b_{ph+det}} b_{ph+det}(\lambda) \left(\frac{600}{\lambda}\right)^\gamma + \bar{b}_{b_{non-ph}} b_{non-ph}(\lambda) \left(\frac{600}{\lambda}\right)^{\gamma_{non-ph}} \quad (2.28)$$

where $\bar{b}_{b_{non-ph}}$ is the backscattering ratio for the additional particles and $b_{non-ph}(\lambda)$ is its respective scattering coefficient. As was done for phytoplankton plus detritus, once $\bar{b}_{b_{non-ph}}$ is estimated, a spectral dependency, i.e., γ_{non-ph} , has to be assumed. Particles such as clay can have a backscattering ratio of up to 0.08 (Bukata *et al.*, 1988), and if a dependency of λ^{-1} is assumed, significant deviations from the general trend can result from increasingly larger inputs of these particles (2.10A and B). The input of these additional particles is simulated by increasing the value of their scattering coefficient, $b_{non-ph}(660)$.

On the other hand, the input of particles with low backscattering ratios, small slopes, and no spectral dependency for the scattering coefficient (for example, organic

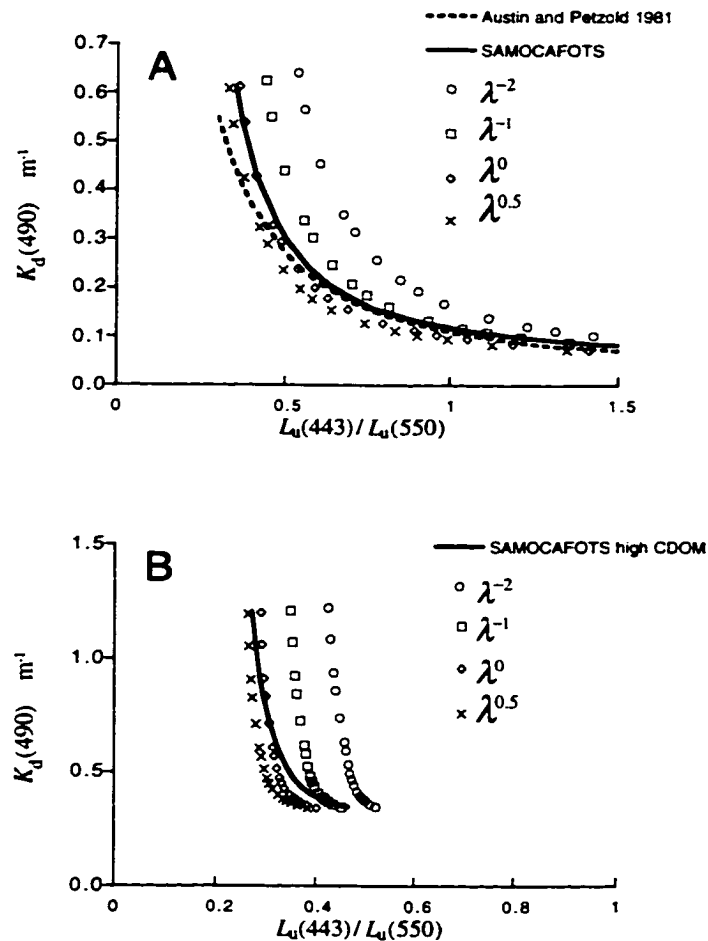


Figure 2.9 Sensitivity of A) SAMOCAFOTS and B) SAMOCAFOTS high CDOM to the wavelength dependence of the particle scattering coefficient (γ), varying as described in the legend. More negative exponents are associated with the importance of smaller particles. All the other parameters (packaging, pigment composition and CDOM plus detrital absorption) are a function of C , as in SAMOCAFOTS. The empirical relationship by Austin and Petzold (1981) is plotted in A for comparison.

2.10C and D), especially in situations where the proportion of $a_{\text{cdom+det}}$ to $a_{\text{ph}}(\lambda)$ is high. Nevertheless, a large input of organic particles (for example in Bedford Basin) with absorption spectra that differ from those of the oceanic phytoplankton and detritus will affect the relationship between total absorption and C , as described below.

2.6.3.3 CDOM and detrital absorption

The effects of $a_{\text{cdom+det}}(\lambda)$ can be analyzed by varying D_o , the absorption attributed to a “background” concentration; d_s , the fraction covarying with phytoplankton absorption; and S , the slope of the decay of $a_{\text{cdom+det}}(\lambda)$ with wavelength. Values of D_o were selected to represent environments ranging from oligotrophic oceanic waters to estuarine waters (based on Kirk (1994b)). The range of d_s was based on the absorption data from a variety of coastal waters (not shown), in which measured values of the absorption coefficient by phytoplankton were compared to measured values of the combined contribution of absorption by CDOM and detritus at 443 nm. Values for S vary over published ranges for CDOM absorption (e.g., Carder *et al.*, 1989; Green and Blough, 1994).

Changes in D_o (Figure 2.11A) affected the relationship between $K_d(490)$ and $L_u(443)/L_u(550)$ slightly at low C , and changes in d_s (Figure 2.11B) hardly influenced the shape of the relationship. This may be one of the reasons why the empirical relationship of *Austin and Petzold* has been shown to hold in more turbid environments (Cullen *et al.*, 1994). In fact, if SAMOCAFOTS were to be extrapolated to very high (and unreasonable) C , and the empirical relationships to lower values of $L_u(443)/L_u(550)$, the curves would explain from 40 to 60% of the variability of the data with high $K_d(490)$. In other words, despite the variability in $a_{\text{cdom+det}}(\lambda)$ in Bedford Basin (see Figure 2.6), empirical relationships can still predict $K_d(490)$ with some degree of accuracy.

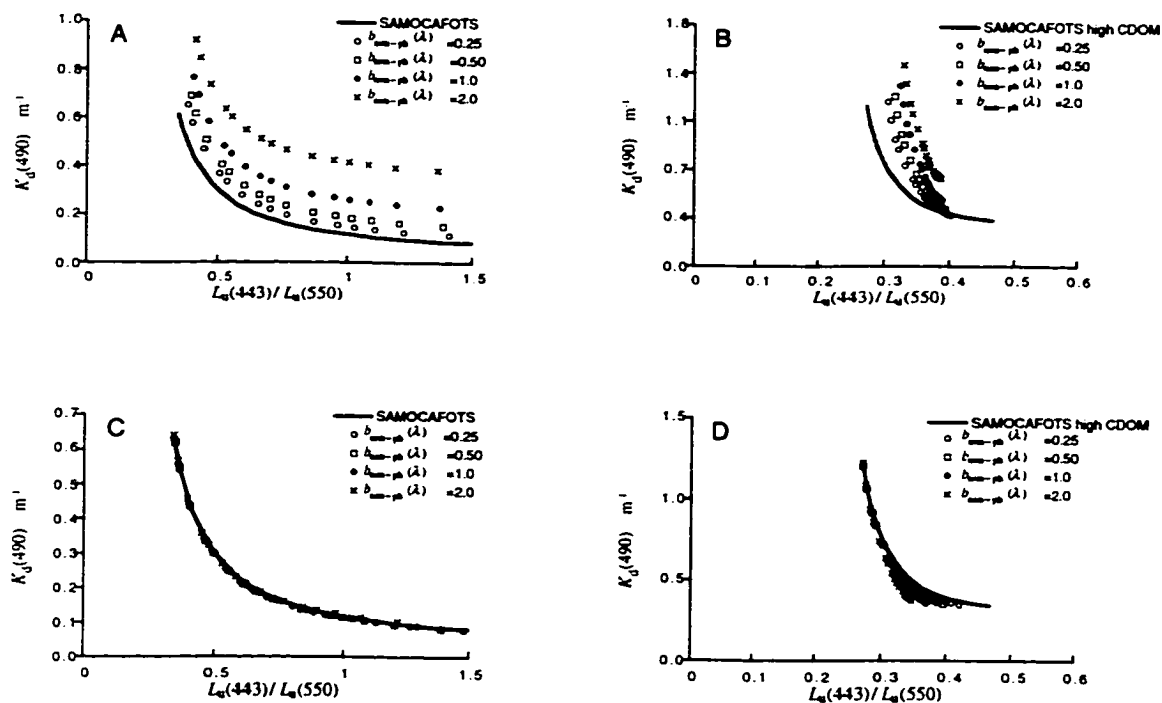


Figure 2.10 Influence of an additional input of particles simulated by their attenuation coefficient at 660 nm, $b_{\text{non-ph}}(660)$. **A and B)** Increments of $b_{\text{non-ph}}(660)$, simulating the input of particles with backscattering ratio equal to 0.08, low absorption coefficient and dependency of λ^{-1} for the scattering coefficient, for SAMOCAFOTS and SAMOCAFOTS high CDOM, respectively. **C and D)** Same as **A and B**, only for input of particles with backscattering ratio of 0.01 and no spectral dependency for the scattering coefficient.

The effect of increasing $a_{\text{cdom+det}}(\lambda)$ is to reduce the overall sensitivity of the radiance ratios to distinguish between the different levels of C , as anticipated (Gordon *et al.*, 1983 and references therein) and verified in the field (e.g., Hochman *et al.*, 1995). Figures 2.11C and 2.11D show the effects of varying D_o and d_s , respectively, on the ratio of upwelling radiance at 490 to that at 550 nm and the resulting changes in C retrieved using the SeaWiFS algorithm (O'Reilly *et al.*, 1998). Changes in d_s affected the results modestly (less than 40%); however, changes in D_o resulted in an overestimation of the retrieved C by a factor of more than 10 when *in situ* C is low, and by a factor of 2 when *in situ* C is high.

The attenuation coefficient remained sensitive to changes in C at all final concentrations of $a_{\text{cdom+det}}(\lambda)$ (Figures 2.11A and B), but will respond to both D_o and d_s in a similar manner as $L_u(443)/L_u(550)$ does. Because in the parameterization the relationship between $a_{\text{cdom+det}}$ and a_{ph} is linear, it is not surprising that the effects of both D_o and d_s on $L_u(443)/L_u(550)$ and $K_d(490)$ are proportional to one another and, therefore, the form of original relationship is maintained.

So far, the comparisons of the influence of varying total amounts of CDOM plus detrital absorption were done for a constant spectral shape. This shape, however, is expected to change depending on the composition and origin of CDOM, which is manifested by changes in the slope, S (Carder *et al.*, 1989). Because of that, S could be expected to vary seasonally. In addition, in waters such as Bedford Basin, the variability in S could follow a range of different time scales, associated with tidal and wind mixing as well as river outflow and precipitation rates. The sensitivity of SAMOCAFOTS to S (Figure 2.12) shows that it can influence significantly the relationship when $a_{\text{cdom+det}}(\lambda)$ is high. The range of variability around the central tendency explained by SAMOCAFOTS high CDOM (Figure 2.12B) is consistent with the range of variability found during the time series experiment in Bedford Basin, suggesting that models should incorporate terms to account for the variability in S for water bodies in which CDOM is an important

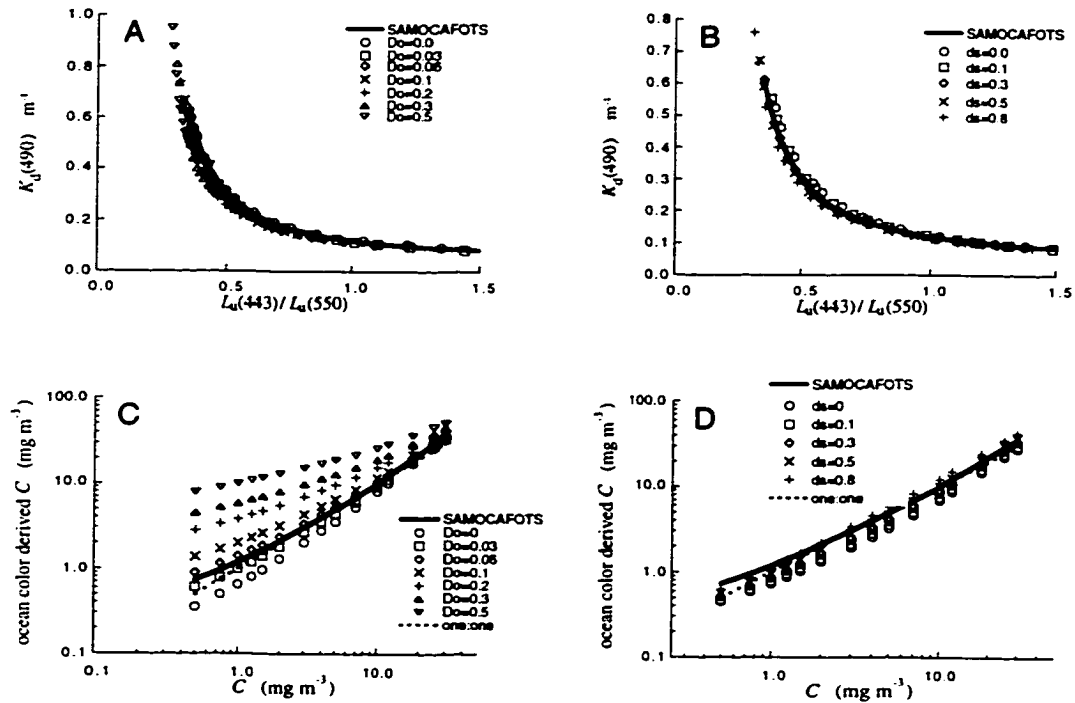


Figure 2.11 A) Sensitivity analysis of SAMOCAFOTS to changes in D_0 , the absorption by the background concentration of CDOM and detritus, representing ranges found from oligotrophic to estuarine waters. B) Sensitivity to d_s , the slope of the assumed linear relationship between phytoplankton and CDOM and detritus absorption, representing ranges found in a variety of coastal waters. C and D) Same as in A and B, only for the relationship between C and $L_u(490)/L_u(550)$ which was parameterized as in equation (2.26) with the relevant parameters modified from 443 to 490 nm.

contributor to total absorption.

2.7 Summary and Conclusions

A semi-analytical model was constructed to explore the effects of diverse optical components on the relationship between upwelling radiance ratios and diffuse attenuation. The model was based on well described, fundamental sources of optical variability in the ocean. The terms were parameterized as functions of C , consistent with observations from the field, reconciled with theoretical and laboratory-derived optical relationships. Although C is a poor descriptor of phytoplankton biomass (Cullen, 1982), the construction of a general (or "expected") relationships as a function of C allowed developing more mechanistic approaches to interpret changes in phytoplankton optical properties as a function of trophic status (Yentsch and Phinney, 1989). In addition, analysis and interpretation of deviations from the expected trend can be useful tools (e.g., Morel, 1997).

The resulting general relationship between $K_d(490)$ and $L_u(443)/L_u(550)$ reproduced well both empirical models and independent bio-optical data from a variety of environments. The individual parameterizations of diffuse attenuation and radiance ratios also agreed well with patterns in data from the field. The model reconciles relationships between inherent and apparent optical properties, as well as theoretical, laboratory and field observations. The agreement between statistical models and the semi-analytical expressions was above 80% for $L_u(443)/L_u(550)$ above 0.5. The parameterization of phytoplankton absorption can be modified to include a range of phytoplankton communities for a given value of C .

Variability around the central tendency explained by the general model was modeled by varying the original relationship between the input parameters and C . The estimated deviations from the general model could be related to the variability observed in the field measurements. Substantial deviations were produced by:

- (a) changes in packaging at high accessory pigment concentration;
- (b) changes in the spectral shape of the scattering coefficient (implying changes in the

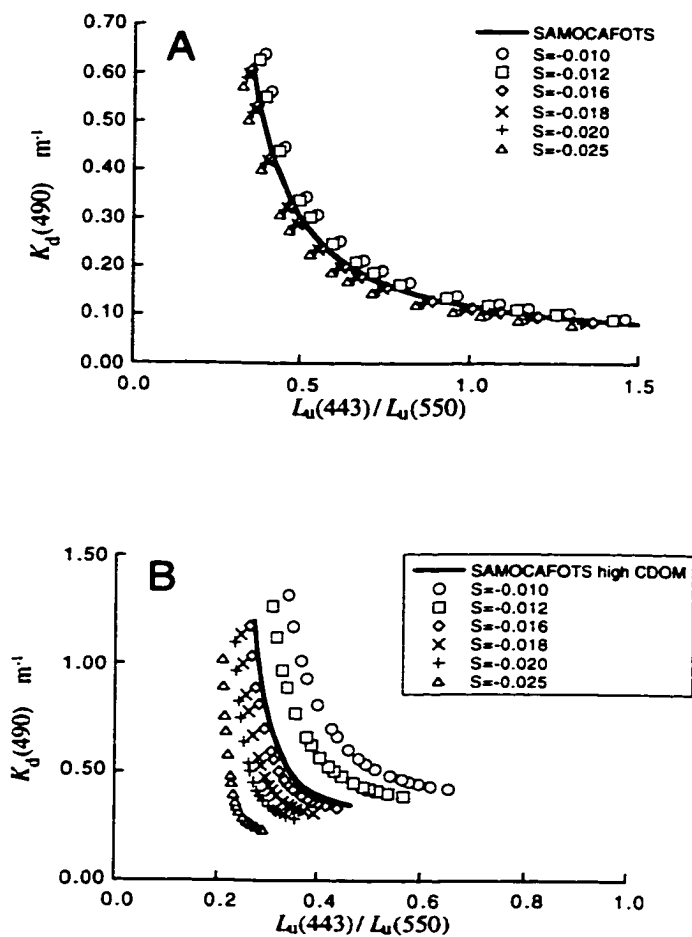


Figure 2.12 Sensitivity of **A)** SAMOCAFOTS and **B)** SAMOCAFOTS high CDOM to changes in S , the slope of the decrease of CDOM plus detrital absorption with wavelength. Values of S represent ranges found in the literature and in the data base collected in this study.

size distribution of the particles and also different types of particles) in environments where CDOM and detrital absorption are important and;

(c) variability in non-phytoplanktonic absorption, particularly changes in S , the slope of the decrease in absorption with wavelength, in environments expected to have a large contribution of CDOM and/or detrital absorption.

Although with the set of wavebands used in this analysis it is difficult to distinguish among these effects, one can speculate that packaging and high accessory pigment concentration explain in large part the deviations found during a red tide event (BBS93), because during this experiment, absorption by CDOM remained relatively consistent. These deviations could be applied in monitoring such events using simple passive optical instruments (Cullen *et al.*, 1997). The analyses suggest that SAMOCAFOTS-like relationships could be constructed to discriminate rough features among different phytoplankton communities (i.e., packaging), given a set of optimized wavelengths which minimizes the influence of CDOM and detrital absorption. Algorithms using two or more radiance ratios (with SeaWiFS wavelengths) to estimate chlorophyll concentrations in waters with CDOM and detrital influence are being developed and tested (Aiken *et al.*, 1995 and references therein).

Another important point can be made regarding the predictive skills of the semi-analytical relationship compared to the empirical ones: in the independent data set presented in this paper, the forecast skill of $K_d(490)$ from $L_u(443)/L_u(550)$ was about the same using the model as with the empirical relationships. This is not unexpected, as both the general semi-analytical and empirical equations represent general trends or averages of the variability in optical properties by phytoplankton and other components. The main goal of expressing optical properties through semi-analytical expressions, rather than improving their statistical forecast skill, is to produce tools to understand quantitatively the factors that influence these properties. Once these factors are defined, some forecast skill improvement can be made if independent and concurrent optical measurements are made to account for first order deviations from the general trend.

Chapter 3

Dominant cell size and its effects on the spectral shape of natural phytoplankton absorption spectra

3.1 Introduction

Changes in phytoplankton species composition are a central feature of marine ecosystem dynamics. Description and prediction of these changes are important goals to many fields in oceanography, such as evaluation of eutrophication (Hallegraeff, 1993), prediction and monitoring of harmful algal blooms (Riegman, 1998), or the distinction of different biogeographical provinces in the ocean (e.g. Longhurst *et al.*, 1995).

Much effort has been dedicated to investigating the extent to which changes in phytoplankton species composition will affect optical properties of surface waters (e.g. Bricaud and Morel, 1988; Ackleson *et al.*, 1990; Stramski and Kiefer, 1991; Hoepffner and Sathyendranath, 1992; Johnsen *et al.*, 1994b; Subramaniam and Carpenter, 1994; Brown *et al.*, 1995; Morel, 1997; Stuart *et al.*, 1998), so that variability of phytoplankton could be observed continuously or synoptically, using techniques such as *in situ* optical instruments or remote sensing. This is a complicated topic, because phytoplankton communities include species with variable size, shape, external and internal structures, pigment composition and different patterns of mobility. All these characteristics will influence the optical properties of the ocean to some degree, and thus it is likely that a

large number of parameters will have to be considered for a complete description of different communities of phytoplankton. A central goal of the research in this field is to determine how much information is required in order to use ocean color for discriminating different types or communities of phytoplankton.

There is good evidence that variability in ocean color spectra alone may not give enough independent information to reveal changes in species composition of phytoplankton (Mueller, 1976; Garver and Siegel, 1994) because most of the variability can be attributed to a few components (but see Hoge and Swift, 1990; Sathyendranath *et al.*, 1994). Therefore, an important step in the study of the influence of different communities of phytoplankton on ocean color is to analyze quantitatively relevant parameters that influence their optical properties.

In the previous chapter, it was shown explicitly that average changes in phytoplankton communities with trophic status (i.e., chlorophyll concentration) were consistent with the proposition that groups of larger cell sizes are added to a relatively constant “background” of smaller cells (cf. Yentsch and Phinney, 1989). Consequently, both pigment packaging and the concentration of accessory pigments also have an expected relationship with chlorophyll concentration. However, nature seldom conforms to such idealized terms: smaller cell sizes can often form large standing crops, and phytoplankton communities can be dominated by a diverse variety of phytoplankton groups, which in principle, will have distinct optical properties.

In this chapter near-surface bio-optical data from a wide variety of natural situations were analyzed to determine the degree to which different communities of phytoplankton, that were explicitly discriminated in terms of cell size, affect the shape of phytoplankton absorption spectra. Comparisons included absorption measurements on samples that were physically separated into size ranges. Phytoplankton communities were also categorized according to taxonomic composition of the dominant organisms to quantify the role of both size and taxon on the spectral shape of phytoplankton absorption coefficient. The results were analyzed in the context of retrieving features of

phytoplankton communities from optical measurements. A large fraction of the variability in the spectral shape of phytoplankton absorption can be related to the cell size range of the organism which dominates phytoplankton biomass. As a direct consequence, the influence of different communities can be substantially accounted for with a parameterization of phytoplankton absorption using two basis vectors, representing absorption of small and large cells, and a “size” parameter specifying the contribution of each.

3.2 Background

Trends in the composition of phytoplankton communities can be related to local trophic status (Margalef, 1978; Kiørboe, 1993). In oligotrophic environments, phytoplankton biomass is dominated by prokaryotic cells (Chisholm *et al.*, 1988; Olson *et al.*, 1990) which are small and have characteristic pigmentation (Goericke and Repeta, 1992; Moore *et al.*, 1995). Because specific rates of nutrient uptake tend to decrease with increasing cell size (see Joint, 1991), only under higher nutrient conditions (i.e., eutrophic environments) can larger cells compete for nutrients, grow, and complement the small-size groups (Malone, 1980; Yentsch and Phinney, 1989; Chisholm, 1992). These groups of larger cells will belong to distinct groups of species depending mainly on both environmental conditions and on the ability of these species to exploit light and nutrients effectively (cf. Margalef, 1978).

Ecologically, changes in community structure with trophic status can be attributed to a balance between growth rates, turbulence and efficiency of predation (Thingstad and Sakshaug, 1990; Kiørboe, 1993; Riegman *et al.*, 1993). Small cells have an advantage in using both light and nutrients as a result of their high surface to volume ratios (Chisholm, 1992), and because of their small size (implying low sinking rates), they tend to remain easily in the euphotic zone. Larger cells have an advantage regarding predation, because the relative density of predators tends to decrease with increasing prey size, while their generation times increase. The abundance of small cells is thus controlled more

effectively by their similar-sized predators (Banse, 1982). Because of that, most of the variability in phytoplankton biomass can be related to pulses of larger cells, formed by a combination of nutrient supply to the euphotic zone, stratification of the water column combined with turbulence levels capable of maintaining larger cells in suspension, and a considerable time lag in the numerical response of their predators (Kjørboe, 1993; Carr, 1998). It is not surprising that both cell size and analyses of pigment composition (as a proxy for taxonomy) are the main focus of studies describing the role of natural phytoplankton in modifying the optical properties of the ocean. An important point to make is that, in conjunction with these changes in favored cell size with trophic status, nutrient availability itself will influence physiological attributes of pigment composition, so that when nutrients are scarce, cells will tend to have a higher concentration of accessory pigments (including photoprotective pigments) than when nutrients are abundant (Sosik and Mitchell, 1991; Geider *et al.*, 1993; Stuart *et al.*, 1998).

The optical properties of phytoplankton are determined by absorption, scattering and backscattering coefficients of assemblages of cells (Gordon *et al.*, 1975; Morel and Prieur, 1977). Data from different optical platforms, such as satellites (Subramaniam and Carpenter, 1994), aircraft (Sathyendranath *et al.*, 1994) and *in situ* instruments (Morel, 1997), as well as laboratory (Johnsen *et al.*, 1994b) and field (Millie *et al.*, 1997) comparisons of absorption spectra, suggest that differences in pigment composition, detectable in measurements of ocean color, can in some cases, be used as “pigment signatures” for different groups (but see Garver and Siegel, 1994).

The spectral absorption of pigments inside phytoplankton cells and organelles is reduced compared to that of the same pigments in solution. This “package effect” (Duysens, 1956; Kirk, 1994b) depends upon cell size and intracellular pigment concentration (Bricaud *et al.*, 1983). Different degrees of packaging in natural populations of phytoplankton have been shown to influence the relationship between phytoplankton absorption and chlorophyll concentration (Bricaud *et al.*, 1995; Cleveland, 1995; Stuart *et al.*, 1998), and optical measurements such as ratios of upwelling radiance

(Carder *et al.*, 1991) and diffuse attenuation coefficients (Mitchell and Holm-Hansen, 1991). Measurements in laboratory using monospecific cultures combined with modeling exercises (Mobley and Stramski, 1997) have also predicted that different dominant species can produce changes in the relationship between ocean color and the amount of chlorophyll.

In contrast, Garver and Siegel (1994) showed that the variability found in a large data set of particulate absorption spectra from different environments could be practically explained by only two spectral components: material containing pigments (phytoplankton) and the material that does not (detritus), inferring that the differences in the shape of phytoplankton absorption for different communities of phytoplankton are too small to be useful.

Ocean color is also dependent on the spectral shape of the backscattering coefficient (Gordon *et al.*, 1988), which changes with particle size-distribution (Morel, 1987) and is expected to be related to the optical characteristics of the dominant species (Stramski and Kiefer, 1991; Ahn *et al.*, 1992). However, the bulk backscattering coefficient in the ocean has been attributed principally to components other than phytoplankton, such as submicron particles and bacteria (Stramski and Kiefer, 1991; Ahn *et al.*, 1992; Ulloa *et al.*, 1994) and more recently, bubbles (Stramski, 1994; Zhang *et al.*, 1998). To date, only a few measurements of spectral backscattering in the field have been presented (e.g. Maffione and Dana, 1997) to validate theoretical predictions. Because of that, generalizations of how the spectral backscattering changes with trophic status are problematic and have to be accessed through simplifying assumptions (Roesler and Perry, 1995).

3.3 Approach

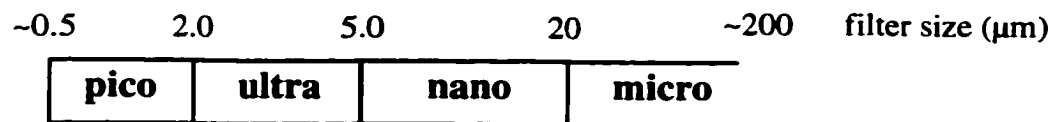
In order to provide a context for describing the variability of phytoplankton composition in coastal waters, a simple classification of different communities of phytoplankton was developed, based on size and dominant taxa. Using a division of

phytoplankton by size (cf. Sieburth *et al.*, 1978), this classification was achieved in two steps (Figure 3.1). First, the dominant “size fraction” was determined by physical separation and quantification of fluorometrically determined chlorophyll (see methods) among 4 size ranges: picoplankton ($< 2 \mu\text{m}$), ultraplankton (between 2 and 5 μm), nanoplankton (between 5 and 20 μm) and microplankton ($> 20 \mu\text{m}$). The dominant size fraction was assumed to be the one containing more than 50% of the total chlorophyll when only two ranges were present, or the one containing more than 40% of the total chlorophyll when three or four ranges were present. Samples that did not meet either criterion were not included in the data set (3 samples of a total of 55). When chlorophyll size fractionation was not available, the dominant size fraction was established through microscopic analysis and/or sizing and enumeration of particles using a Coulter Counter.

Once the dominant size fraction was defined, the dominant organism within that fraction was identified through either microscopic or flow cytometric analyses. That is, only the cells retained in the dominant size fraction were counted and sized. For colonies and chain-forming organisms, which were always included in the microplankton size fraction by the physical separation, cell size could be smaller than the designated size fraction and was thus reassessed. The dominant organism or group within the designated dominant size fraction was determined by using the product of cell number and surface area of the cells (see details in methods). Each community was thus characterized by both taxon and respective cell size of the dominant group of organisms.

This approach provides a simple technique to obtain the dominant organism in the phytoplankton biomass, rather than only the numerical dominance. Throughout this chapter, “whole” refers to non-fractionated samples; “size fractions” refers to samples that were physically separated into the 4 size ranges, and “cell sizes” refer to the actual cell size measured using microscopic analyses. It is important to note that, in most cases, the ranges for “size fractions” and “cell size” will be the same, except when chain or colonial forms are present in large numbers.

Physical separation of particulate fraction



Classification: Dominant size fraction

Measurement: chlorophyll concentration:

Criteria: >50% when 2 fractions were present

>40 % when 3 or 4 fractions were present



Classification: Dominant cell size

Measurement: microscope and flow cytometer

Criteria: cell size of dominant organism in dominant size fraction

Figure 3.1 Procedure followed to discriminate among different communities. Dominant cell size was attributed to the organism or group with the higher product of cell number and cell area.

3.4 Sampling design

Bio-optical characteristics were measured in three different environments: coastal waters off Oregon, the southeastern Bering Sea and Bedford Basin (Nova Scotia, Canada), the last being sampled on several occasions (Figure 3.2; Table 3.1). Our goal was to represent as many different field conditions as possible. A general sampling design was followed during all cruises: a cast was made with a CTD equipped with a fluorometer and a 25 cm path length transmissometer; a second CTD cast was made for water samples. Sampling depths were chosen with reference to the vertical profiles of fluorescence and/or beam transmission from the first CTD cast. Water samples were obtained from 2 to 3 depths within the mixed layer using Niskin bottles, and at the surface with a clean plastic bucket. An additional sample was collected at the chlorophyll maximum layer, when present. In Bedford Basin, samples were also collected with a peristaltic pump (Masterflex 7518-12) whose intake (opaque) hose was attached to the CTD frame, close to the fluorometer's viewing window. During the time series in Bedford Basin from July to December of 1996, water samples were collected at two fixed depths (1 and 3 meters) using a 5 L Niskin bottle.

3.5 Methods

Chlorophyll a (chl, mg m^{-3}) was determined fluorometrically using a Turner Designs 10-005R fluorometer, equipped with the following filters: Corning 5-60 (excitation), Corning 3-66 (reference) and Corning 70 and 16 (emission). Pigments were extracted at -10°C or below, for at least 24 hours, in pre-cooled 90% acetone: DMSO solution (6:4 by volume, Shoaf and Lium, 1976) immediately after filtration. Samples were corrected for pheopigments by acidification with 10% HCl. The fluorometer was calibrated during each cruise, with a series of known chlorophyll a concentrations, derived from volumetric dilutions of a standard solution using pure chlorophyll a from Sigma. The concentration of the standard was determined spectrophotometrically by

Table 3.1 Location, dates, and measurements in each cruise.

Location	Dates	Cruise	Measurements
Bedford Basin	Aug. 1992	BBS92	chl, particulate absorption and floristics
Bedford Basin	Aug. 1993	BBS93	chl, cell size, floristics, particulate and dissolved absorption
Bedford Basin	Aug. 1996 Jul. to Dec. 1996	BBS96 BBTS96	chl (total and size classes), particulate and dissolved absorption and floristics (weekly plus intensive sampling Aug 20-22)
Oregon coast	Sep. 1994	ORE94	chl (total and size classes), floristics, particulate (total and size classes) and dissolved absorption
Bering Sea	Apr. 1996	BS96	chl (total and size classes), particulate (total and size classes) and dissolved absorption
Bering Sea	Jun. 1997	BS97	chl, particulate and dissolved absorption

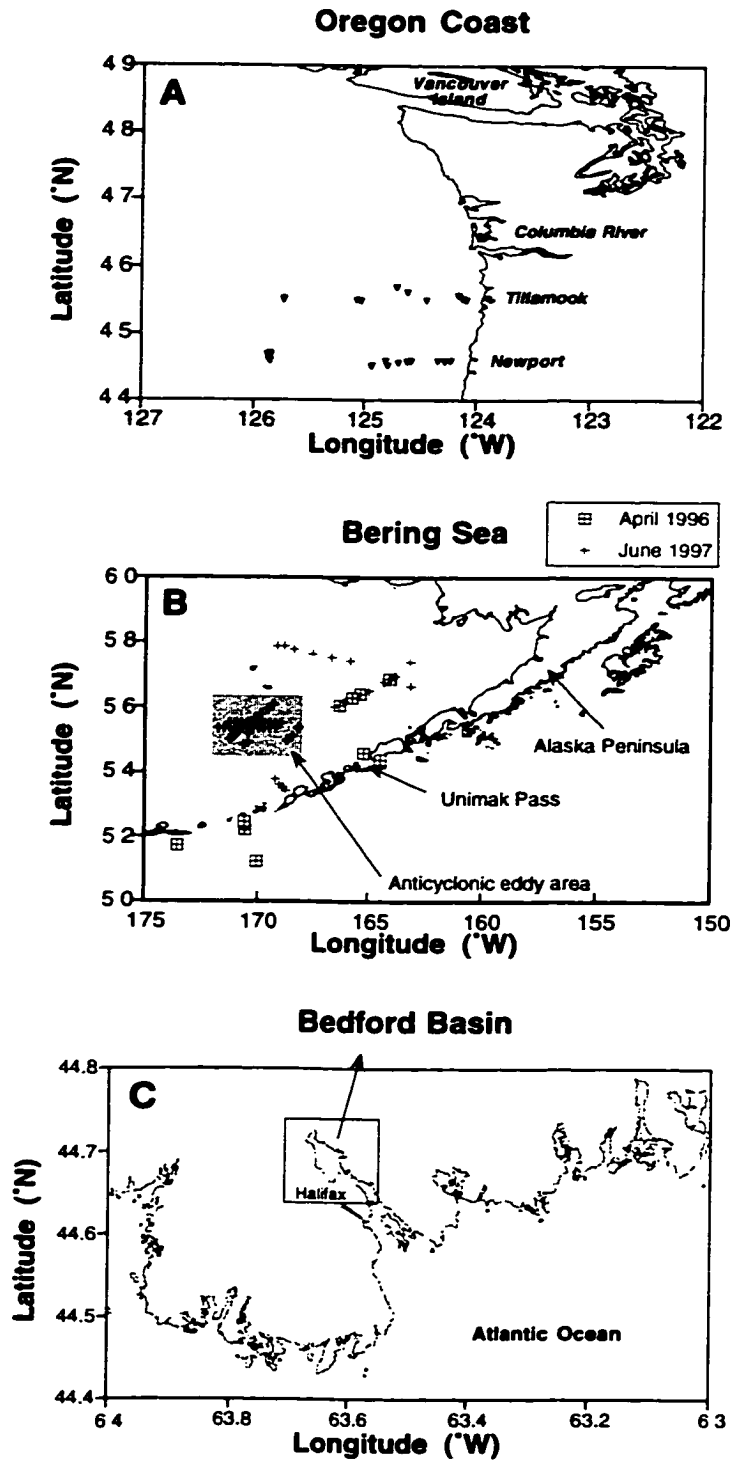


Figure 3.2 Sampling areas and stations visited. **A)** Off the coast of Oregon state in September 1994. **B)** Bering Sea in 1996 and 1997. **C)** Bedford Basin on several occasions. See Table 3.1 for dates and measurements.

using the extinction coefficient of pure chlorophyll from Jeffrey and Humphrey (1975). For the time series in Bedford Basin a single calibration was used, made immediately before the experiment. This calibration was verified every other week by using standard solutions and did not vary more than 3%. It is important to note that the relatively wide spectral responses of the filters in the fluorometer will allow the influence of accessory pigments on the final chl. For example, high concentrations of chlorophyll *c* will tend to overestimate chl, while high concentrations of chlorophyll *b* will tend to underestimate chl (Mantoura *et al.*, 1997)

Particulate absorption was measured on samples concentrated onto GF/F filters. Samples were either preserved in liquid nitrogen (maximum of 2 months) until analysis or analyzed immediately after filtration. Absorption of particulate material was determined following the method described by Yentsch (1962) modified by Mitchell and Kiefer (1983). Two different Cary 3 Dual-Beam spectrophotometers were used, and a pathlength amplification correction (beta) was determined for each instrument, using monospecific cultures (Ciotti, unpublished; Roesler, 1992). Filters were scanned against a blank filter, dampened with 250 μ l of artificial sea water pre-filtered through a 0.2 μ m polycarbonate filter (Poretics® and or Nuclepore®). Blank and sample filters were taken from the same lot. Immediately after the scans, blank and sample filters were extracted with pure methanol and rinsed with 100 ml of artificial sea water, pre-filtered through a clean 0.2 μ m polycarbonate filter, which was intended to extract both hydrophobic and hydrophilic pigments (see Roesler and Perry, 1995). Once the beta correction was applied, each scan was smoothed using a 5 nm running average, and corrected for both differential scattering (setting the mean absorption between 740 to 750 nm to zero) and volume filtered and area of the filter. This assumes that the differential scattering is wavelength independent. Phytoplankton absorption was computed by subtraction of scans before (total particulate) and after (“detritus”) the methanol and water extraction.

Size-fractionated chl and particulate absorption were determined for 4 size fractions: picoplankton (cells < 2 μ m), ultraplankton (cells between 2 and 5 μ m),

nanoplankton (cells between 5 and 20 μm) and microplankton (cells > 20 μm). Filtrates from 20, 5 and 2 μm Poretics® and or Nuclepore® polycarbonate filters were concentrated onto GF/F filters (nominal pore size of 0.7 μm). GF/F filters have been shown to be as effective as 0.2 μm pore size filters retaining phytoplankton cells even in oligotrophic waters (Chavez et al., (1995) addressing Dickson and Wheeler, (1993)) thus significant losses of small cells in this procedure are not anticipated. Filtration using polycarbonate filters was driven by gravity or very low pressure (around 25 mm Hg). The concentration in each size fraction was then determined as shown in Table 2. Fractionation was done only on samples from the surface and the chlorophyll maximum.

Flow cytometric analyses were done with a FACScan flow cytometer (Becton Dickinson) equipped with a 15 mW air-cooled argon laser (488 nm). Samples were processed during the cruise and these data are courtesy of T. Cucci. For all detected particles, forward light scatter, 90 degree light scatter, phycoerythrin fluorescence emission (560-590 nm) and chlorophyll fluorescence emission (>650 nm) were measured. The volume of the sample analyzed was estimated by the addition of a known number of fluorescent microspheres (10 μm in diameter) to each sample immediately before analysis. Samples were run at approximately 10-12 $\mu\text{l min}^{-1}$. The identification of the different groups in each sample was done by using a combination of forward light scattering and red and orange fluorescence (Yentsch *et al.*, 1983).

Microscopic analyses were performed with an inverted microscope on samples fixed with a mixture of glutaraldehyde and formaldehyde (0.5 to 1% final concentration; D. V. Subba Rao, pers. com.; see also Lazinsky (1979)). The lower limit of detection was about 3 μm . This analysis was only relevant for samples in which picoplankton did not dominate. The cells in the sample were concentrated using sedimentation chambers (cf. Utermöhl, 1958) and scanned under the microscope using magnifications of 100 and 400 times. Only cells within the dominant chl size fraction (see section 3.3) were counted and sized, and the dominant organism was chosen by computing the product of cell number and an average surface area for each group identified in that fraction. It is important to

note that the reported cell sizes from the microscopic analyses tend to underestimate the actual sizes, due to fixative effects (Klein-Breteler, 1985). The reduction in size depends on the organism and storage time.

Particle size was also determined with a Coulter Multisizer II Particle Analyzer using a tube with a 75 μm aperture. Upper and lower limits of detection for this tube are 3 and 50 μm , respectively. These measurements were done during one experiment only, in the Summer of 1993 in Bedford Basin.

3.6 Results

The three environments and times sampled represented contrasting oceanographic regimes, with a variety of sizes and groups of phytoplankton. The results will be presented in three parts. First, a brief summary will be given of the physical characteristics and chl (total and size classes) in the upper layers. Second, based on the chl sizes and identification of main genera, different “communities” are classified in each environment. These communities are summarized on Table 3.3, presented at the end of this section. Finally, the relative influence of cell size and taxonomy on the shape of the phytoplankton absorption coefficient spectra of these communities is assessed.

For the comparison amongst the different communities, phytoplankton absorption spectra ($a_{\text{ph}}(\lambda)$, m^{-1}) were normalized using the average absorption computed between 400 and 700 nm, following the equation below:

$$\langle a_{\text{ph}} \rangle = \frac{1}{301} \sum_{\lambda=400}^{700} a_{\text{ph}}(\lambda) \Delta\lambda, \quad (3.1)$$

where $\Delta\lambda=1$ nm, and $\langle a_{\text{ph}} \rangle$ (m^{-1}) is designated optical-biomass index (see Garver and Siegel, 1994). For comparison with other works, the phytoplankton absorption spectra will be also normalized to the sum of chlorophyll plus pheopigments concentration (C , mg m^{-3}), hereafter denominated C -specific phytoplankton spectra ($a_{\text{ph}}^*(\lambda)$, $\text{m}^2 \text{mg}^{-1}$).

3.6.1 Hydrography and chlorophyll concentration in the different size ranges and main groups of organisms

3.6.1.1 Off the Oregon coast

The surface waters off the Oregon coast are influenced by coastal upwelling and freshwater outflow from the Columbia River, which in turn affects the mixed-layer depth, the concentration of nutrients (Thomas and Strub, 1989), and colored dissolved organic mater (CDOM) in these waters. During the cruise in September of 1994, a gradient of chl decreasing from the coast ($>20 \text{ mg m}^{-3}$) to open ocean ($>0.2 \text{ mg m}^{-3}$) was observed, accompanying an increase of the mixed layer depth (Figure 3.3). In some stations in the mid-shelf, however, a pycnocline was not clearly distinguished in the upper 50 meters, and in these stations chl was low (Figure 3.3B).

The relative contributions of the 4 different size classes to the total chl are illustrated by lines relating chl in each size class to the total (Figure 3.4). Note that in this data set, picoplankton chl remains approximately constant and the variability in total chl is explained by changes in the larger size classes, thus illustrating well the hypothesis that different phytoplankton communities are formed due to the addition of bigger cells (cf. Yentsch and Phinney, 1989). Although in Figure 3.4 (and in similar ones made for the data collected in other cruises) a linear regression was applied on the log-transformed chl data, the equations and coefficients of determination are not shown, because the total and the size fractionated chl are not independent variables (see Table 3.2) and the statistical relationships are compromised.

Flow cytometric and microscopic analysis indicated that each of the size fractions was dominated by distinct groups. Picoplankton was dominated by *Synechococcus* spp. and *Prochlorococcus* spp., although the latter was not detected in some coastal stations. Ultraplankton was dominated by small unidentified flagellates and cryptomonads. Both nanoplankton and microplankton cell sizes were dominated by chain-forming diatoms,

Table 3.2 Physical separation of samples into 4 size fractions for chlorophyll *a* and particulate absorption, as determined by differential filtration. Filtrates from 20, 5 and 2 μm Poretics® polycarbonate filters, filtered either by gravity or very low pressure, were concentrated onto GF/F filters. The concentration of each size class was determined following the second column.

Name	Operational Definition	Size Ranges
total	whole sample	all sizes
microplankton	total minus filtrate of 20 μm	bigger than 20 μm
nanoplankton	filtrate 20 μm minus filtrate of 5 μm	5 to 20 μm
ultraplankton	filtrate of 5 μm minus filtrate of 2 μm	2 to 5 μm
picoplankton	filtrate of 2 μm	less than 2 μm

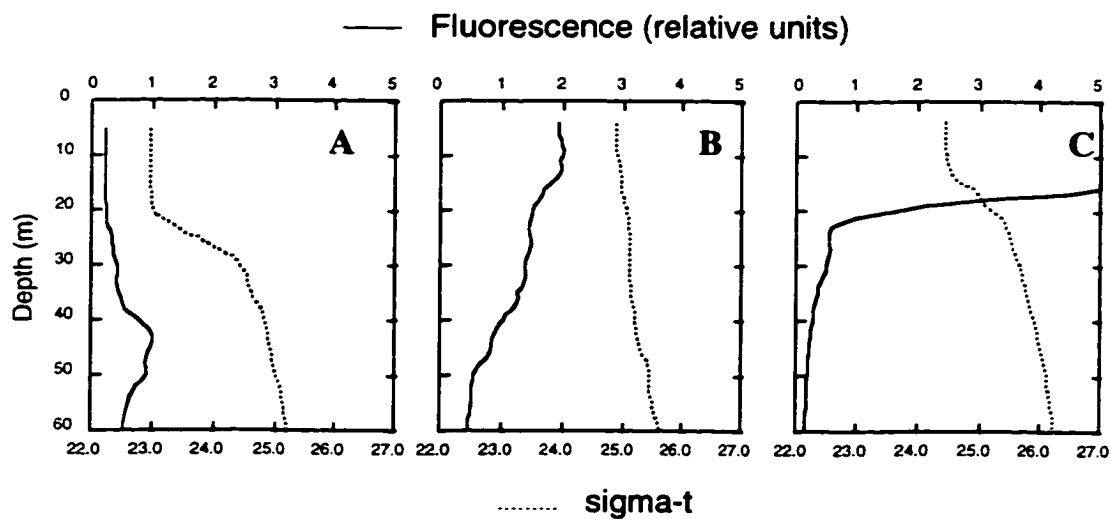


Figure 3.3 Selected vertical profiles of sigma-t (dotted line) and fluorescence in relative units (solid line) for the upper 60 meters during the cruise off the Oregon coast. **A)** Open ocean (surface chl $< 0.3 \text{ mg m}^{-3}$). **B)** Mid shelf (surface chl $< 1 \text{ mg m}^{-3}$). **C)** Coastal waters (surface chl $> 10 \text{ mg m}^{-3}$). Note that the fluorometer was off scale in the upper 15 m.

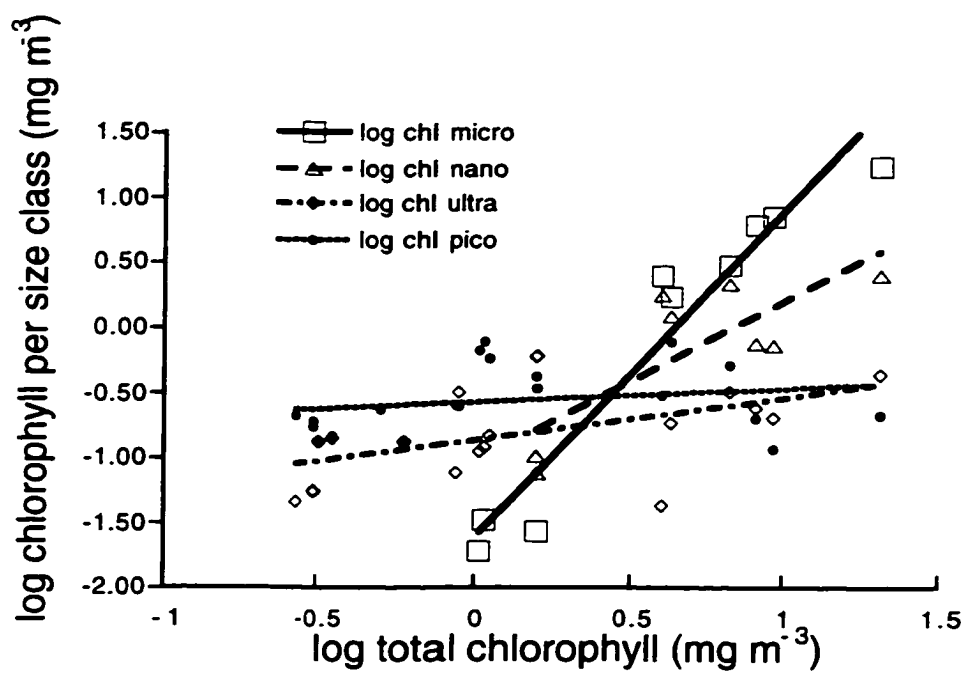


Figure 3.4 Chlorophyll size-fractions (see Table 3.2) versus total chlorophyll during the cruise off Oregon in 1994. Samples are from surface (20 stations). Note that concentrations are in log scale. Lines are linear regressions on log-transformed data, and are included to illustrate trends only. Coefficients of determination and fit parameters are not shown, as size fractions are not independent of total chlorophyll.

from genera *Chaetoceros* and *Leptocylindrus*, and *Pseudo-nitzschia* and *Lauderia*, respectively.

The diverse groups of phytoplankton present off Oregon during this cruise were reflected in the variety of spectral shapes of the phytoplankton absorption (Figure 3.5A). When whole samples were grouped according to the dominant chl size fractions in that sample, a strong indication was given that size was a major factor controlling the shape of the phytoplankton absorption spectra in this data set. Note, however, the high variability where the picoplankton size fraction was most important. The degree of variance among and within groups was tested with a one-way analysis of variance (Kruskal-Wallis). This non-parametric test does not assume that the samples are normally distributed or that the variance within each group is the same. The differences among the groups were significant at the 0.05 level in almost all wavelengths from 400 to 700 nm, except for the range between 502 and 507 nm (see discussion). A parametric one-way anova test yielded the same results.

The same procedure used to separate chl fractions was used to separate particulate absorption. The goal was to compare the shapes of phytoplankton absorption in each fraction without the influence of the other size fractions (Figure 3.5B), as whole samples dominated by large size fractions will include the smaller sizes. Results from sample of phytoplankton absorption separated in size fractions were similar to those from simply grouping whole samples according to the most important chl fraction. Note also that the variability within each size range comparatively increased, particularly in the smaller size fractions. This is probably a result of errors associated with the filter pad method. This method is very sensitive to the amount of material concentrated on the filters, and the fractionation produced very diluted samples, which in turn generated high instrument noise and statistical uncertainties in the beta correction (Mitchell, 1990). In fact, some of the fractionated samples had to be eliminated from the data set due to the high noise. The criterion for elimination was applied through visual inspection: fractionated spectra lacking the two main characteristic peaks of chlorophyll *a* absorption (i.e., around 436

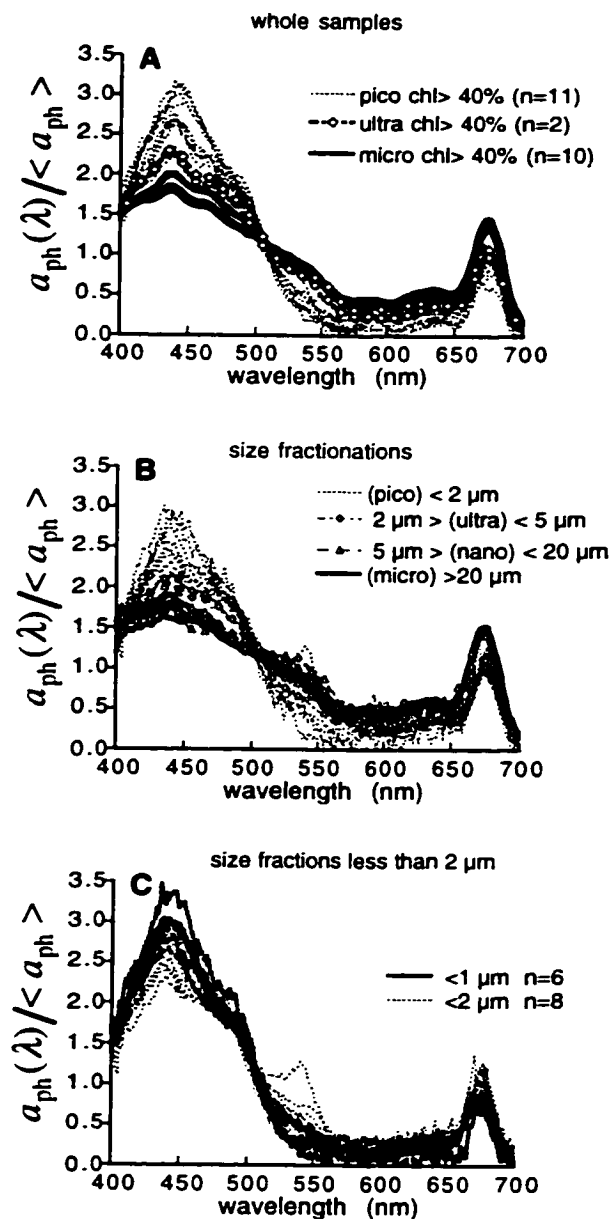


Figure 3.5 A) Phytoplankton absorption spectra measured in whole surface samples during the Oregon cruise. Spectra were normalized to the average phytoplankton absorption between 400 and 700 nm. Legend indicates the dominant chl size fractions (i.e., more than 50% when two size ranges were present or more than 40% when 3 or more size ranges were present). B) Phytoplankton absorption spectra measured directly for different size fractions collected on GF/F filters (see Figure 3.1 and Table 3.2). C) Comparison of absorption for size fractions using 1 µm and 2 µm filters.

and 675 nm) when these peaks were observed on the respective whole samples, were not included in Figure 3.5B.

As a way to examine the variability in the picoplankton fraction in more detail, when a population of *Prochlorococcus* was detected in the flow cytometer samples (which were being analyzed in real time), filters with 1 μm pore in diameter were also used in the fractionation. The intention was to separate the influence of *Prochlorococcus* spp. (average diameter less than 1 μm) from the influence of *Synechococcus* (average diameter bigger than 1 μm), the two main components of the picoplankton fraction. By comparing these two fractions, part of the variability found in the stations dominated by picoplankton (Figure 3.5C) could be attributed to different proportions of these two groups and, thus, their respective sizes and pigment composition. The expected peak in the green region, due to phycoerythrin, was clearly found only in samples from the chl maximum (not shown) and one station in the proximity of the Columbia river plume.

3.6.1.2 Southern Bering Sea

The main oceanographic features influencing the southeastern Bering Sea are the mid-shelf and shelf-break fronts, formed and maintained by topographical features, tides and wind mixing (Coachman, 1986). The fronts create 3 distinct environments on the shelf: coastal, middle shelf and outer shelf (see Springer *et al.*, 1996 and references therein). These environments have distinct seasonal features influencing the succession of phytoplankton communities among them (Kocur, 1982). Eddies, related to the flow of the Bering Slope Current, can also be present on the shelf at times (Verkhunov and Tkachenko, 1992; Schumacher and Stabeno, 1994), also affecting nutrient input, mixing depth, and in turn, phytoplankton composition.

During the cruise in April 1996, sampling was concentrated in the middle shelf especially at two points: one at each side of the 100 m isobath. Shallow waters were characterized by cold temperatures, weak vertical stratification and low chl ($<1 \text{ mg m}^{-3}$) (Figure 3.6A). In deeper waters, a surface mixed layer of 40 m was observed and chl was

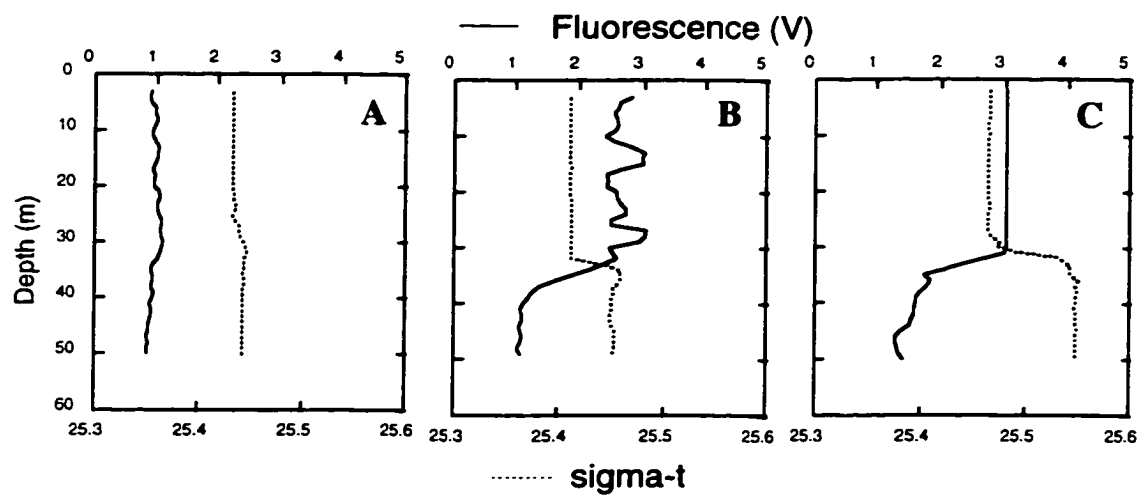


Figure 3.6 Selected vertical profiles of sigma-t and fluorescence (relative units) for the upper 60 meters during the cruise in the Bering Sea in April 1996 (see Figure 3.2). **A)** Mid-shelf inside the 100 meters isobath (surface chl $<1 \text{ mg m}^{-3}$). **B)** Mid-shelf outside the 100 meters isobath (surface chl $>1 \text{ mg m}^{-3}$). **C)** Station by Unimak Pass (surface chl $>3 \text{ mg m}^{-3}$).

between 1 and 2 mg m⁻³ (Figure 3.6B). High chl (>3 mg m⁻³) were found in the coast near the Unimak Pass (see Figure 3.2B), with mixed layers of 30 meters (Figure 3.6C).

Size fractions of chl (Figure 3.7) showed a different trend from the one observed during the Oregon cruise. According to our criteria (Figure 3.1), the picoplankton fraction never dominated the total chl (i.e., maximum concentration was smaller than 50% of the total). At stations where chl was low, picoplankton and nanoplankton contributed approximately with equal concentrations. Picoplankton chl also tended to increase slightly with total chl. The increments in the total chl, however, were mainly explained by increases in ultra and microplankton, with the nanoplankton fraction having less importance. Although no samples for floristic analyses were available during this cruise, fresh samples from 20 µm zooplankton net casts could be observed. This fraction was composed of chain-forming diatoms with small cell size (mainly *Chaetoceros* spp.). The ultraplankton is probably dominated either by isolated diatoms or fragments of chains, based on the work by Kocur (1982) who compared the phytoplankton community in the 3 main provinces of the shelf before and after the onset of the Spring bloom. However, there are no means to confirm the taxon in this fraction. Thus, this group will be treated as “unknown” with respect to taxonomic composition, but it will be considered for the comparisons among different sizes.

Variability in absorption spectra during BS96 was smaller than for the Oregon cruise, and grouping the spectra measured on whole samples according to the dominant chl size fraction did not allow for a clear distinction among different size fractions (Figure 3.8A). Both non-parametric and parametric one-way ANOVA tests indicated that the spectra were not significantly different. Although taxonomic changes cannot be accounted for, the little information available suggests that changes in cell size in this data set were not as remarkable as those encountered during the Oregon cruise: when microplankton fraction dominated chl, phytoplankton was composed of chain-forming diatoms containing small (nano-sized) cells. Normalized size-fractionated absorption coefficients were even noisier than the ones measured during the Oregon cruise (not

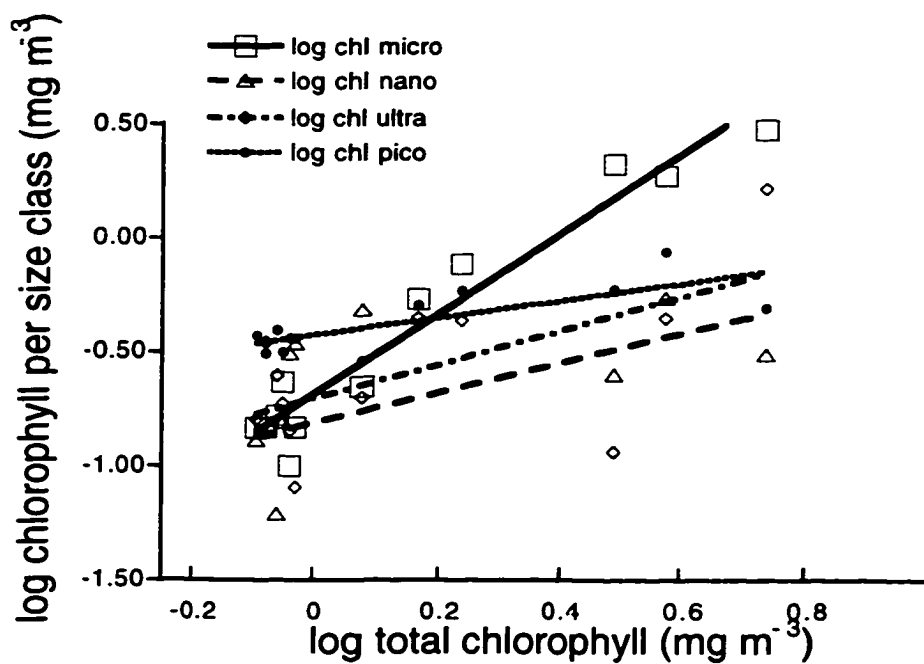


Figure 3.7 Chlorophyll size-fractions (see Table 3.2) versus total chlorophyll during the cruise in the Bering Sea in April 1996. Samples are from surface (12 stations). Note that the concentrations are in log scale. Lines are linear regressions on log-transformed data, and are included to illustrate trends only. Correlation coefficient and parameters are not shown, as size fractions are not independent of total chlorophyll.

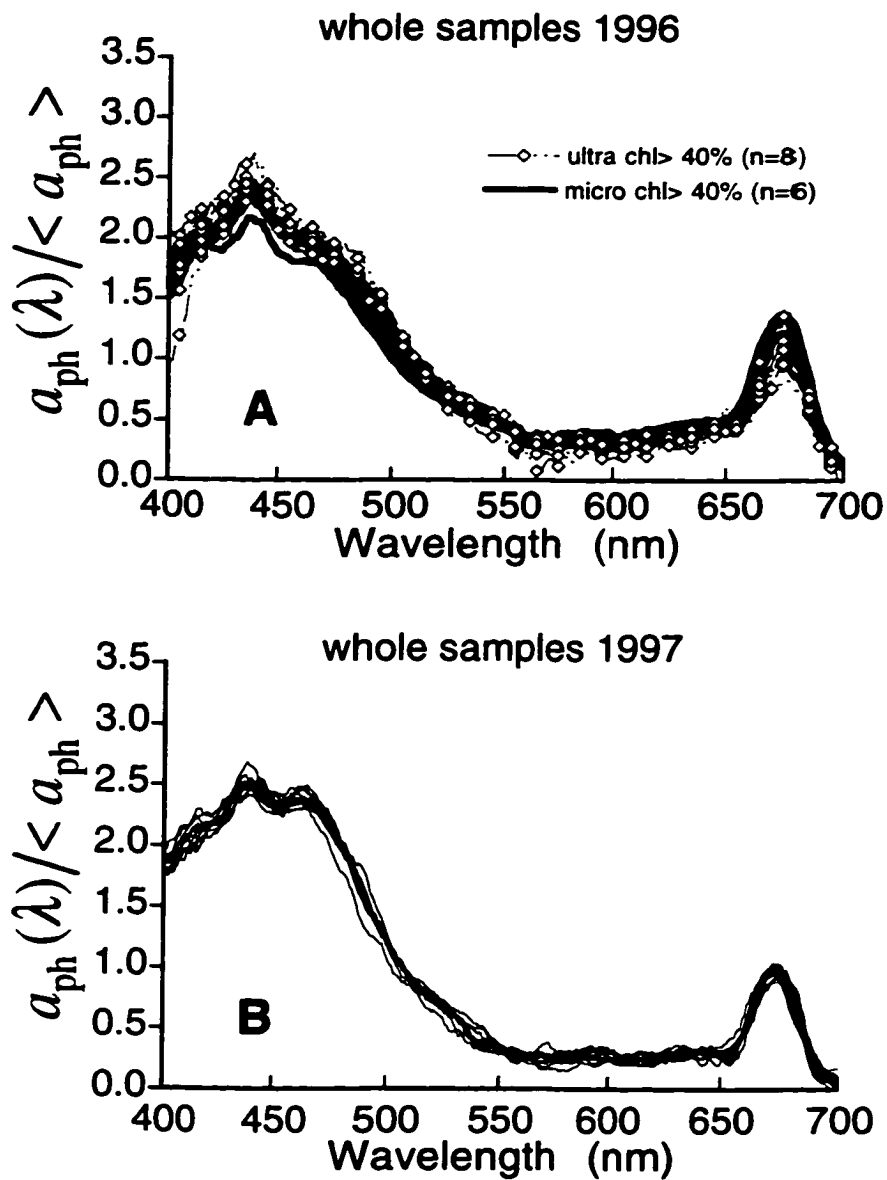


Figure 3.8 Shape of phytoplankton absorption spectra for surface samples collected in the southern Bering Sea. Spectra were normalized to the average phytoplankton absorption between 400 and 700 nm. **A)** April 1996. Legend indicates the dominant chlorophyll size range. **B)** June 1997.

shown), but similar trends and shapes as in Figure 3.8A were observed for micro and ultraplankton fractions.

The data set from the cruise in June 1997 was obtained in the area highlighted in Figure 3.2B, during transects through an anticyclonic eddy. The position of the eddy was monitored by a combination of drifters and satellite imagery (TOPEX) computing sea surface height (Dr. P. J. Stabeno, pers. comm.). Chlorophyll in the eddy varied from about 2 to 7 mg m⁻³. No samples for size fractionation were taken during this cruise and microscopic analyses indicated the presence of small flagellates and some chain-forming diatoms containing cells of nano to micro size. Nevertheless, a large number of colonies of what was believed to be the prymnesiophyte *Phaeocystis* spp., were observed in surface waters (J. J. Cullen, pers. comm.), and it is possible that the colonies were poorly preserved for the microscopic analysis. Data from a limited number of samples for pigments using high performance liquid chromatography analysis collected in this area (J. P. Parkhill, unpublished results) showed high ratios of 19-Hexanoyloxyfucoxanthin to chlorophyll *a* and also chlorophyll *c*₃, suggesting the presence of prymnesiophytes (Jeffrey and Wright, 1994). Thus, a single "community" will be characterized for these data: ultraplankton dominated by a prymnesiophyte (e.g., *P. pouchetti* have cells between 4 and 8 μm in length (Tomas, 1997)).

Normalized phytoplankton absorption spectra for stations in the proximity of the eddy (Figure 3.8B) were remarkably similar. A t-test for all wavelengths indicated that all spectra have the same mean value at the 0.05 level of significance. The spectra suggested abundance of cells with a relatively low degree of pigment packaging, and a relatively high absorption around 460–470 nm, consistent with high concentrations of carotenoids (see Bidigare *et al.*, 1990). An absorption peak in this waveband is consistent with the presence of fucoxanthin, 19-Hexanoyloxyfucoxanthin and chlorophyll *c*₃ (see Jeffrey *et al.*, 1997), but because their absorption peaks overlap, it is difficult to assign the observed peak to a unique pigment. In addition, the maximum absorption of individual accessory

pigments *in vivo* will be slightly shifted in wavelengths, when compared to measurements using organic solvents (as reported by Jeffrey et al., (1997)).

3.6.1.3 Bedford Basin

Bedford Basin is an enclosed embayment with an area of approximately 17 km² (Figure 3.21C). It is connected to the Atlantic Ocean by a channel with a shallow sill of 20 meters. Freshwater runoff, tides and winds regulate the exchange of waters between the Basin and the ocean (Platt and Irwin, 1971). Due to its location in an urban area, the Basin receives large inputs of nutrients, particulate and dissolved organic matter from both land drainage and the untreated sewage discharge. Because of that, for most of the year (except for blooms in Spring, Fall and Summer), the Basin is an optically complex environment, corresponding to case 2 (Morel, 1988) coastal waters.

3.6.1.3.1 Summer experiments

In August 1992, August 1993 and August 1996, intensive experiments were conducted for at least 3 days, with samples collected during early morning, mid-day and late afternoon. All the samples were collected in a single point approximately in the middle of the Basin. During the Summer, Bedford Basin is a 2 layer system and the mixed layer depth will change by the influence of tides and wind.

In August 1992, microscopic analysis indicated that the dominant size fractions were ultra and nanoplankton, both dominated by naked flagellates from the classes Chlorophyceae, Cryptophyceae, Dinophyceae and Prymnesiophyceae, with diameters up to 8 µm. Diel changes in species composition were not substantial, and changes in chl were associated with increases in the numbers of flagellates. Few microplanktonic dinoflagellates were observed, always at depth.

In August 1993, the microscopic analyses were complemented with measurements of particle size, but no measurements of chl size fractions were available. Similar groups of species to the ones found in 1992 (ultra and nanoflagellates,

represented by a size mode centered at 6 μm) were present, together with two additional and distinct “populations” of dinoflagellates: a nanoplanktonic group dominated by the genus *Prorocentrum* (mode of 12 μm in diameter) and a microplanktonic group dominated by *Gonyaulax digitale* and *Dinophysis* spp. (mode of 35 μm in diameter). To make the particle size data consistent with the classification for different communities used before, the cell numbers measured in each size mode were converted into approximate chl values. For that, an intracellular chl for each group was assumed, by using data from monospecific cultures of species having similar sizes and taxonomical composition as the main species identified with the microscopic analyses (e.g., *Dunalliella tertiolecta*, *Prorocentrum minimum* and *Alexandrium tamarense*, representing ultra-flagellates, nano-dinoflagellates and micro-dinoflagellates), respectively. It is acknowledged that this calculation will likely overestimate the chl in each class, to the extent that natural cells are usually growing in higher light and lower nutrient concentration than cultures. Nonetheless, only relative concentrations are needed, and the sum of estimated chl in the three modes agreed relatively well with the measured total chl concentration in each station. Thus, estimated chl per size was used to classify the communities similarly to what was done in other cruises. During this experiment, diel changes in species composition at the surface, as well as chlorophyll concentrations, were a direct result of the vertical displacement of micro-size population of dinoflagellates. Three typical profiles were observed (Figure 3.9): a) a dense and thin layer found at depth, reaching at times chl above 100 mg m^{-3} , where microplanktonic dinoflagellates were found in large numbers; b) in the first two days of the experiment, this layer was entrained in surface waters by winds at mid-day, visibly changing the color of the water (Cullen *et al.*, 1994); and c) cells well dispersed in the mixed layer. In the last day, the nanoplanktonic dinoflagellates reached high numbers at the surface by late afternoon, whereas the microplanktonic population remained at depth. In August 1996, microscopic analyses were complemented by chl size fractionation. The results of the chl size fractionation (Figure 3.10) showed that the main size fraction at the surface was the ultra-

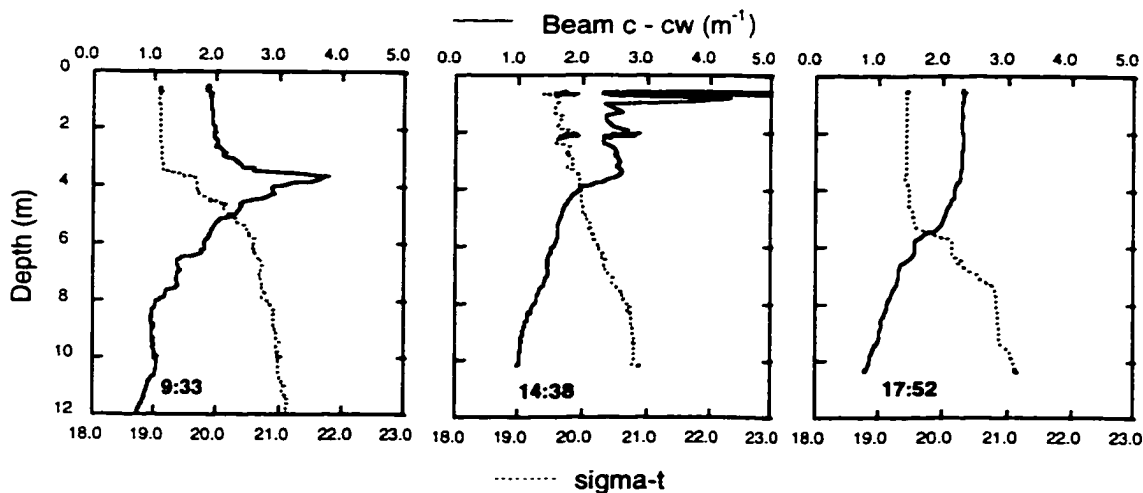


Figure 3.9 Three typical vertical profiles of sigma-t (dotted line) and beam attenuation minus attenuation by sea water, 0.367 m^{-1} (solid line), which was used as a proxy for total particle concentration during the intensive sampling in 1993 in Bedford Basin. Examples refer to August 18. Figures are identified with sampling time shown on the bottom of figures. At 9:33, a dense layer was detected at depth, related to large numbers of large dinoflagellates (mode of $32 \mu\text{m}$ in diameter) and surface chl ranged between 6 and 36 mg m^{-3} . At 14:38, the cells entrained in the surface due to wind mixing, and surface chl ranged between 27 and 135 mg m^{-3} . At 17:52 a well mixed upper layer was observed and surface chl ranged between 10 and 40 mg m^{-3} .

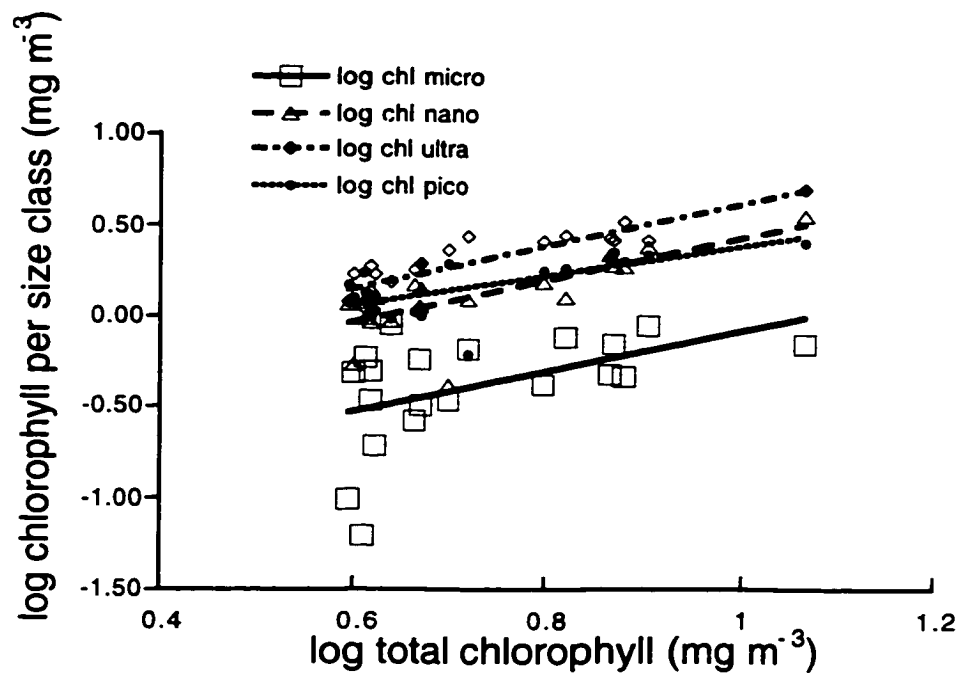


Figure 3.10 Chlorophyll size-fractions versus total chlorophyll during the Summer of 1996 in Bedford Basin. Data refer to samples from mixed layer ($n=21$). Note that concentrations are in log scale. Lines are linear regressions on log-transformed data, and are only illustrating the tendency.

and nanoplankton. Abundant phytoplankton groups present were ultra and nano-sized flagellates and a nano-sized silicoflagellate (*Dictyocha* spp.) was also present in high numbers in the last day of the experiment. The weather was very calm throughout the experiment and a chl maximum was observed at depth in the first two days, containing few micro dinoflagellates (*Prorocentrum* spp. and *Dinophysis* spp.). The picoplankton fraction was present in concentrations of about one order of magnitude higher than the ones found in Oregon and in the Bering Sea, and it also increased as total chl increased, thus, not remaining as a constant background. Although samples to identify picoplankton organisms were not taken during these experiments, the results of Li *et al.* (1998) done in the Basin during the same period, indicate that the picoplankton fraction was dominated by cyanobacteria, reaching concentrations of 10^5 to 10^6 cells ml^{-1} .

For simplicity, the normalized absorption coefficients observed during the three Summer intensive samplings in Bedford Basin are presented together (Figure 3.11). The spectra were grouped and averaged according to the communities defined above. The shape of the absorption coefficient for the distinct groups were very similar in the blue and green portions of the spectra, except during the red tide event (i.e., micro dinoflagellates) in the Summer of 1993, which showed relatively lower values. In the red tide spectra a slight shift in the red peak towards shorter wavelengths was observed. This is peculiar to some dinoflagellates as the peridinin-chlorophyll-protein complex peaks at 671 nm (see Johnsen *et al.*, 1994a).

3.6.1.3.2 Time Series from July to December 1996

During July to December 1996, a spectral radiometer buoy (TACCS) was moored in Bedford Basin (see details in chapter 2). During this period, the site was visited weekly, and water samples for absorption (particulate and dissolved fractions), chl (total and size fractions) and microscopic analysis were collected. In July, chain-forming diatoms (ultra-sized *Skeletonema* spp.) were observed. These were replaced by ultra-flagellates in August (see Summer experiments). Dinoflagellates were dominant in the

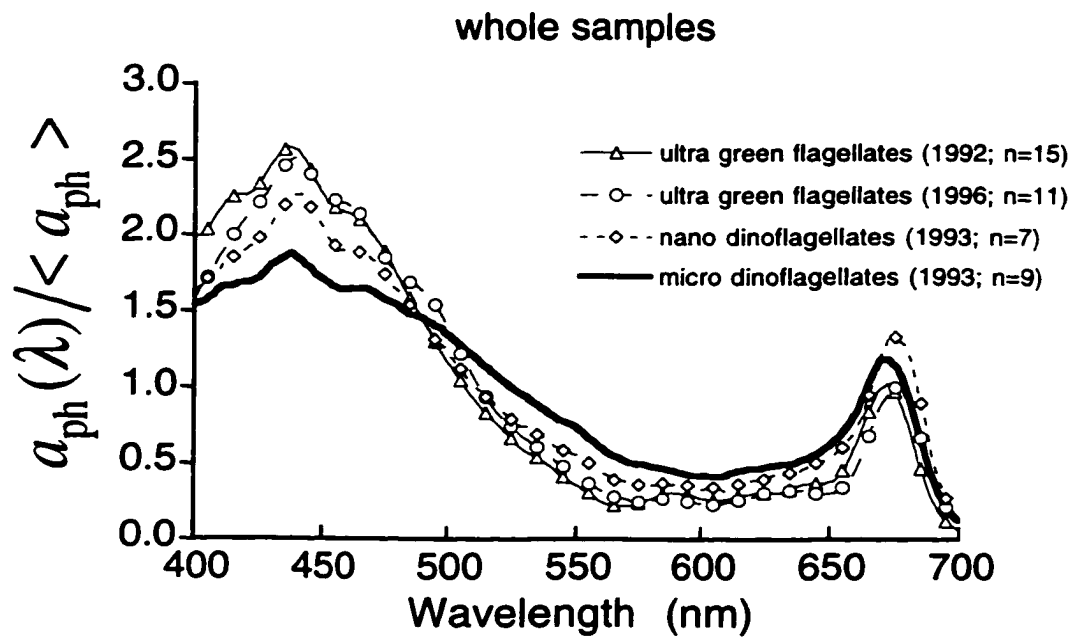


Figure 3.11 Spectral shape of phytoplankton absorption coefficient for whole water samples collected at the surface during the three intensive samplings in the summer in Bedford Basin. Legends indicate the communities characterized according to cell size and dominant group (see text). Lines are averages for the number of samples (n) indicated in the legend.

beginning of October, and were present in small numbers throughout the fall bloom, which was initially composed of chain-forming diatoms with small (ultra to nano) cell sizes (*Skeletonema* spp.), followed by the development of larger-sized diatoms (*Thalassiosira* spp.). Chlorophyll size-fractionation (Figure 3.12) shows the development and replacement of these communities by size. Intense rain periods (Figure 3.13) occurred in the Summer, which on one hand “disturbed” the blooms by flushing waters out of the Basin, and on the other, promoted growth of diatoms by the input of nutrients, especially silicates (see tables in Li *et al.*, 1998).

The changes in phytoplankton composition through time are reflected in normalized absorption coefficients, which are presented as averages according to our classification (Figure 3.14). Clear changes in packaging can be observed in the blue part of the spectra, and throughout July, the chain forming diatoms present showed an additional peak (not related to chlorophyll *a*) in the blue end (centered around 412 nanometers), possibly related to high concentrations of U.V. protectant pigments (Yentsch and Yentsch, 1982). The presence of these pigments could affect bio-optical models, as 412 nm is commonly used to interpret CDOM absorption.

3.6.2 Influence of the different communities on the spectral shape of phytoplankton absorption

Combining all the cruises and intensive sampling, 16 communities were characterized (Table 3.3), some of them being represented in more than one environment. These communities were named after the cell size range and genera or group of the dominant organisms present. “Repeated” communities were numbered sequentially, according to sampling date. By grouping the communities according to the size range of the dominant organism fraction (Figure 3.15), one can compare the relative influence of both size and taxon, which is one of our goals. It is important to keep in mind, however, that as our classification refers to ranges of size, there is still a degree of variability in

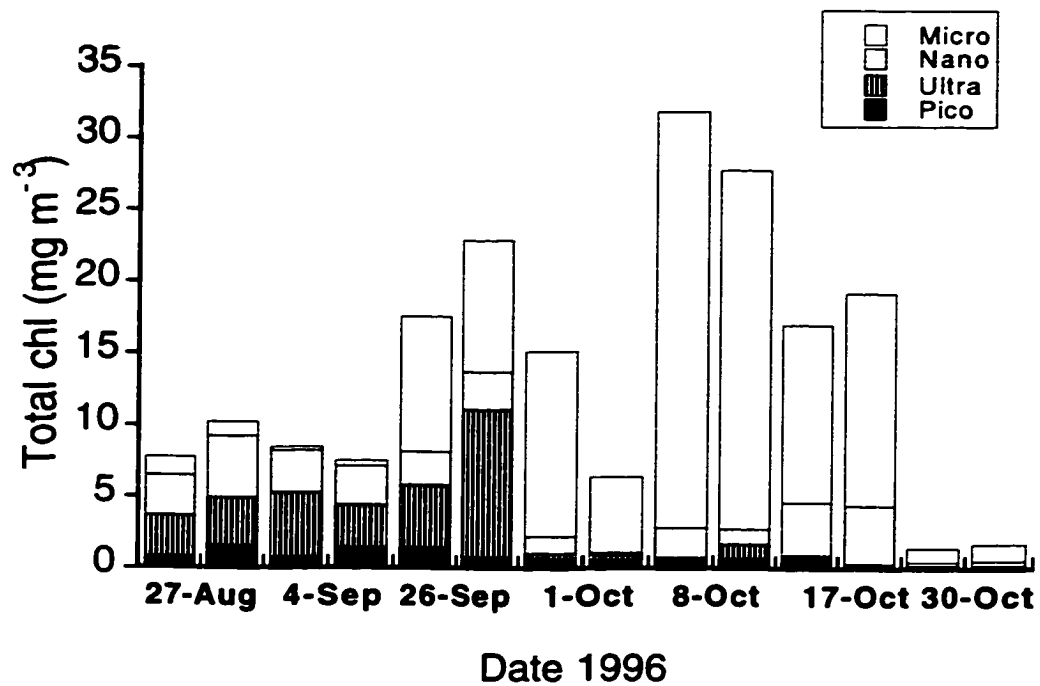


Figure 3.12 Weekly chl size-fractions (see Table 3.2) as proportions of total chl during the time series in 1996 in Bedford Basin, including the fall bloom. Samples from 1 and 3 meters, respectively, for each day.

size within each group. For example, the nano chain-forming diatoms found in Bedford Basin in the Summer (N-cdf2) and in the Bering Sea (N-cfd1) were close to the lower limit attributed to this size range (i.e., 5 μm), while the nano-dinoflagellates found in 1993 during the red tide in Bedford Basin (N-din) were close to the upper limit of this range (i.e., 20 μm). The more noticeable differences within sizes were found in the picoplankton fraction (Figure 3.15A). Nevertheless, the differences in spectral shape between the communities dominated by *Prochlorococcus* and by *Synechococcus* could also be related to their size (see results in Figure 3.5C). The distinction between the spectra classified as ultra (Figure 3.15B) and those classified as nanoplankton (Figure 3.15C) was less evident, except in the samples collected in the Bering Sea in 1997 (where *Phaeocystis* spp. was present), which had a distinct peak centered around 465 nm. In addition, samples dominated by ultra-flagellates during the Oregon cruise showed a peak centered around 545 nm which was associated with high numbers of *Synechococcus* spp. (flow cytometer measured 1.59×10^5 cells ml^{-1}), and which probably results from a high concentration of phycoerythrin (see Moore *et al.*, 1995). In the nanoplankton fraction (Figure 3.15C), peaks centered around 412 were present when *Skeletonema* spp. was the dominant organism. This was more noticeable during the Summer in Bedford Basin. In the microplankton fraction (Figure 3.15D), differences between diatom-dominated and dinoflagellate-dominated spectra were very small in the visible wavelengths. Figure 3.15E shows the average spectrum for each cell size range, and illustrates the main trends; as the size of the dominant organism increases, the spectra flatten consistently with the increase in pigment packaging.

For comparison with previous works, the phytoplankton absorption spectra of the 16 communities were also normalized to the concentration of chl plus pheopigments (Figure 3.16). It is noteworthy that, although the same trends observed in Figure 3.15 were repeated, the variability within each cell size range was somewhat higher when reported as $a_{\text{ph}}^*(\lambda)$. This may be attributed to a number of causes. Biases in the measurement of chl plus pheopigments due to accessory pigments can either under or overestimate

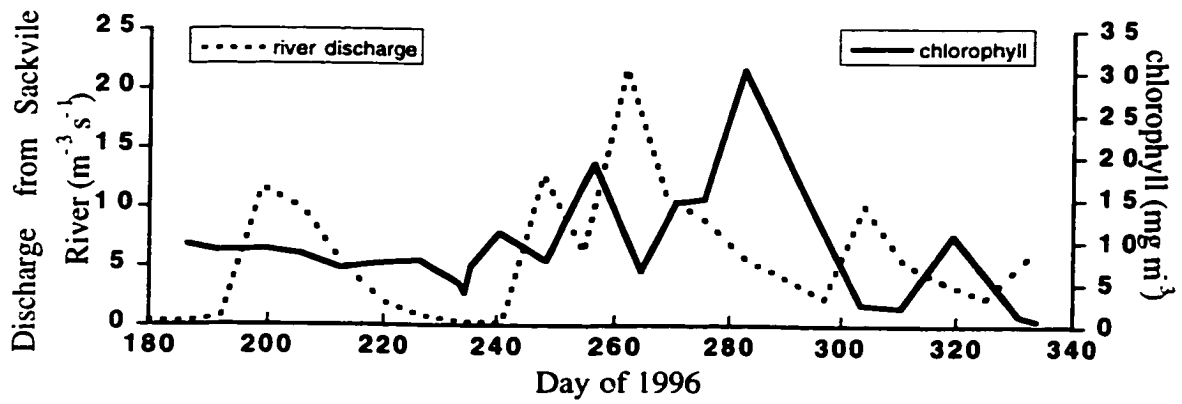


Figure 3.13 Weekly river discharge (Sackville River, data from Environment Canada) and surface chlorophyll concentration during the time series in Bedford Basin in 1996 (July to December).

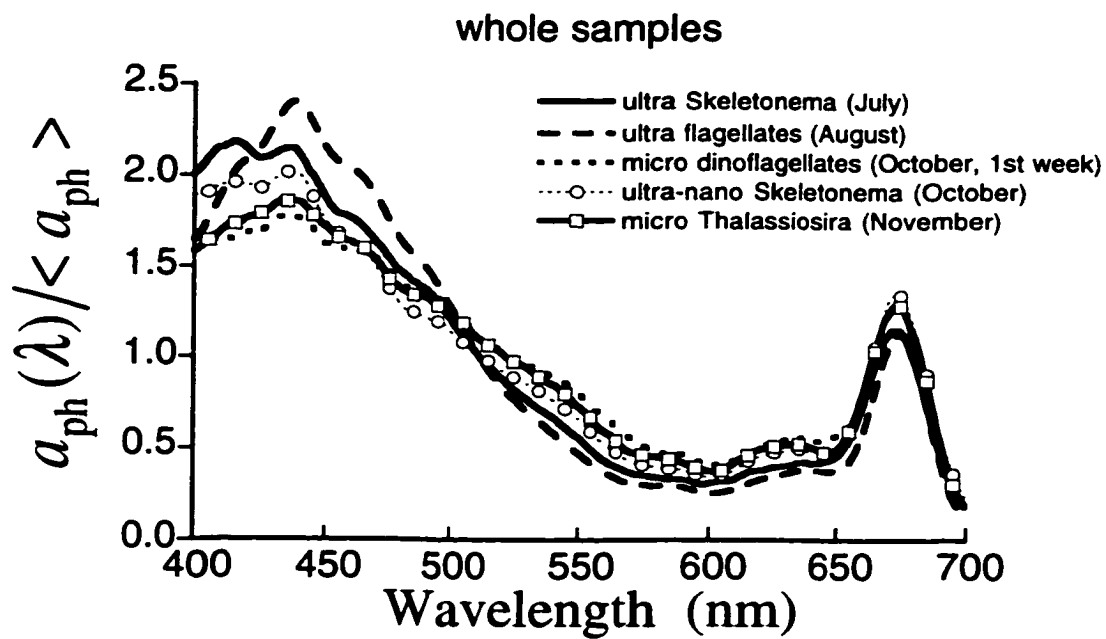


Figure 3.14 Spectral shape of phytoplankton absorption coefficient for surface samples collected in from July to November 1996 in Bedford Basin. Legends indicate the communities characterized according to size range and dominant group (see text). Lines are averages.

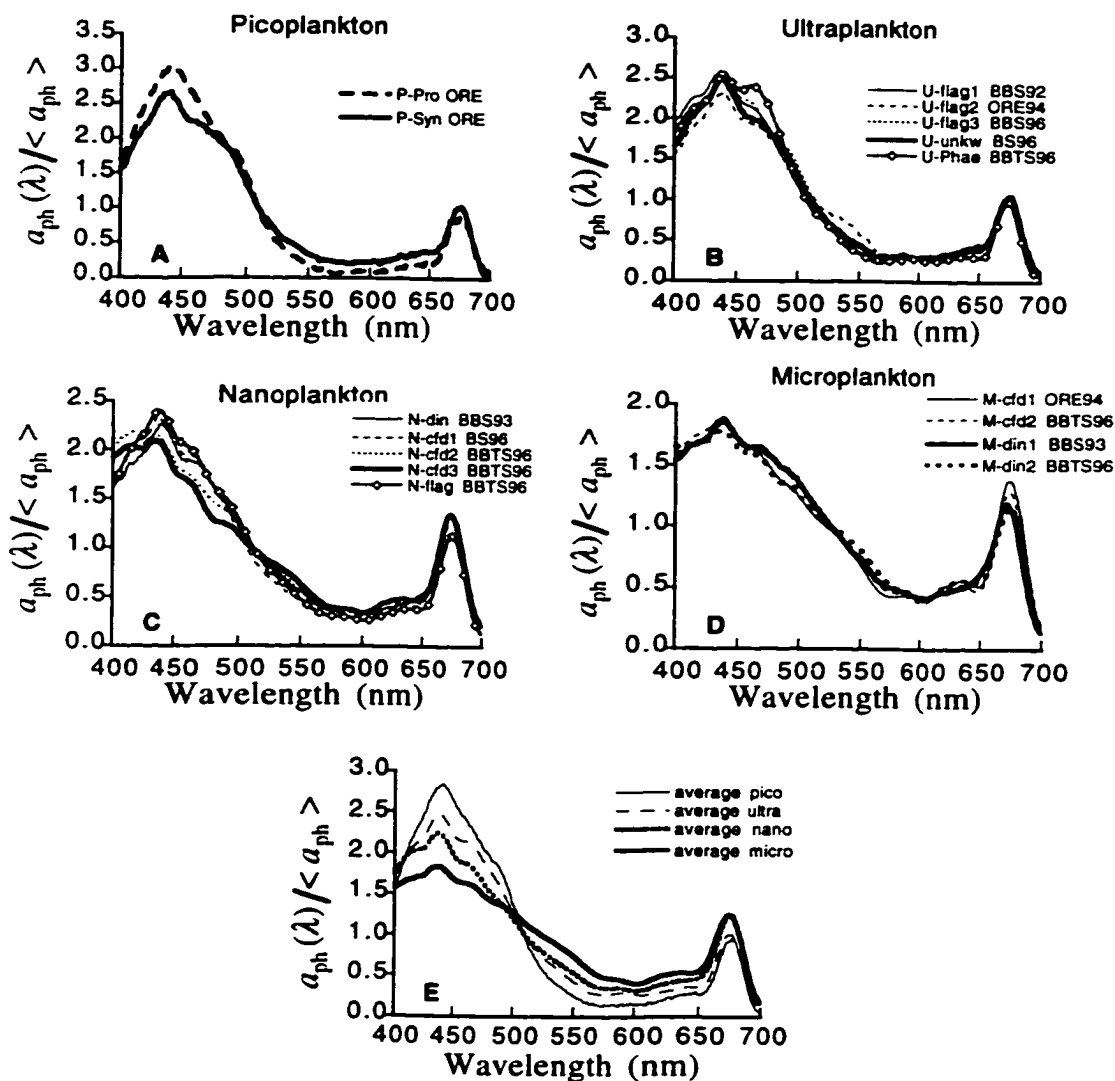


Figure 3.15 Spectral shape of phytoplankton absorption coefficient for whole-water surface samples collected in all experiments, according to cell size range of the dominant organism (see Figure 3.1). **A)** Picoplankton. **B)** Ultraplankton. **C)** Nanoplankton. **D)** Microplankton. **E)** Average for each cell size. Legends indicate the communities characterized in Table 3.3 and the cruises: ORE (off Oregon coast); BS96 (Bering Sea April 1996); BS97 (Bering Sea 1997), BBS92, BBS93 and BBS96 (intensive samplings in Bedford Basin in 1992, 1993 and 1996, respectively) and BBTS96 (time series in Bedford Basin from July to November 1996). See Table 3 for number of samples. CFD stands from chain-forming diatoms. Note changes in the scale on Y-axis.

Table 3.3 Summary of the distinct communities of phytoplankton characterized in the combined data sets. Name describes cell size range (P is pico; U is ultra; N is nano and M is micro) and species or groups of the dominant organism. N.S. is number of samples, na means not available. For details on cruises, refer to Table 3.1.

Name	Cruise	N.S.	Dominant chl size fraction	Chl conc. Range (mg m ⁻³)	Main genera or group	Dominant cell size fraction	Comments
P-Pro	ORE94	10	pico	less than 0.3	<i>Prochlorococcus</i>	pico	flow cytometer
P-Syn	ORE94	6	pico	0.5 to 0.6	<i>Synechococcus</i>	pico	flow cytometer
U-flag1	BBS92	12	na	2.5 to 7.5	flagellates	ultra	microscope
U-flag2	ORE94	2	ultra	1.5 to 1.7	cryptomonads	ultra	flow cytometer
U-flag3	BBS96	14	ultra	4 to 8	flagellates	ultra	microscope
U-unkw	BS96	5	ultra	0.5 to 0.7	unknown	assumed ultra	na
U-Phae	BS97	20	na	2 to 7	<i>Phaeocystis</i>	assumed ultra	HPLC and literature
N-din	BBS93	14	nano	6 to 36	<i>Prorocentrum</i>	nano	Coulter
N-cfd1	BS96	5	micro	0.9 to 2.3	<i>Chaetoceros</i>	nano	microscope
N-cfd2	BBTS96	5	na	9 to 10	<i>Skeletonema</i>	nano	microscope
N-flag	BBTS96	5	nano	6.5 to 8	flagellates	nano	microscope
N-cfd3	BBTS96	3	micro	17 to 30	<i>Skeletonema</i>	nano	microscope
M-din1	BBS93	5	micro	27 to 135	<i>Gonyaulax</i>	micro	Coulter
M-cfd1	ORE94	12	micro	8 to 20	<i>Pseudo-nitzschia</i> and <i>Lauderia</i>	micro	microscope
M-din2	BBTS96	4	micro	8 to 16	<i>Prorocentrum</i>	micro	microscope
M-cfd2	BBTS96	5	micro	3 to 15	<i>Thalassiosira</i>	micro	microscope

$\alpha_{ph}^*(\lambda)$ (see methods). Different degrees of activity of chlorophyllases (especially where diatoms dominate the community (Jeffrey and Hallegraeff, 1987)) can also produce biases, because, in general, the time required for concentrating samples for particulate absorption is always much longer than that for chl samples. The influence of the filter pad method itself, however, cannot be overruled. The distinct amounts of material concentrated on the filters in each situation (i.e., combination of the volume filtered and the amount of local phytoplankton) will be corrected by a different beta factor, and uncertainties will be higher for dilute samples.

3.6.2.1 Quantification of the effects of cell size

A simple visual inspection of Figures 3.15 and 3.16 suggests that, despite the potential influence of the different accessory pigments on the phytoplankton absorption coefficient, a metric descriptor of the size of the dominant organism can be an effective parameter for explaining the changes in shape of the phytoplankton absorption coefficient in whole phytoplankton assemblages. If the dominant cell size range described much of this variability, it could be as a proxy for many changes acting together; particularly pigment packaging and the concentration and composition of accessory pigments (see chapter 2). Therefore, when we refer to the effects of cell size, we are actually referring to the combined effects of a group of covariant variables.

In order to evaluate the effect of cell size quantitatively, 301 multivariate regression analyses were performed, one for each wavelength, using normalized absorption for each wavelength from the 16 communities (Figure 3.15) as variables. The following linear model was assumed:

$$\hat{y}(\lambda) = \beta_0(\lambda) + \beta_1(\lambda)x_1 + \beta_2(\lambda)x_2 + \beta_3(\lambda)x_3, \quad (3.2)$$

where $\hat{y}(\lambda)$ is the predicted value for the normalized absorption at each wavelength, x_1 to x_3 are “dummy” variables identifying the size range to which the observed spectrum

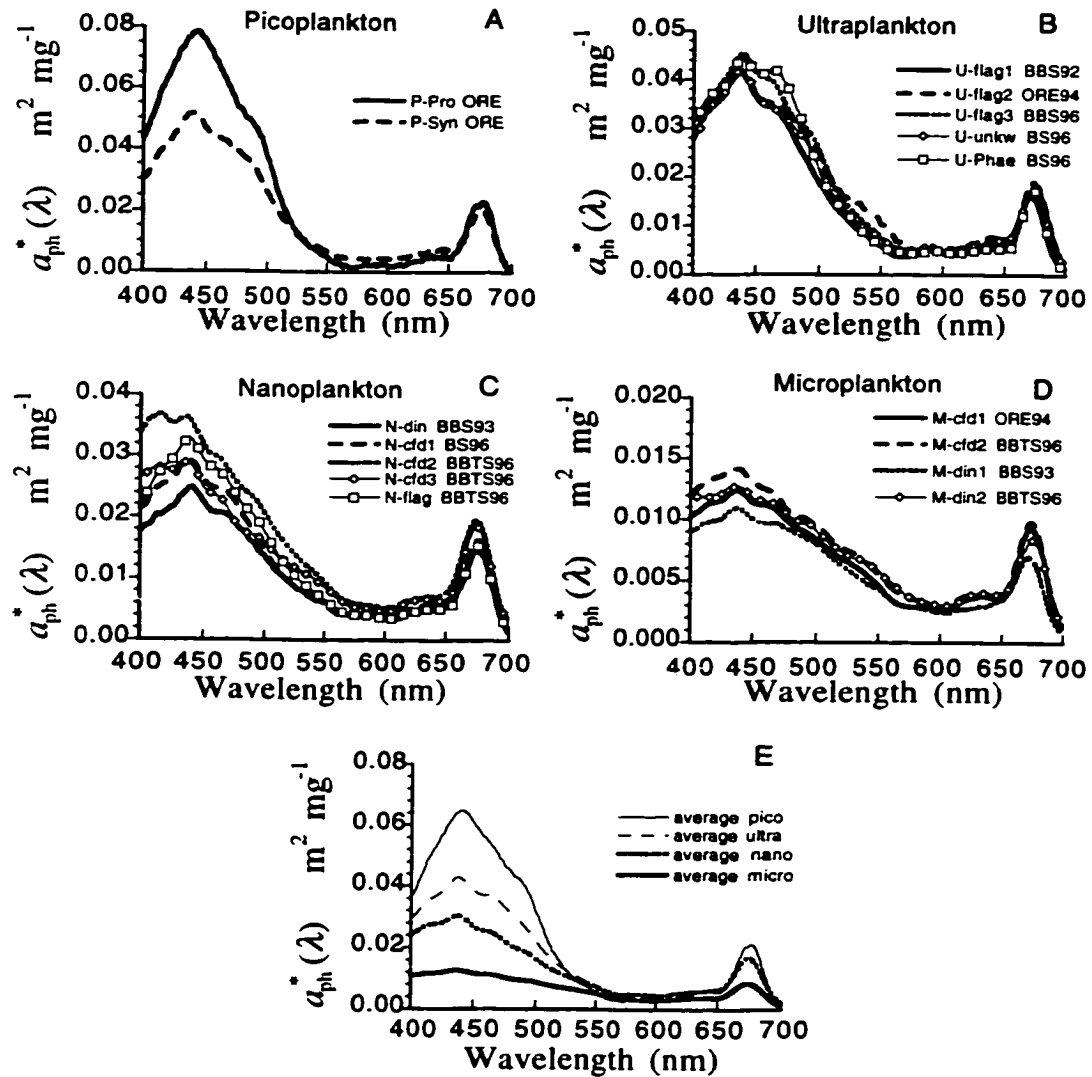


Figure 3.16 Same as in Figure 3.14 except that phytoplankton absorption spectra were normalized by chl plus pheopigments. Note changes in the scale on Y-axis.

belongs, and $\beta_0(\lambda)$ to $\beta_3(\lambda)$ are the parameters to be estimated by the regression. The identification of the size range by the “dummy” variables is achieved as follows: the spectra classified as pico have x_1 , x_2 and x_3 set to zero, the spectra classified as ultra have x_1 set to one while x_2 and x_3 are zero; the spectra classified as nano have x_2 set to one while x_1 and x_3 are zero, and the spectra classified as micro have x_3 set to one while x_1 and x_2 are zero. Thus, the use of the dummy variables will either include or exclude the pertinent parameters from the model, making the multiple regressions analyses similar to analyses of variance. The regressions yield the expected spectrum for each of pre-defined size classes, because the intercept, $\beta_0(\lambda)$, corresponds to the expected spectrum for pico, and $\beta_1(\lambda)$ to $\beta_3(\lambda)$ correspond to the difference between $\beta_0(\lambda)$ and the expected spectra for ultra, nano and micro, respectively. The expected shape for each size (Figure 3.17A) is in fact equivalent to the average spectrum for each size shown in Figure 3.15E. The initial variance among the 16 normalized spectra is shown in Figure 3.17B, along with the coefficient of determination (r^2) at each wavelength (Figure 3.17C), that represents the variance in the absorption coefficient explained by the model at each wavelength. These results strongly suggest that the dominant cell size in the community can be used as a parameter explaining most of the variability in the shape of the absorption coefficient for distinct phytoplankton communities. Note that the values for r^2 are relatively low for wavelengths around 500 nm, but this is rather a result of the low variability in the original spectra than a problem with the model.

3.6.2.2 Estimation of a “size” parameter from the phytoplankton absorption coefficient

The results of the previous section leads one to question whether the normalized absorption spectra for all 16 phytoplankton communities could be “reconstructed” with a linear combination of two “constant” spectra representing the smallest (average of all samples dominated by *Prochlorococcus* spp.) and largest (average of all the samples dominated by microplakton-sized organisms) cell sizes found in our data set, so that:

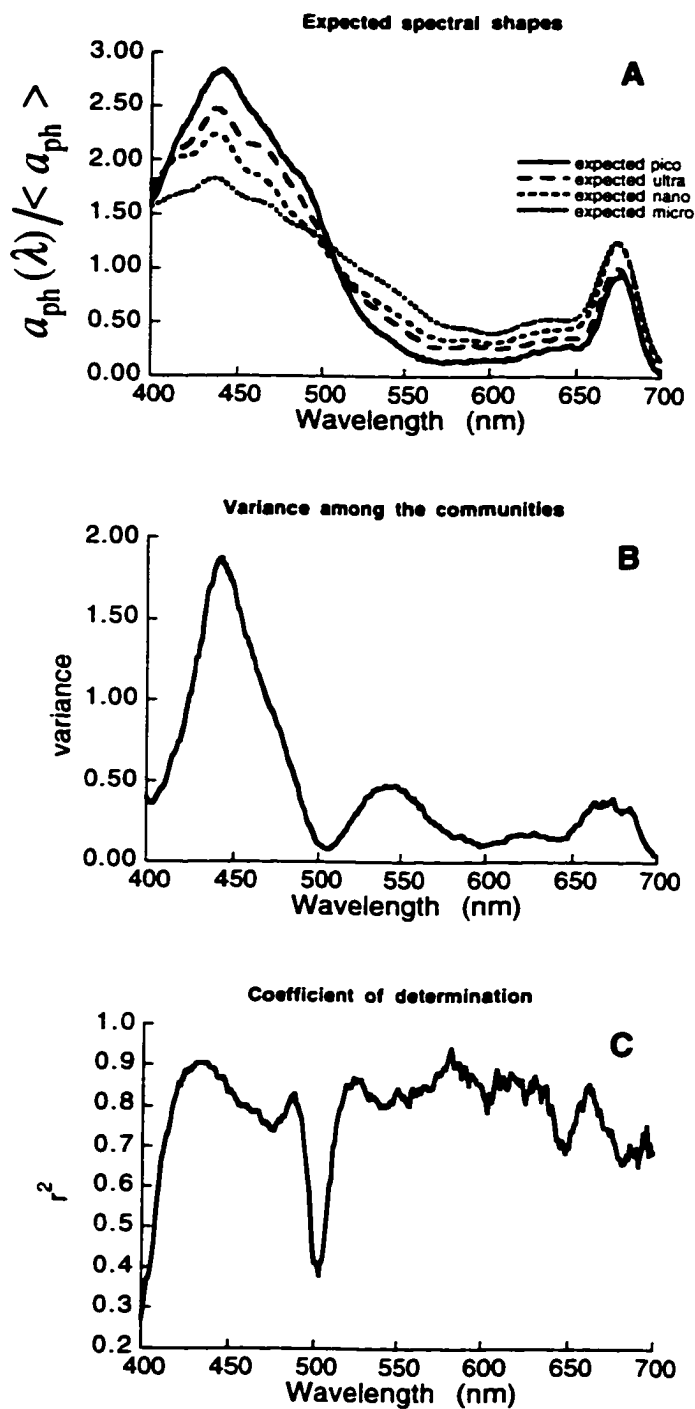


Figure 3.17 Results of the multiple regression analyses for 301 wavelengths. **A)** Expected spectral shapes for phytoplankton absorption for each cell size fraction. **B)** Initial variance of the data set (16 different communities). **C)** Variability of the data explained by predefining cell size range of the dominant organism.

$$a_{<ph>}^*(\lambda) = F_{<p>} \hat{a}_{<pico>}^*(\lambda) + F_{<m>} \hat{a}_{<micro>}^*(\lambda), \quad (3.3)$$

where $\hat{a}_{<pico>}^*(\lambda)$ and $\hat{a}_{<micro>}^*(\lambda)$ are the “basis vectors” or shapes describing the smallest and biggest cells (see Appendix 3.9A), and $F_{<p>}$ and $F_{<m>}$ are respective magnitudes. Note that these vectors differ from the spectral shapes described in the previous analysis, which used the average spectrum for all samples dominated by picoplankton, that is, *Prochlorococcus* spp. and *Synechococcus* spp.

Using a least-squares routine to fit the observed normalized spectra to equation 3.3, it is observed that all 16 spectra were indeed well reconstructed ($r^2 > 0.9$), and because of the nature of this normalization, the sum of $F_{<p>}$ and $F_{<m>}$ tended to be very close to one. Thus, a linear equation subjected to constraints was applied (see Appendix 3.9B), in which the sum of $F_{<p>}$ and $F_{<m>}$ was forced to be equal to 1. Conversely, given a value of $F_{<p>}$, a full spectrum can be estimated as

$$a_{<ph>}^*(\lambda) = F_{<p>} \hat{a}_{<pico>}^*(\lambda) + (1 - F_{<p>}) \hat{a}_{<micro>}^*(\lambda). \quad (3.4)$$

In other words, considering the entire visible range, the spectral shape of the absorption coefficient for a variety of natural communities could be decomposed into two basis vectors and a parameter representing the degree to which the observed spectra is like each of the basis vectors (assumed to be the two possible extremes). Some examples of observed versus “recomposed” spectra (i.e., using equation 3.4) are shown in Figure 3.18.

3.7. Discussion and conclusions

Communities of phytoplankton are complex mosaics of different species (Sournia *et al.*, 1991), the composition of which can be related to environmental conditions such as turbulence and nutrients (Margalef, 1978; Kiørboe, 1993). Our goal was to illustrate and justify, with a diverse variety of field examples, that despite the physiological and

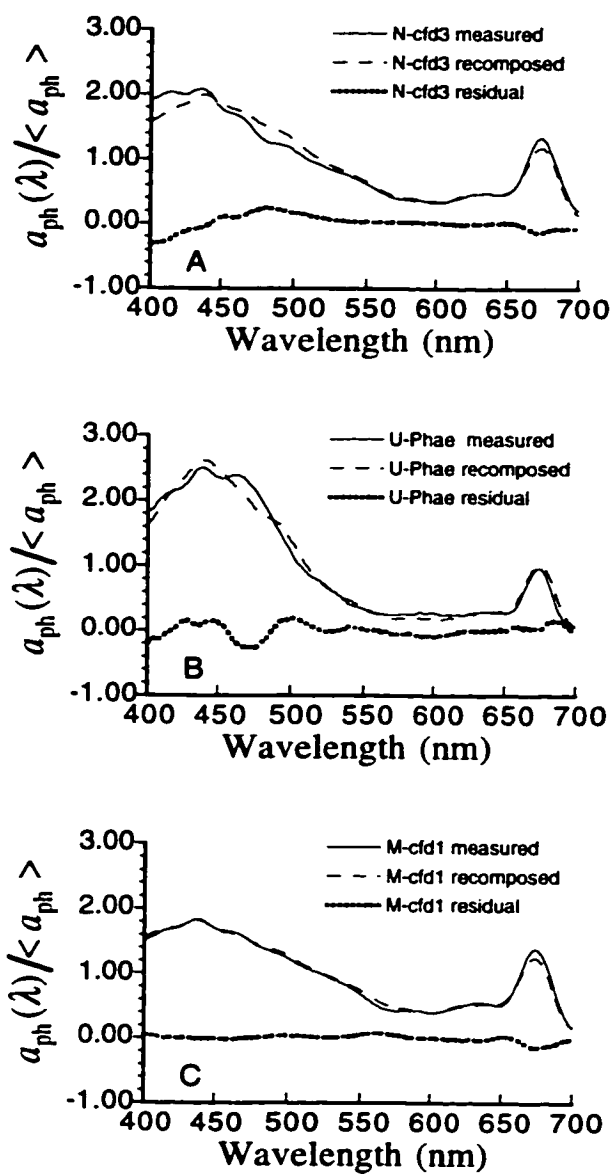


Figure 3.18 Three examples for recomposed normalized spectra of phytoplankton absorption using equation 3.4 and two basis vectors, representing the average for the smallest and largest cell sizes found in our data set. See Table 3.3 and 3.4 for details.

taxonomic variability associated with changes in community structure of phytoplankton, variation in the spectral shape of their bulk absorption coefficient can be described by simple relationships, representing covarying changes in a suite of factors that influence their optical properties.

It is well established that changes in phytoplankton community structure are linked to changes in phytoplankton abundance (Chisholm, 1992). The concept of increasing phytoplankton biomass by the addition of groups of larger species to a background of smaller species proposed by Yentsch and Phinney (1989) seems to hold in a variety of natural communities (Figures 3.4, 3.7, 3.12). Still, our results show, not surprisingly, that the size ranges and taxonomic composition of these additional groups, for a given chlorophyll concentration (proxy for phytoplankton abundance), vary among different environments and seasons. Our results also suggest that the background of small cells will not remain constant during some situations, as for example, the substantial increase in the standing stock (chl) of the picoplankton fraction observed during the Summer experiment in Bedford Basin in 1996 (Figure 3.10), associated with high numbers of cyanobacteria. This could be related to seasonal trends in their abundance (e.g., Delgado *et al.*, 1992) and also to particular conditions of the Basin, such as the combined effects of sewage inputs (eutrophication) and seasonal changes in the mixing regime (see Eppley and Weiler, 1979). Nevertheless, the Yentsch and Phinney (1989) approach seems to be appropriate for comparing effects of different communities of phytoplankton on the variability of optical properties in the ocean.

Despite the differences in taxonomic composition and in the relative proportions of chl size fractions observed during the different cruises, the shape of the absorption spectra for the whole phytoplankton assemblage seem to vary systematically with the cell size range of the dominant organism (Figures 3.15 and 3.16). The comparison of the 16 communities characterized in this study indicated that, when this size range was specified (that is, pico-, ultra-, nano- and microplankton), more than 80% of the variability in the shape of absorption spectra between 400 and 700 nm could be explained (Figure 3.17C).

Table 3.4 Results from a linear decomposition of the phytoplankton absorption spectra for the different communities (see Table 3.3) using a linear regression subjected to constraints (see Appendix 3.9B). $F_{<p>}$ is the factor estimated and varies from 1 to 0 for small and big cell sizes, respectively, and r^2 is the coefficient of determination between observed and estimated spectrum. The linear regression uses two basis vectors representing the minimum and maximum cell size found in our data set (see text and Appendix 3.9A). For reference, maximum $a_{ph}^*(\lambda)$ at the red peak (and respective wavelength) are presented, so $a_{ph}^*(\lambda)$ curves can be reconstructed for each community.

Community	$F_{<p>}$	r^2	a_{ph}^* ($m^2 mg^{-1}$)	λ (nm)
P-Pro	1.000	na	0.0231	676
P-Syn	0.663	0.993	0.0200	676
U-flag1	0.598	0.979	0.0165	673
U-flag2	0.369	0.992	0.0192	674
U-flag3	0.558	0.995	0.0182	676
U-unkw	0.491	0.992	0.0179	676
U-Phae	0.664	0.982	0.0171	675
N-din	0.287	0.987	0.1459	674
N-cfd1	0.370	0.981	0.0163	676
N-cfd2	0.266	0.963	0.0195	674
N-cfd3	0.151	0.954	0.0186	674
N-flag	0.442	0.995	0.0153	675
M-cfd1	0.002	0.989	0.0092	675
M-cfd2	0.014	0.993	0.0098	674
M-din1	0.025	0.987	0.0070	672
M-din2	0.000	0.990	0.0084	675

The systematic variability observed can be related to both pigment packaging and the composition of accessory pigments.

Pigment packaging (or self-shading) is a well documented source of variability for phytoplankton absorption and is a function of cell size and intracellular concentration of pigments (Bricaud and Morel, 1986; Sathyendranath *et al.*, 1987); see also chapter 2. In monospecific laboratory cultures, grown in nutrient replete media, cell diameter (d) correlates negatively with the concentration of intracellular pigments (c_i). This has been described as a strategy to minimize self-shading (see Agusti, 1991), and a similar correlation is expected in the field. In natural environments, however, cell size can be positively correlated to the availability of nutrients (Yentsch and Phinney, 1989), which in turn can be positively correlated with c_i (e.g. Geider *et al.*, 1993; Richardson *et al.*, 1996). Furthermore, nutrient availability can be also related to pigment composition (Claustre, 1994; Wozniak *et al.*, 1994; Aiken *et al.*, 1995) due to the competition among different taxa (i.e., prokaryotes are more important in oligotrophic environments (Chisholm, 1992)) and also to physiological responses (i.e., the concentration of accessory pigments, including photoprotective, tend to be higher when the community is dominated by small cells (Stuart *et al.*, 1998)). In other words, a suite of factors that controls the spectral shape of the absorption of phytoplankton shows a strong co-variation with the size range of dominant organism in the community. Because of that, size can be used as a parameter to explain a large portion of the variability observed in the spectral shape of the phytoplankton absorption (Table 3.4). Residual variability is expected to be derived mainly from changes in pigment composition and intracellular concentration which do not covary with cell size, and also from variability in cell size within the pre-defined size ranges (see Figure 3.5C) and, therefore, the residuals contain some taxonomic and physiological information. Most of the residual variability was observed in narrow spectral bands (see Figure 3.18) that could be related to different accessory pigments (Bidigare *et al.*, 1990; Hoepffner and Sathyendranath, 1991; Millie *et al.*, 1997). Very distinct peaks were observed in the ultraviolet region (not shown in the

results) when both nano and micro dinoflagellates dominated the community, probably related to the presence of mycosporine-like amino acids (MAAs, Karentz *et al.*, 1991). Nevertheless, MAAs are not exclusive to dinoflagellates (e.g. Richardson *et al.*, 1996), and peaks associated with MAAs in dinoflagellates can also be present or absent, depending on nutrient availability (A.M. Ciotti and J.G. MacIntyre, unpublished data).

The strong co-variation between size of dominant organism and several factors controlling the shape of the spectral absorption leads to a tentative parameterization of phytoplankton absorption which could be implemented in inverse models for retrieving spectral absorption for ocean color. A linear decomposition of the observed phytoplankton absorption spectra of the 16 different communities into a factor, $F_{\langle p \rangle}$, and two basis vectors representing the two “extreme” possible spectral shapes (from the smallest and biggest dominant cell size observed), reproduced well ($r^2 > 0.95$) all of observed spectral shapes (see examples in Figure 3.18).

In inverse modeling techniques (e.g., Sathyendranath *et al.*, 1989; Doerffer and Fischer, 1994; Roesler and Perry, 1995; Garver and Siegel, 1997) ocean color spectra are fit to theoretical expressions that relate ocean color to inherent optical properties (IOPs), that is, absorption and backscattering (Morel and Prieur, 1977). The values for the bulk IOPs, by definition, can be computed as the sum of the absorption or backscattering by all the optical components (i.e., water, particles and dissolved material). These are represented by known values (e.g., absorption and backscattering by water) and by spectral shapes and magnitudes of the unknown components. The spectral shape for phytoplankton absorption is usually represented by $a_{\text{ph}}^*(\lambda)$ and, thus, the retrieved magnitude is chlorophyll. In the case of the parameterization of phytoplankton absorption suggested in this work, the retrieved magnitude would be $\langle a_{\text{ph}} \rangle$, that is, the average value of phytoplankton absorption from 400 to 700 nm, which can have application in primary production models (e.g., Kyewalyanga *et al.*, 1997, but see Sosik and Mitchell, 1995). More work has to be done to establish how well the other retrieved parameter, $F_{\langle p \rangle}$, the size factor can be related to the features of phytoplankton communities or ecology.

Nonetheless, our results suggest a robust relationship between $F_{<p>}$ and the cell size of the dominant organism. If indeed a relationship can be established, the potential retrieval of $F_{<p>}$ from ocean color will have several applications in oceanography, as many biogeochemical processes are directly related to the distribution of phytoplankton size classes in a given environment or time (Platt and Denman, 1977; Margalef, 1978; Malone, 1980; Michaels and Silver, 1988; Legendre and Fèvre, 1989; Chisholm, 1992).

Appendix 3.9A: Basis vectors

Basis vectors representing the normalized absorption for the smallest ($\hat{a}_{<pico>}^*(\lambda)$, pico) and biggest ($\hat{a}_{<micro>}^*(\lambda)$, micro) cell sizes in our data set. Basis vectors for $a_{ph}^*(\lambda)$ can be constructed by setting $\hat{a}_{<pico>}^*(676)$ to 0.023 and $\hat{a}_{<micro>}^*(674)$ to 0.0086.

wavelength	pico	micro	wavelength	pico	micro	wavelength	pico	micro
400	1.682	1.574						
402	1.734	1.584	502	1.373	1.242	602	0.068	0.400
404	1.800	1.600	504	1.270	1.222	604	0.078	0.403
406	1.890	1.617	506	1.162	1.196	606	0.069	0.408
408	1.978	1.633	508	1.040	1.169	608	0.090	0.416
410	2.057	1.654	510	0.961	1.141	610	0.096	0.429
412	2.162	1.669	512	0.886	1.118	612	0.094	0.443
414	2.269	1.674	514	0.794	1.096	614	0.084	0.458
416	2.327	1.684	516	0.734	1.075	616	0.105	0.473
418	2.398	1.697	518	0.665	1.057	618	0.128	0.487
420	2.457	1.708	520	0.617	1.035	620	0.119	0.495
422	2.533	1.710	522	0.544	1.013	622	0.126	0.499
424	2.614	1.716	524	0.522	0.992	624	0.138	0.504
426	2.663	1.737	526	0.486	0.977	626	0.146	0.514
428	2.749	1.763	528	0.448	0.959	628	0.135	0.521
430	2.804	1.793	530	0.391	0.944	630	0.175	0.525
432	2.840	1.812	532	0.375	0.927	632	0.189	0.532
434	2.915	1.827	534	0.336	0.909	634	0.176	0.535
436	2.947	1.830	536	0.305	0.888	636	0.203	0.534
438	2.978	1.834	538	0.292	0.868	638	0.190	0.535
440	3.014	1.824	540	0.288	0.847	640	0.190	0.532
442	3.032	1.800	542	0.261	0.826	642	0.191	0.528
444	3.011	1.771	544	0.245	0.806	644	0.174	0.526
446	2.965	1.741	546	0.214	0.785	646	0.197	0.528
448	2.937	1.712	548	0.194	0.764	648	0.176	0.538
450	2.888	1.685	550	0.187	0.737	650	0.168	0.549
452	2.816	1.667	552	0.138	0.711	652	0.160	0.574
454	2.783	1.650	554	0.137	0.682	654	0.217	0.605
456	2.706	1.641	556	0.111	0.653	656	0.244	0.655
458	2.655	1.631	558	0.094	0.626	658	0.286	0.720
460	2.590	1.631	560	0.095	0.604	660	0.381	0.798
462	2.526	1.623	562	0.070	0.580	662	0.437	0.889
464	2.455	1.616	564	0.053	0.555	664	0.520	0.979
466	2.402	1.606	566	0.076	0.535	666	0.660	1.068
468	2.331	1.592	568	0.064	0.514	668	0.716	1.147
470	2.281	1.568	570	0.043	0.501	670	0.824	1.207
472	2.205	1.542	572	0.050	0.487	672	0.846	1.243
474	2.136	1.509	574	0.051	0.478	674	0.816	1.249
476	2.063	1.481	576	0.065	0.475	676	0.891	1.227
478	2.049	1.459	578	0.067	0.468	678	0.869	1.174
480	1.998	1.437	580	0.084	0.464	680	0.812	1.096
482	1.930	1.415	582	0.111	0.459	682	0.741	1.004
484	1.918	1.399	584	0.072	0.452	684	0.605	0.893
486	1.897	1.387	586	0.073	0.452	686	0.496	0.767
488	1.867	1.377	588	0.073	0.449	688	0.372	0.635
490	1.812	1.367	590	0.099	0.443	690	0.278	0.516
492	1.776	1.349	592	0.070	0.433	692	0.215	0.409
494	1.701	1.338	594	0.095	0.424	694	0.113	0.323
496	1.648	1.319	596	0.085	0.416	696	0.075	0.253
498	1.522	1.301	598	0.090	0.406	698	0.047	0.200
500	1.439	1.271	600	0.086	0.401	700	0.009	0.158

Appendix 3.9B: Linear regression subject to constraints

The retrieval of the size parameter, $F_{<p>}$, was established by minimizing the sum of squared errors in the following expression:

$$a_{<ph>}^*(\lambda) = F_{<p>} \hat{a}_{<pico>}^*(\lambda) + F_{<m>} \hat{a}_{<micro>}^*(\lambda) + \text{error} \quad \text{I}$$

where $a_{<ph>}^*(\lambda)$ is the observed spectrum of the phytoplankton absorption coefficient, normalized to the average between 400 and 700 nm, $\hat{a}_{<pico>}^*(\lambda)$ and $\hat{a}_{<micro>}^*(\lambda)$ are the “basis vectors” or shapes describing the smallest and biggest cells (see Appendix 3.9A for values), and $F_{<p>}$ and $F_{<m>}$ are their respective magnitudes. Equation I holds for 301 wavelengths, and can be written:

$$Y = X\beta + \varepsilon, \quad \text{II}$$

where Y is a 301 by 1 vector of $a_{<ph>}^*(\lambda)$, X is a 301 by 2 matrix containing $\hat{a}_{<pico>}^*(\lambda)$ and $\hat{a}_{<micro>}^*(\lambda)$, and ε is a vector of the observation errors.

β is the regression coefficient, which is a 2 by 1 matrix, so that :

$$\beta = [F_{<p>} \quad F_{<m>}] \quad \text{III}$$

The regression coefficient β is estimated by minimizing the sum of squared errors (SSE), which in a linear regression model is given by:

$$\text{SSE} = (Y - X\beta)'(Y - X\beta). \quad \text{II}$$

The constraint to be applied in this case is

$$F_{<p>} + F_{<m>} = 1.$$

If w' is an unitary 2by 1 matrix,

$$w' \beta = 1.$$

A standard solution was applied using a Lagrange multiplier in the constraint minimization (Graham, 1981) of equation II, yielding:

$$\frac{\partial \text{SSE}}{\partial \beta} = 2X'(Y - X\beta) + Lw = 0. \quad \text{III}$$

Solving III for β :

$$\beta = (X'Y(X'X)^{-1} + \frac{L}{2}w(X'X)^{-1}) \quad \text{IV}$$

as $w'\beta = 1$, we can multiply IV by w' and solve it for the unknown L:

$$\frac{L}{2} = 1 - \frac{(w'(X'X)^{-1}X'Y)}{(w'(X'X)^{-1}w)} \quad \text{V}$$

Solving V and applying it in IV, β is found.

Chapter 4

Analyses of the influence of different cell sizes of phytoplankton on relationships between apparent optical properties

4.1 Introduction

The effective use of ocean color to estimate the abundance of phytoplankton depends on understanding how changes in species composition and the physiological status of phytoplankton assemblages, along with changes in other colored and refractive components of the sea water, quantitatively affect the fate of the incident irradiance (Gordon *et al.*, 1988; Morel, 1988). Corrections for these effects are required for the development of improved global algorithms for chlorophyll and primary production (see Aiken *et al.*, 1995). In the process, concentrations of optically active components other than chlorophyll can potentially be retrieved from optical measurements using both *in situ* and satellite platforms (Carder *et al.*, 1991; Doerffer and Fischer, 1994).

Changes in species composition accompany spatial and temporal gradients of phytoplankton abundance in the upper ocean (Malone, 1980; Chisholm, 1992). Generally, at low chlorophyll concentration (as a proxy for phytoplankton abundance), communities of phytoplankton are dominated by smaller cells (Thingstad and Sakshaug, 1990;

Riegman *et al.*, 1993) with relatively high concentrations of accessory pigments (Claustre, 1994; see also Stuart *et al.*, 1998). Depending on environmental conditions, as the trophic status changes to more eutrophic, distinct groups of larger organisms are added to a "background" of small cells (Yentsch and Phinney, 1989). The increase in phytoplankton cell size with trophic status is thus expected to affect bulk optical properties of phytoplankton as a result of pigment packaging (Bricaud *et al.*, 1995 and references therein) and a tendency of species from eutrophic waters to have relatively less accessory pigmentation (Claustre, 1994). Indeed, the analysis of a large set of data from the field (chapter 2) suggested that the optical properties of phytoplankton assemblages along a trophic gradient follow a strong central tendency which is consistent with experimental and theoretical work, and could reproduce some well-recognized empirical relationships between apparent optical properties, such as ratios of upwelling radiance or diffuse attenuation versus chlorophyll concentration (e.g., Morel, 1988; O'Reilly *et al.*, 1998). In chapter 2 it was also demonstrated that deviations from this general tendency occur, and that predictable departures can be expected when assemblages, treated as populations of a single cell type, differ from the central trend in the degree of pigment packaging and accessory pigmentation.

Spectral reflectance of the sea surface, and thus ocean color, is related to the absorption and backscattering coefficients (Morel and Prieur, 1977) of all the combined optically active components, including the water itself, organic and inorganic particles, and dissolved substances (Kirk, 1994b). The major contribution of phytoplankters to ocean color derives from their absorption coefficient, because of their relatively unimportant backscattering efficiency (Bricaud *et al.*, 1983; Stramski and Kiefer, 1991; Ahn *et al.*, 1992). When a wide variety of phytoplankton communities were compared (chapter 3), changes in the spectral shape of the absorption coefficient of the entire phytoplankton assemblage was largely explained by the cell size range of the dominant organisms, due to the covariance of many physiological factors (mainly cellular concentration of chlorophyll and accessory pigments) with cell size. The results of both

chapter 2 and chapter 3 suggest that, along a trophic gradient, phytoplankton assemblages will differ optically and that the optical changes with trophic status can be generalized and related to dominant cell size.

In coastal areas with significant influence of continental outflows, dissolved substances and particles other than phytoplankton will affect significantly ocean color through contributions to absorption and backscatter (Kirk, 1994b). For example, colored dissolved organic matter can absorb strongly in shorter wavelengths, overwhelming contributions of phytoplankton to total absorption. Also, a considerable portion of sunlight reflected from surface waters can be generated by components having high backscattering efficiency, such as very small inorganic particles (Stramski and Kiefer, 1991; Ulloa *et al.*, 1994), bacteria (Morel and Ahn, 1990) and even bubbles (Stramski, 1994; Zhang *et al.*, 1998). Because of that, the effective extraction of information about phytoplankton with different cell size ranges from ocean color relies on either accounting quantitatively for these other components or on effectively minimizing their influence.

Biological and non-biological information from ocean color spectra have been retrieved using three main procedures: 1) statistical and semi-analytical algorithms relating the value to be retrieved to either two-band ratios of upwelling radiance, or to a linear combination of more than two ratios (Gordon and Morel, 1983; Aiken *et al.*, 1995); 2) inverse modeling techniques which relate the contribution of the different colored and refractive substances to theoretical expressions (Sathyendranath *et al.*, 1989; Doerffer and Fischer, 1994; Roesler and Perry, 1995; Garver and Siegel, 1997) using known spectral shapes for the relevant coefficients, and 3) empirical algorithms relating sun-induced chlorophyll fluorescence (i.e., the height of the peak of chlorophyll fluorescence centered around 683 nm, Neville and Gower, 1977; Gower and Borstad, 1981) to the concentration of chlorophyll *a*. Differences in the absorption spectra of communities of phytoplankton will influence these procedures in different ways.

In this chapter our initial goal is to investigate quantitatively how the dominant cell size of phytoplankton influences relationships between ocean color and chlorophyll

concentration, as well as relationships between vertical diffuse attenuation and ocean color. To do so a wide variety of situations were compared, where measurements of surface reflectances and near-surface diffuse attenuation coefficient at selected wave bands were complemented by measurements of chlorophyll and the spectral absorption coefficients of phytoplankton, detritus and colored dissolved organic matter. Independent measurements of phytoplankton absorption allow us to quantify the effects of different communities on the retrieval of information from optical measurements. By analyzing the diverse bio-optical data set and results from a semi-analytical model as function of chlorophyll, combinations of measurements that best discriminate changes of phytoplankton community structure in surface waters will be selected.

4.2 Background

In chapter 2, it was discussed in detail how different assemblages of phytoplankton are expected to influence radiance ratios and spectral diffuse attenuation in surface waters. Briefly, consistent changes in inherent optical properties, IOPs (e.g., absorption, $a(\lambda)$, and backscattering, $b_b(\lambda)$), as functions of chlorophyll plus pheopigments (C , mg m^{-3}) were parameterized. In particular, the semi-analytical model (SAMOCAFOTS) described changes in pigment packaging and accessory pigmentation as functions of C . Main trends in $a(\lambda)$ and $b_b(\lambda)$ were computed, and deviations were simulated by changing specific parameter values. The parameterization of apparent optical properties, AOPs (e.g., reflectance spectra and attenuation coefficient), were made by combining theoretical expressions relating AOPs to IOPs (Gordon *et al.*, 1975; Morel and Prieur, 1977; Gordon *et al.*, 1988; Sathyendranath and Platt, 1988) and simplifications regarding the geometrical distribution of the light field.

4.2.1 Reflectance and attenuation

Following the approximations and assumptions described in chapter 2, remote sensing reflectance ($R_r(\lambda)$, sr⁻¹) just below the sea surface, that is, the ratio of upwelling radiance, $L_u(\lambda)$, to the downwelling irradiance, $E_d(\lambda)$, is given by:

$$\frac{L_u(\lambda)}{E_d(\lambda)} = R_r(\lambda) = \frac{f(\lambda)b_b(\lambda)}{Q(\lambda)a(\lambda)}, \quad (4.2)$$

where $Q(\lambda)$, sr, is the ratio of the upwelling irradiance to the nadir upwelling radiance and $f(\lambda)$, dimensionless, is a parameter that depends on the geometrical distribution of the light field. As a first approximation, the spectral variability of $f(\lambda)/Q(\lambda)$ in the blue and green wavebands can be assumed to be very small (Morel and Gentili, 1993; Morel and Gentili, 1996), so when ratios of $R_r(\lambda)$ at two wavelengths, λ_1 and λ_2 , are estimated:

$$\frac{R_r(\lambda_1)}{R_r(\lambda_2)} = \frac{b_b(\lambda_1) a(\lambda_2)}{b_b(\lambda_2) a(\lambda_1)}. \quad (4.3)$$

The diffuse attenuation coefficient, $K_d(\lambda)$, is given by

$$K_d(\lambda) = \frac{a(\lambda) + b_b(\lambda)}{\bar{\mu}_d(\lambda)}, \quad (4.4)$$

where $\bar{\mu}_d(\lambda)$ is the average cosine for downwelling irradiance, that can be assumed relatively constant in coastal waters (Kirk, 1994b). The variability imposed by communities of phytoplankton with distinct cell sizes on the relationships between AOPs will be, therefore, manifested in their differential influence on $a(\lambda)$ and $b_b(\lambda)$.

4.2.2 Total backscattering

Direct measurements of backscattering were unfortunately not available during our sampling programs. Theoretical studies, however, suggest that the spectral shape of the backscattering coefficient can be approximated as a power function of wavelength, which is a result of the combined effects of the backscattering by water with an exponent

of -4.65 (Morel and Smith, 1974), and backscattering by the local particles with exponents varying from around -2 to zero (Morel, 1988; Sathyendranath *et al.*, 1989; Mobley, 1994). Consequently, in equation 4.3 the term $b_b(\lambda_1)/b_b(\lambda_2)$ will depend both on the proportion of backscattering by water versus particles, and on the optical characteristics and size distribution of the local particle assemblage, which defines the spectral slope of their backscattering coefficient (Stramski and Kiefer, 1991; Ulloa *et al.*, 1994). For reflectance ratios commonly used for retrieval of C , e.g., 443 to 555 nm or 490 to 555 nm (Gordon and Morel, 1983; Aiken *et al.*, 1995), $b_b(\lambda_1)/b_b(\lambda_2)$ can vary by more than a factor of 2 (Table 4.1). It is thus expected that in some situations the spectral changes in backscattering may override the effects of absorption on spectral reflectance, as for example, during coccolithophore blooms (Balch *et al.*, 1996). In most oceanic waters, however, $a(\lambda)$ is anticipated to be the dominant factor changing spectral reflectance.

On the other hand, in coastal waters the input of inorganic particles will increase the importance of backscattering (Bukata *et al.*, 1995). Blooms of phytoplankton can also affect the shape of the size distribution by the addition of modes of particular sizes (Yentsch and Phinney, 1989; Chisholm, 1992; Mobley, 1994) or by affecting the concentration of small particles by aggregation (Hill, 1992). These processes can influence the shape of the size distribution and in turn, influence $b_b(\lambda)$ (Ulloa *et al.*, 1994). Bubbles were also shown to potentially influence $b_b(\lambda)$ (Stramski, 1994; Zhang *et al.*, 1998). All these different factors combined with the uncertainties of $b_b(\lambda)$ due to the lack of measurements in the field, make it difficult to predict the influence of different cell sizes of phytoplankton on $b_b(\lambda)$.

4.2.2.1 Minimizing the effects of total backscattering on reflectance ratios

If the general power shape of $b_b(\lambda)$ is applicable in nature, so-called curvature or inflection ratio algorithms (see Campbell and Esaias, 1983) can be used to minimize the

Table 4.1 Expected values of $b_b(\lambda_1)/b_b(\lambda_2)$ when the proportion of backscattering by particles at 555 nm, $b_{b_{ph+det}}(555)$, is varied (first column). This range represents the approximate values predicted by the semi-analytical model SAMOCAFOTS (i.e., from around 3 when C is 0.5 mg m^{-3} to 25 when C is 30 mg m^{-3} , see chapter 2). Backscatter by water, $b_{b_w}(\lambda)$, follows a power function with wavelength; the slope is -4.65 , corresponding to a $b_{b_w}(490)/b_{b_w}(555)$ of 1.631 and $b_{b_w}(443)/b_{b_w}(555)$ of 2.579. Backscattering by particles also follows a power function with wavelength: the value of γ indicates the slope.

		$b_b(\lambda_1)/b_b(\lambda_2)$				
		$\frac{b_{b_{ph+det}}(555)}{b_{b_w}(555)}$	$\gamma=-2$	$\gamma=-1$	$\gamma=0$	$\gamma=0.5$
$\lambda_1 = 490$ and $\lambda_2 = 555$	0.500	1.522	1.395	1.262	1.195	
	1.000	1.440	1.297	1.157	1.090	
	2.000	1.376	1.227	1.087	1.022	
	5.000	1.325	1.174	1.037	0.975	
	10.000	1.305	1.154	1.019	0.958	
	20.000	1.294	1.143	1.010	0.949	
$\lambda_1 = 443$ and $\lambda_2 = 555$	0.500	2.180	1.897	1.618	1.484	
	1.000	1.970	1.656	1.371	1.241	
	2.000	1.807	1.483	1.206	1.084	
	5.000	1.676	1.354	1.088	0.974	
	10.000	1.625	1.305	1.045	0.935	
	20.000	1.598	1.279	1.023	0.914	

influence of the backscatter term on reflectance ratios (Zaneveld *et al.*, 1998). For example, in the curvature algorithm

$$\frac{R_r(443)R_r(555)}{R_r(490)^2} = \frac{b_b(443)b_b(555)}{b_b(490)^2} \frac{a(490)^2}{a(443)a(555)}, \quad (4.5)$$

the value of the $b_b(\lambda)$ term in the equation will vary from 0.94 to 1.04, for the same ranges for the proportion of backscattering by particles and by water at 555 nm exemplified in Table 4.1. If surface reflectance, absorption and backscattering are computed with the semi-analytical model presented in Chapter 2 for the minimum and maximum values of C (0.5 and 30 mg m⁻³, respectively), changes in $R_r(490)/R_r(555)$ and in $(R_r(443)R_r(555))/R_r(490)^2$ can be associated with either the absorption or the backscattering terms in each expression. The relative contribution of backscattering term in equations 4.3 and 4.5 was estimated as follows:

$$\frac{\ln\left(\frac{B2}{B1}\right)}{\left(\ln\left(\frac{A2}{A1}\right) + \ln\left(\frac{B2}{B1}\right)\right)},$$

where A1 and B1 refer to the absorption and the backscattering terms when C is 0.5 mg m⁻³, and A2 and B2 refer to the absorption and the backscattering terms when C is 30 mg m⁻³. This calculation suggests that $b_b(490)/b_b(555)$ explains about 15% of the changes in $R_r(490)/R_r(555)$ when C varies from 0.5 to 30 mg m⁻³, and that $(b_b(443)b_b(555))/b_b(490)^2$ explains only about 2% for $(R_r(443)R_r(555))/R_r(490)^2$. Therefore, even when extreme spectral shapes for backscattering are used, absorption will be the more important factor in equation 4.5.

Note that equations 4.3 to 4.5 are only valid in the spectral regions not influenced by inelastic scattering, such as Raman scattering by water molecules (Stavn and Weidemann, 1992) and fluorescence by chlorophyll (above 600 nm) and other pigments (Neville and Gower, 1977; Gordon, 1979; Gower and Borstad, 1981; Yentsch and Phinney, 1985). Raman scattering affects the entire visible spectrum, especially from 500

to 700 nm (Stavn, 1993; Bartlett, 1996). For example, at 550 nm the contribution of Raman scattering to the reflectance signal has been estimated to be around 20% for pure water, decreasing to 3% when C is 1 mg m^{-3} (Waters, 1995). For the C range considered in this chapter, therefore, the contribution of Raman scattering can be neglected. In the blue part of the spectrum, fluorescence by organic dissolved substances may be important in waters in which their concentration is very high (Vodacek *et al.*, 1994) and the validity of these equations can be compromised. It will be assumed in this chapter that CDOM fluorescence is negligible. Accordingly, with the instruments used in the present study, analysis between AOPs and IOPs can be conducted for 4 wavebands: 412, 443, 490 and 555 nm.

4.2.3 Spectral shape of total absorption coefficient

The spectral shape of total absorption depends both on the relative contributions of water, phytoplankton, detritus and CDOM (Kirk, 1994b) and on the respective spectral shapes of their absorption coefficients. Absorption by water has been measured (Pope and Fry, 1997) and can be assumed invariant. Absorption by CDOM and detritus can be analyzed together (i.e., $a_{\text{cdom+det}}(\lambda)$, m^{-1}) due to the similarity of their spectral shapes (Roesler *et al.*, 1989) which can be represented by:

$$a_{\text{cdom+det}}(\lambda) = a_{\text{cdom+det}}(\lambda_0) e^{[S(\lambda-\lambda_0)]}, \quad (4.6)$$

where S (nm^{-1}) is the slope of the exponential decrease with wavelength and $a_{\text{cdom+det}}(\lambda_0)$ is the absorption coefficient for CDOM plus detritus at a reference wavelength (i.e. 443 nm). In chapter 3 changes in the spectral shape of phytoplankton absorption ($a_{\text{ph}}(\lambda)$, m^{-1}) were compared, and for a wide variety of phytoplankton communities, the spectral shape of $a_{\text{ph}}(\lambda)$ for entire phytoplankton assemblages from surface waters was strongly related to the cell size range of the dominant organisms. A given spectral shape of $a_{\text{ph}}(\lambda)$ from surface waters could be duplicated almost exactly with a linear combination of two spectra (or basis vectors) representing the assumed extremes for assemblages dominated

by small and big cell sizes, respectively (see Table 3.4), and a single parameter, $F_{<p>}$, which varies from 1 to 0, designating the proportion of the small cells. Thus, the size parameter, $F_{<p>}$, in combination with the two basis vectors, can be used to represent quantitatively the spectral shape of phytoplankton absorption, as will be shown below.

4.3 Approach

The effects of communities of phytoplankton with different cell sizes and also the influence of $a_{\text{cdom+det}}(\lambda)$ on the retrieval of information from AOPs is analyzed by comparing forward modeling (using the semi-analytical model SAMOCAFOTS presented in chapter 2) to observations of $F_{<p>}$ and $a_{\text{cdom+det}}(\lambda)$. The good agreement between SAMOCAFOTS and empirical relationships (see chapter 2), allows us to assume that the model results represent expected values of AOPs as functions of C , so that one can relate the deviations in the observations from the model results to either changes in cell size or CDOM plus detrital absorption.

4.4 Methods

4.4.1 Sampling design

The bio-optical data examined in this chapter were collected during the same cruises described in chapter 3 (see section 3.5 for the general sampling design). Water samples were taken and CTD casts were conducted while a spectral radiometer buoy was deployed to measure ocean color (see Table 4.1 for instruments used and wavelengths measured in each occasion). Radiometer data were collected at 6 Hz throughout the occupation of stations, which varied from about 15 minutes to several hours. Immediately after water was sampled from the CTD-rosette system, vertical profiles of spectral downwelling irradiance were taken. During the time series in Bedford Basin from July to December of 1996 (BBTS96), the spectral radiometer buoy was moored, collecting data

Table 4.2 Location, dates, measurements and instruments used in each cruise. **TSRB:** Tethered spectral radiometer buoy, **TACCS:** Tethered attenuation coefficient chain sensor, **SPMS:** SeaWifs profiling multichannel radiometer, **OCI-200:** Ocean color radiometer with irradiance sensors, **OCTS:** Ocean color and temperature sensor. All instruments from Satlantic, Inc.

Location	Dates	Cruise name	Measurements	Instruments
Bedford Basin	Aug. 1992	BBS92	L_w (412, 443, 490, 510, 555, 670 and 683), E_d 490, K_d 490, chl and particulate absorption	TSRB and pair of E_d sensors
Bedford Basin	Aug. 1993	BBS93	L_w (412, 443, 490, 510, 555, 670 and 683), E_d 490, K_d (412, 490 and 555), chl, particle size, particulate and dissolved absorption	TSRB and pairs of E_d sensors
Bedford Basin	Aug 1996	BBS96	L_w (412, 443, 490, 559, 670, 683 and 705), E_d 490 daily, E_d (412, 443, 490, 555 and 700) weekly, K_d 490 daily, K_d (406, 413, 435, 444, 456, 490, 510, 532, 556, 590, 670, 683, 700) weekly, chl, particulate and dissolved absorption (weekly plus intensive sampling Aug 20-22)	TACCS, SPMS and OCI-200
	Jul. to Dec. 1996	BBTS96		
Bering Sea	Apr. 1996	BS96	L_w (412, 443, 490, 555, 670, 683 and 700), E_d (412, 443, 490, 555 and 700), K_d 490, chl, particulate and dissolved absorption	TSRB, single E_d sensor and OCI-200
Bering Sea	Jun. 1997	BS97	L_w , E_d and K_d (412, 443, 490, 511, 531, 555, 590, 673, 683, and 700), chl, particulate and dissolved absorption	OCTS-100

at 6 Hz for one minute in 10 minute intervals. The site was visited every week for water samples and profiles of spectral downwelling irradiance. An intensive sampling was conducted on August 21 and August 22 1996, with CTD and spectral downwelling irradiance taken every hour, along with surface samples for chlorophyll.

4.4.2 Optical measurements

Spectral diffuse attenuation coefficients for downwelling irradiance ($E_d(\lambda)$, $\text{W m}^2 \text{nm}^{-1}$), were measured using free-falling radiometers (SPMR and OCTS-100, see Table 4.2). Vertical profiles of $E_d(\lambda)$ were used to compute the diffuse attenuation coefficient ($K_d(\lambda)$, m^{-1}), defined as the slope of the natural logarithm of $E_d(\lambda)$ versus depth for each waveband. Only $E_d(\lambda)$ within the first optical depth was included (i.e., depth in which measured $E_d(\lambda)$ was 37% of the value measured at the surface). In-water $E_d(\lambda)$ was not corrected for variations of $E_d(\lambda)$ measured in air during the vertical cast. Although variable downwelling irradiance can affect $E_d(\lambda)$ measured at depth during the casts, this variability is not expected to affect $K_d(\lambda)$ much because only data from the uppermost layers were used and the casts were completed in a relatively short time. The SPMR was equipped with a tilt sensor and data taken when the instrument was more than 3 degrees of the vertical were excluded. In general, multiple casts (3 or more) were available at each station, and $K_d(\lambda)$ was calculated as above for each cast and then averaged. When free-falling radiometers were not available, $K_d(\lambda)$ was measured with vertical profiles of pairs of $E_d(\lambda)$ sensors, or by profiling with a single $E_d(490)$ sensor attached to the frame of the CTD (see Table 4.2),.

Spectral upwelling radiance was measured with three different spectral radiometer buoys (Table 4.1). In both the TSRB and TACCS buoys, the radiance sensors are located at a depth of 0.45 m ($L_{u\text{-tsrb}}(\lambda)$). Thus, to compute upwelling radiance just below the surface ($L_u(\lambda)$), $K_d(\lambda)$ must be taken into account, such that:

$$L_u(\lambda) = L_{u\text{-tsrb}}(\lambda) \cdot \exp(0.45K_d(\lambda)). \quad (4.1)$$

When spectral K_d was not available (see Table 4.2) the different wavebands of vertical attenuation were estimated as a function of surface chlorophyll plus pheopigments (BS96) using the relationships described by Morel (1988), or as a function of $K_d(490)$ (Bedford Basin) using the statistical relationships by Austin and Petzold (1986). Equation 4.1 assumed that $K_d(\lambda)$ is constant in the upper 45 cm. Measurements with OCTS-100 (i.e., Bering Sea 1997) were not corrected for attenuation, because the sensors were located approximately 0.1 m below the surface.

Spectral downwelling irradiance was also measured in air by different instruments (Table 4.1), equipped with cosine-collector sensors. These data were used for computation of surface remote sensing reflectance, that is the ratio of upwelling to the downwelling irradiance. The spectral irradiance measured in the air ($E_d(\lambda, 0^+)$) was corrected for reflection at the air-ocean interface, computed using the Fresnel equation (see Mobley, 1994), thereby yielding $E_d(\lambda)$, the irradiance just below the surface. Note that if reflectances were computed just above the surface instead, their values would be about two times smaller due to the transmission of radiance at the ocean-air- interface. Nonetheless, the changes in Fresnel reflectance for upward and downward fluxes with zenith angle are not spectrally dependent, and the data discussed here refer solely to ratios of reflectance. Data for solar zenith angles greater than 70 degrees were excluded from the data set, due to limitations of the cosine response of the sensors (see Bartlett *et al.*, 1998). Measurements of $E_d(490)$ were taken in all experiments and when data in other wave bands were not available (i.e., BS92 and BS93), $E_d(\lambda, 0^+)$ was estimated by multiplying $E_d(490, 0^+)$ by a factor. The factors were computed as median values for $E_d(\lambda, 0^+) / E_d(490, 0^+)$ using a clear sky solar irradiance model (Gregg and Carder, 1990) that was run several times with the input parameters ranging within pertinent ranges for Bedford Basin in the summer. The use of a clear sky model ignores the effects of clouds on $E_d(\lambda, 0^+)$, which can introduce variability on reflectance ratios independently of the composition of the water or of the geometrical distribution of the light field. The main spectral changes in irradiance due to clouds are in the blue region, and in Bedford Basin

area studies show that the maximum error for using the clear sky model to determine irradiance at 555 nm from $E_d(490, 0^\circ)$ is around 7% (Bartlett *et al.*, 1998).

4.4.3 Water samples

Samples for fluorometrically-measured chlorophyll plus pheopigments (C , mg m^{-3}) and for particulate absorption using the filter-pad method were analyzed as described in chapter 3. Phytoplankton absorption was computed by measuring the absorption by total particulate material and subtracting the absorption of the same material after an extraction with methanol and water (see section 3.5).

Absorption by dissolved material (hereafter referred to as colored dissolved organic matter, CDOM) was measured using filtrates of GF/F (Bedford Basin), 0.2 μm polycarbonate filters (Bering Sea 1996) or 0.2 μm nylon filters (Bering Sea 1997). Samples were scanned against Nanopure water, filtered through a 0.2 μm polycarbonate filter, with a Cary 3 Dual-Beam spectrophotometer using 10 cm cuvettes. Filtered samples and Nanopure water were brought to room temperature before analysis. All filters were rinsed with approximately 50 ml of sample water and this initial filtrate was discarded. Each scan was smoothed using a 5-nm running average, and corrected for both residual scattering (setting the mean optical density between 740 to 750 nm to zero) and pathlength. The use of different filters for removing particulate matter is not expected to interfere with the results much, as none of the samples showed notable signals between 740 and 750 nm, suggesting that the amount of scattering material that passed through the filter was not important. For comparison with optical data, total absorption was computed as the sum of measured total particulate absorption, CDOM absorption and water absorption, taken from Pope and Fry (1997). Total absorption was estimated with a spectral resolution of 1 nm, then absorption corresponding to relevant wavebands was computed using averages, weighted with the spectral response of the instruments used in each sampling program.

4.4.4 Parameterization of the effects of cell size

In order to examine the effects of cell size explicitly, it was necessary to modify the model to incorporate the size parameter $F_{\langle p \rangle}$. SAMOCAFOTS predicts the central trend in $a_{\text{ph}}(\lambda)$ by computing expected values of phytoplankton absorption normalized to C , $a_{\text{ph}}^*(\lambda)$. One can convert $a_{\text{ph}}^*(\lambda)$ into $F_{\langle p \rangle}$ values by decomposing spectra of a_{ph}^* at each C as described in chapter 3:

1) For a given range of C , $a_{\text{ph}}^*(\lambda)$ is computed for 6 wavebands (412, 443, 490, 510, 555 and 670 nm) using the semi-analytical model. Although a high-resolution spectrum for each C can be inferred, the analysis will refer only to the six wavebands.

2) The estimation of $F_{\langle p \rangle}$ from a_{ph}^* at the six wavebands is done as described in chapter 3, except that the spectra were not normalized to $\langle a_{\text{ph}} \rangle$, that is, to the average phytoplankton absorption computed between 400 and 700 nm. The a_{ph}^* values computed by the model at each C were assumed to vary between two possible extremes of $a_{\text{ph}}^*(\lambda)$, representing small ($a_{\text{pico}}^*(\lambda)$) and larger ($a_{\text{micro}}^*(\lambda)$) cells (see Appendix 3.9A for values). A linear regression of $a_{\text{ph}}^*(\lambda)$ was performed following

$$a_{\text{ph}}^*(\lambda) = F_{\langle p \rangle} a_{\text{pico}}^*(\lambda) + F_{\langle m \rangle} a_{\text{micro}}^*(\lambda), \quad (4.7)$$

where $F_{\langle p \rangle}$ and $F_{\langle m \rangle}$ are the magnitudes of $a_{\text{pico}}^*(\lambda)$ and $a_{\text{micro}}^*(\lambda)$, and the regression is constrained so that $F_{\langle m \rangle} = (1 - F_{\langle p \rangle})$ (see details in Appendix 3.9B). Thus, the entire spectrum can be described with a single parameter, $F_{\langle p \rangle}$ (see slope and coefficient of determination in Table 4.3). Note that dependent and independent variables have only 6 cases. Therefore, a spectrum characteristic of small cells tends towards $F_{\langle p \rangle} = 1$, and a spectrum characteristic of large cells tends towards $F_{\langle p \rangle} = 0$ (Figure 4.1A).

When $a_{ph}^*(\lambda)$ predicted by the semi-analytical model at each C , is decomposed using equation 4.7, the regression yields $F_{<p>}$ as a function of C (Figure 4.1b) illustrating the trend toward absorption spectra characteristic of bigger cells with higher C . For comparison, Table 4.3 also shows the slopes and coefficients of determination (r^2) for the regressions of $a_{ph}^*(\lambda)$ predicted by the semi-analytical model and each of the two basis vectors. Two points can be made: first, r^2 of the regression including both vectors are only slightly higher than those from the regression using $a_{micro}^*(\lambda)$ only, however the slopes (which indicate the bias on the magnitude) differ substantially; secondly, r^2 for the regression using both basis vectors tended to increase with C , which is probably a result of the higher uncertainties associated to the parameterization of $a_{ph}^*(\lambda)$ as a function of C when C is low (see chapter 2).

The incorporation of $F_{<p>}$ in the model allows one to modify its central trend with C and in turn, simulate effects of phytoplankton absorption on AOPs for different situations, such as dominance by small and larger cells. For example, if $F_{<p>}$ is fixed to be zero and then to be one, independently of C , the model can generate AOPs for a maximum range of variability imposed by absorption spectra of different cell sizes only. These predictions can be verified with independent measurements of $F_{<p>}$ (i.e., the decomposition of the measured phytoplankton spectra in our data set) and C that were taken concurrent with measurements of AOPs.

4.4.5 Parameterization of the effects of CDOM and detritus

The semi-analytical model also assumes a relationship between CDOM plus detrital absorption ($a_{cdom+det}(\lambda)$) and C . Absorption by CDOM and detritus has a background value (D_o , m^{-1}) (Kirk, 1994b) and increases linearly (slope d_s , dimensionless) with $a_{ph}(\lambda)$ based on published relationships (Bricaud and Stramski, 1990). By changing both D_o and d_s in the relationship (see equation 2.17 in chapter 2) within a factor of 4 of the original values, one can simulate AOPs for situations in which $a_{cdom+det}(\lambda)$ is 1/4 or 4 times the values predicted by SAMOCAFOTS. This range was chosen based on our data

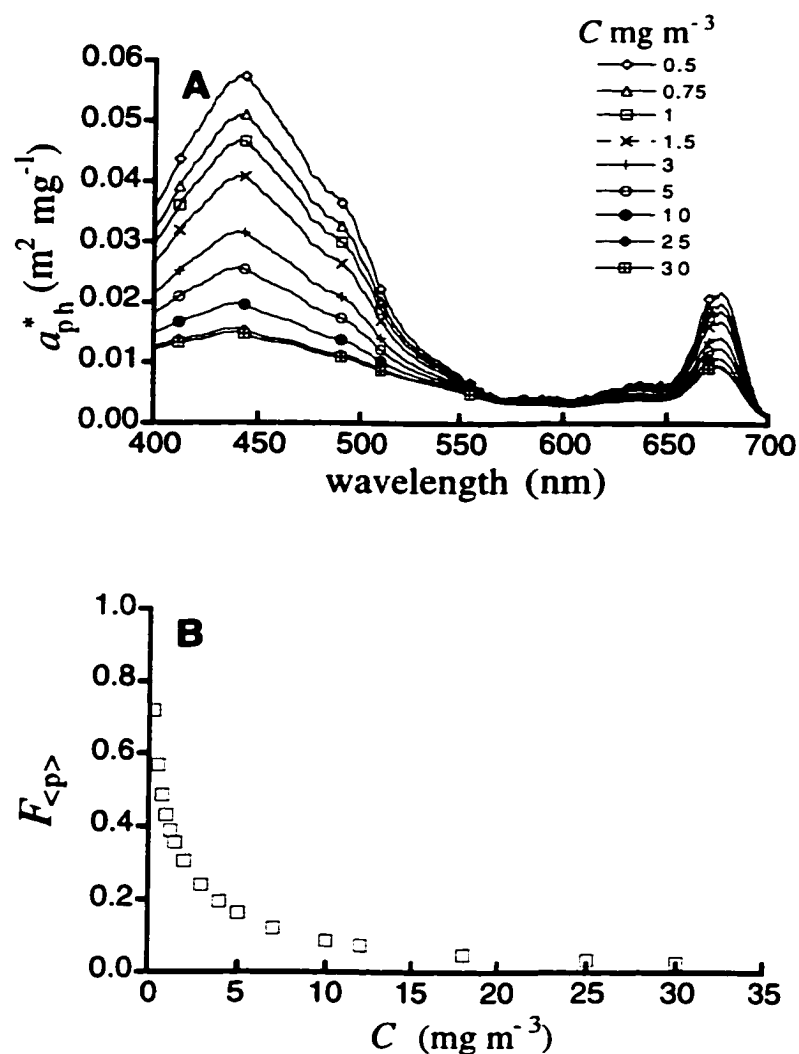


Figure 4.1 Inferred contributions of different size classes to phytoplankton absorption as a function of trophic status. SAMOCAFOTS estimates C -normalized phytoplankton absorption at 6 wavebands (see chapter 2). The set of wavebands at each C were decomposed using a linear combination of two spectra with 1 nm-resolution representing small and large cells, respectively, as described in chapter 3. The decomposition yields the size parameter $F_{<p>}$. **A)** Inferred spectra at each C using a linear combination of the two basis vectors and the estimated $F_{<p>}$ (see equation 4.6). Some spectra are not shown to facilitate visualization. **B)** Estimated $F_{<p>}$ at each C .

Table 4.3 Results for the decomposition of $a_{ph}^*(\lambda)$ computed for 6 wavebands (412, 443, 490, 510, 555 and 670 nm) using the semi-analytical model for the given range of C (see text). Decomposition is a result of a linear combination of two extreme $a_{ph}^*(\lambda)$, representing small and big cells, using a linear regression subjected to constraints (see text). The regression yields the factor $F_{<p>}$. For comparison, coefficients of determination (r^2) and slopes are presented for the regressions using both basis vectors and using each vector separately. Analysis was performed for 6 wavebands only.

C	$F_{<p>}$	r^2 both	slope both	r^2 pico	slope pico	r^2 micro	slope micro
0.500	0.568	0.815	1.015	0.743	0.658	0.766	3.240
0.750	0.486	0.825	1.016	0.722	0.591	0.787	2.921
1.000	0.432	0.833	1.017	0.704	0.547	0.802	2.706
1.250	0.389	0.840	1.018	0.686	0.512	0.815	2.541
1.500	0.356	0.845	1.018	0.666	0.485	0.826	2.412
2.000	0.305	0.854	1.019	0.628	0.444	0.845	2.213
3.000	0.239	0.866	1.020	0.557	0.389	0.868	1.950
4.000	0.194	0.879	1.020	0.494	0.353	0.886	1.775
5.000	0.162	0.892	1.020	0.438	0.327	0.901	1.649
7.000	0.121	0.910	1.019	0.343	0.293	0.919	1.484
10.000	0.086	0.930	1.016	0.251	0.264	0.933	1.345
12.000	0.073	0.945	1.013	0.246	0.253	0.938	1.288
18.000	0.049	0.960	1.006	0.231	0.233	0.943	1.189
25.000	0.033	0.968	1.001	0.209	0.220	0.950	1.124
30.000	0.026	0.970	0.997	0.233	0.214	0.951	1.090

set, so it would include all observed $a_{\text{cdom+det}}(\lambda)$ and C from the diverse cruises (see Figure 4.3 in next section).

4.5 Results and Discussion

4.5.1 Main characteristics of the data sets

To facilitate the interpretation of the trends in the observations presented in the following sections, it is important to describe the measured patterns of both $F_{\langle p \rangle}$ and $a_{\text{cdom+det}}(\lambda)$ relative to C . All measurements refer to surface samples and are assumed to be representative of the mixed layer.

4.5.1.1 Observed $F_{\langle p \rangle}$ and C

Changes in spectral absorption as a function of C during the different cruises can be illustrated by the relationship between $F_{\langle p \rangle}$ and C (Figure 4.2). Comparing observations and model (i.e., “expected”) results, one can observe that the expected trend between $F_{\langle p \rangle}$ and C was approximately followed during the cruise in the Bering Sea in 1996 (BS96) and during only a portion of the time series in Bedford Basin in 1996 (BBTS96) represented by the fall bloom observed in mid-October. During the summer experiments in Bedford Basin in both 1992 and 1996 (BBS92 and BBS96), measured $F_{\langle p \rangle}$ values were representative of dominance by small cells. In the summer of 1993, due to a bloom of large dinoflagellates that remained intermittently at sub-surface, $F_{\langle p \rangle}$ varied mainly reflecting the proportion of dinoflagellates to the small-celled flagellates that were always present at the surface. During the Bering Sea cruise in 1997 (BS97), a large portion of the data collected were derived from radial transects in an anticyclonic eddy showing a relatively constant $F_{\langle p \rangle}$ representative of a bloom of small cells (probably *Phaeocystis*, J.J. Cullen pers. comm.). The eddy was revisited after the presumed crash of this “bloom” observed with ocean color drifters (Cullen *et al.*, 1998),

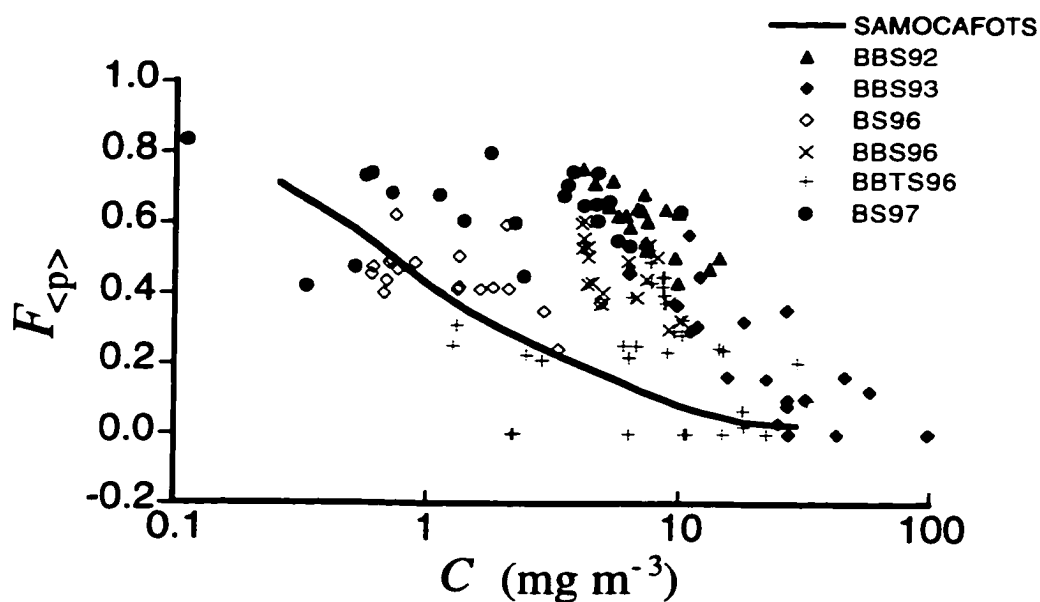


Figure 4.2 Inferred contributions of different size classes to phytoplankton absorption (i.e., values of $F_{<p>}$ computed from measured phytoplankton absorption spectra) as a function of trophic status in the different data sets (see legend) compared to “expected” values as a function of C estimated with SAMOCAFOTS (solid line). Points above the line correspond to spectra characteristic of cells smaller than predicted by the model.

and as will be shown later, resulted in high CDOM plus detrital absorption values at low C .

4.5.1.2 Observed $a_{\text{cdom+det}}(\lambda)$ and C

The relationship between $a_{\text{cdom+det}}(\lambda)$ and C during BS96 (Figure 4.3A) shows that observed $a_{\text{cdom+det}}(\lambda)$ values were similar to the predictions of the model for C above 1 mg m^{-3} but with high values at lower C . This resulted in an inverse relationship between $a_{\text{cdom+det}}(\lambda)$ and C in low- C water. The same inverse relationship was observed during BS97 at low to medium C . Higher $a_{\text{cdom+det}}(\lambda)$ values than those predicted by the model were also observed in high C accompanying the bloom in the Bering Sea in 1997.

The several data sets from Bedford Basin were taken from a single sampling point at different times. The Basin receives large inputs of particulate and dissolved organic matter from both land drainage and untreated sewage discharge, and values of $a_{\text{cdom+det}}$ are high in any season (Figure 4.3B). Because of that, the comparisons between data and model (or expected values) results refer to SAMOCAFOTS high CDOM, which includes a “background” $a_{\text{cdom+det}}(\lambda)$ that encompasses more properly the range of conditions in the Basin (see chapter 2). During the intensive sampling in August 1993 and 1996, $a_{\text{cdom+det}}(\lambda)$ values were similar to those predicted by SAMOCAFOTS high CDOM at a given C . Strong and episodic increases in $a_{\text{cdom+det}}$ during rainy periods were observed in July and also in the end of August of 1996.

4.5.2 Remote sensing reflectance ratios and C

Ratios of remote sensing reflectance have been important tools in bio-optical oceanography, yielding robust empirical relationships with C and other constituents of sea water (Gordon and Morel, 1983; Carder *et al.*, 1991; Aiken *et al.*, 1995; Lee *et al.*, 1998). The ratio $R_r(490)/R_r(555)$ is particularly important, as it has been shown recently

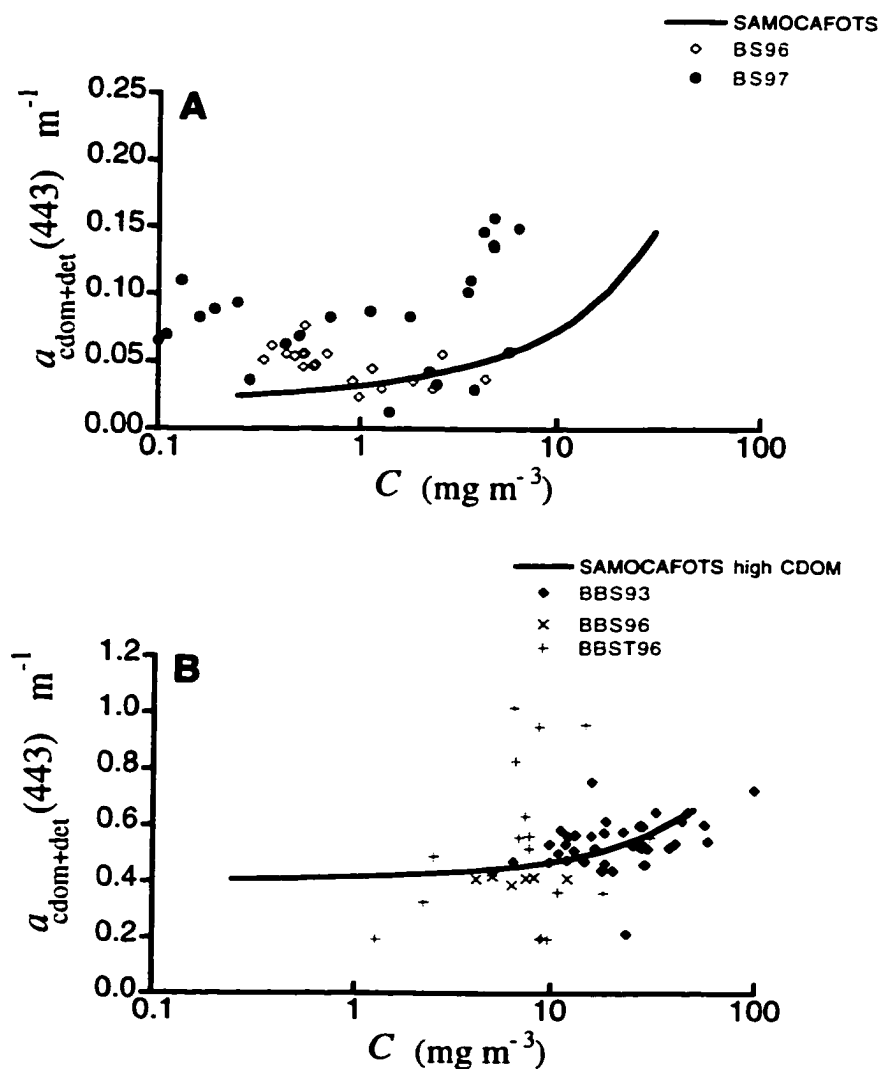


Figure 4.3 Relationship between measurements of absorption by CDOM and detritus at 443 nm versus C in the different data sets (see legends) compared to values estimated by the model (solid lines). **A)** Data from the Bering Sea cruises and estimates from SAMOCAFOTS and **B)** Data from Bedford Basin and estimates from SAMOCAFOTS high CDOM.

to be the single wavelength pair to explain empirically most of the variability found in C in surface waters (O'Reilly *et al.*, 1998). Some evidence of the influence of phytoplankton showing different degrees of pigment packaging on empirical bio-optical relationships has already been presented (Mitchell, 1992; Carder *et al.*, 1999), and it is thus crucial to analyze the extent to which different communities at a given C can affect this ratio. Ratios such as 412:555 and 443:555 are more susceptible to interference by other optically active constituents of the water, such as CDOM and detritus. These components will also affect 490 nm, but less than they affect 412 and 443 nm, due to the spectral shape of their absorption coefficient, typically represented by an exponential decrease with wavelength (Bricaud *et al.*, 1981).

The semi-analytical model recreates well the empirical relationships (e.g., O'Reilly *et al.*, 1998) between $R_r(490)/R_r(555)$ and C for ranges between 0.5 to 30 mg m⁻³ (chapter 2). Because of that, analyses comparing model results and data outside this range of C will be not discussed in depth .

4.5.2.1 Influence of cell size on simple reflectance ratios

In the general formulation of the semi-analytical model, $F_{<p>}$ decreases smoothly with C (Figure 4.2b), representing the changes in the spectral shape of the phytoplankton absorption coefficient with C that are consistent with a gradual increase in the cell size of the dominant organisms. At first approximation, assuming that the shape of phytoplankton absorption coefficient indeed varies between two possible extremes, the model can be run with $F_{<p>}$ fixed to one and zero, thereby simulating relationships between $R_r(490)/R_r(555)$ and C for dominance of small and big cells, respectively, ignoring any systematic differences in backscattering and in CDOM plus detrital absorption. When these formulations are compared to our data set representative of coastal and oceanic waters with small to moderate contributions of continental outflows (i.e., relatively low CDOM Figure 4.4A), it is observed that the lines representing the model simulations create an envelope around most of the data, except at very low C (the

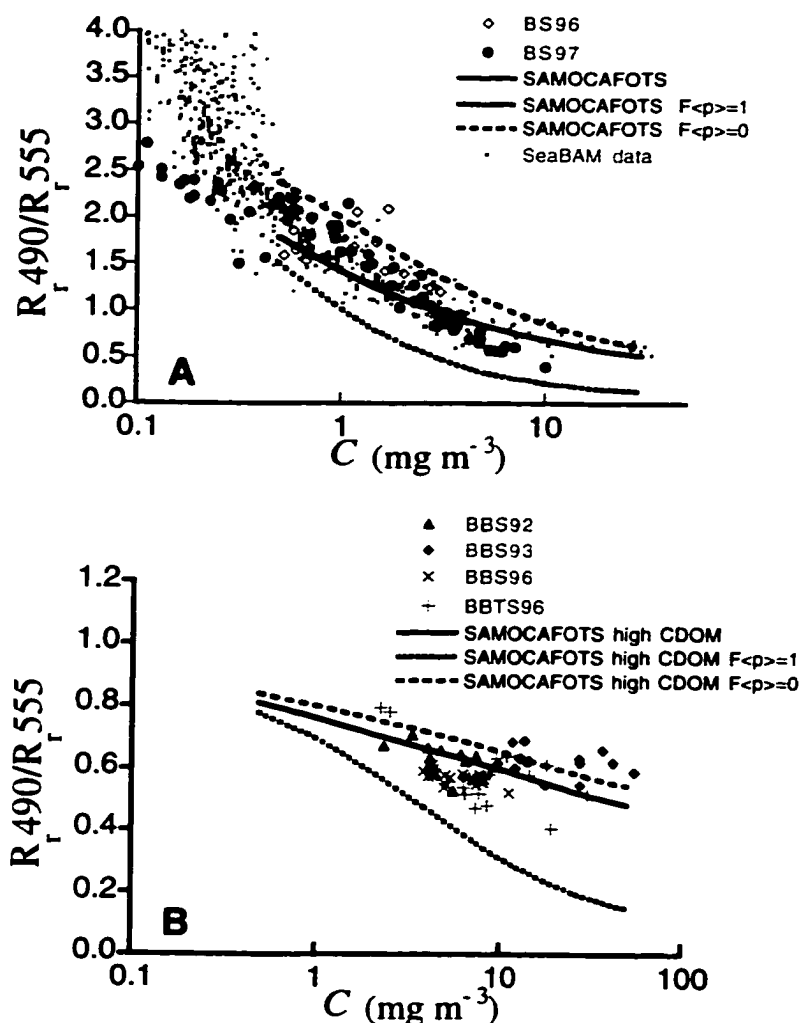


Figure 4.4 Relationships between $R_r(490)/R_r(555)$ and C from all cruises. **A)** Solid line shows results of the semi-analytical model SAMOCAFOTS describing the central trend of the decrease in $F_{\langle p \rangle}$ with C , in which small cells dominate at low C and large cells dominate at high C . Small dashed line represents SAMOCAFOTS with $F_{\langle p \rangle} = 1$ (dominance of small cells). Large dashed line represents SAMOCAFOTS with $F_{\langle p \rangle} = 0$ (dominance of large cells). An independent data set (SeaBAM validation data set, courtesy of Dr. C. McClain) is included for comparison. **B)** Same as **A** only for data collected in Bedford Basin in several occasions compared to SAMOCAFOTS high CDOM. Note change in scales.

SeaBAM validation data set, courtesy of Dr. C. McClain, is plotted for comparison). The envelope suggests that the degree of variability in the relationship between $R_r(490)/R_r(555)$ and C imposed by communities of phytoplankton of distinct cell sizes can be of the order of 40 to 50% around the central trend of the reflectance ratios as a function of C , at a maximum. Deviations above 50% can be expected for dominance of very small cells at C higher than 3 mg m^{-3} . This is somewhat unrealistic (Chisholm, 1992), as “blooms” of very small (usually procaryotic) cells, such as *Synechococcus* are found in nature with relatively low C of about 1 mg m^{-3} (e.g., Morel, 1997). Nonetheless, the trends observed at high C in Figure 4.4A are in agreement with the predictions of the model: deviations in reflectance ratios of about 20 to 40% were observed in the data and could be related to the dominance of small cells during BS97.

Similar envelopes can be created for comparison with the data collected in Bedford Basin (Figures 4.4B). In these data, deviations from the relationship between $R_r(490)/R_r(555)$ and C are consistent with the presence of large cells observed during the red tide event in 1993 (Cullen *et al.*, 1994) and of small cells during the summer of 1996. However, deviations from the relationship between $R_r(490)/R_r(555)$ and C in the Basin are expected to be strongly driven by changes in $a_{\text{cdom+det}}$.

4.5.2.2 Influence of $a_{\text{cdom+det}}(\lambda)$ on simple reflectance ratios

In nature, not only F_{cp} but also CDOM plus detritus absorption is expected to change differently with C than is predicted by the model. For example, the data points below the line predicted by the general formulation of SAMOCAFOTS (Figure 4.4A) are a consequence of increasing $a(490)$ relative to $a(555)$. This can be a result of both a decrease in the flattening of the phytoplankton absorption spectra (i.e., dominance of small cells) or a larger contribution by $a_{\text{cdom+det}}(\lambda)$. By varying the parameter values controlling $a_{\text{cdom+det}}(\lambda)$ in the model, a new envelope around the general formulations of SAMOCAFOTS can be created (Figures 4.5A and 4.5B). If $a_{\text{cdom+det}}(\lambda)$ varies from 1/4 to 4 times of the values assumed in the general model at each C (which is a reasonable

range to include all our observations as shown in Figure 4.3), the expected deviations of reflectance ratio are about 20 to 30% for C less than 2 mg m^{-3} , decreasing to less than 10% at higher C . The deviations in Figure 4.5A emphasize the data points collected in the Bering Sea with low C as a result of higher contribution of CDOM absorption. Note also that points from C between 0.5 and 5 mg m^{-3} during BS97 are in close agreement with the line representing $1/4$ of the values assumed in the general model. It is important to note that in the model, the spectral shape of $a_{\text{cdom+det}}$ was kept constant following an exponential decrease with wavelength with a slope of -0.015 (equation 4.6). Model simulations varying the slope from -0.02 to -0.01 (not shown) produce deviations of 5% at a maximum in $R_r(490)/R_r(555)$ as a function of C with SAMOCAFOTS, but around 20% with SAMOCAFOTS high CDOM (Figure 4.5B).

4.5.3 Inflection ratios and C

In all the $R_r(490)/R_r(555)$ predictions discussed above, it was assumed that changes in backscattering with C in the data follow closely the central tendency described by the model (see chapter 2). Briefly, scattering by phytoplankton plus detritus at 660 nm, $b_{\text{ph+det}}(660)$, and the spectrally-invariant backscatter ratio, $\tilde{b}_{\text{ph+det}}$, are specified as functions of C using published empirical relationships. Their product is used to calculate the backscattering by particles, $b_{\text{ph+det}}(\lambda)$ with the application of an exponential slope (γ) for wavelength dependence. The slope γ changes with C , reflecting larger particle sizes, hence lower γ , at higher C . Backscatter due to pure water comes from the literature (see chapter 2 for details). As changes in backscatter are most likely a result of the influence of components other than phytoplankton, the effects of changes in $F_{<p>}$ on $b_{\text{ph+det}}(\lambda)$ were not taken into account in the modeling exercises.

However, part of the deviations observed in the data could be a result of a different behavior of spectral backscattering in relation to what is predicted by the model. Thus, it is useful to investigate quantitatively the general deviations produced by changes

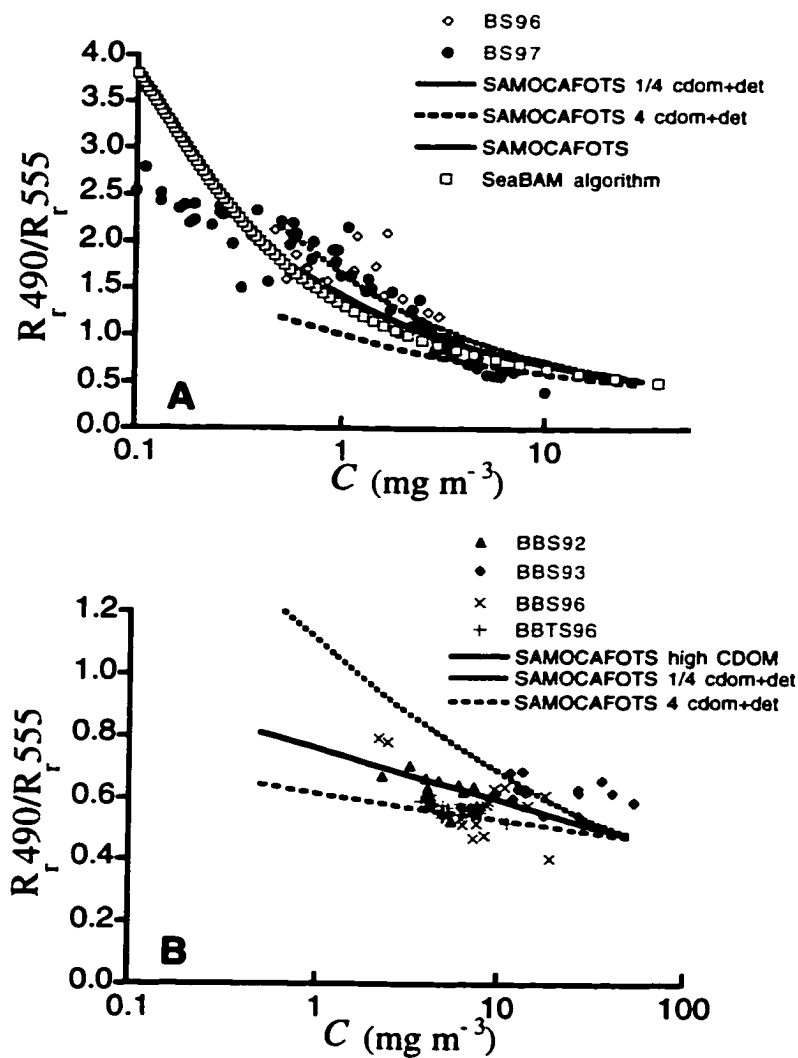


Figure 4.5 Same as Figure 4.4, only the model runs refers to changes in the total value of absorption by CDOM plus detritus of 1/4 of SAMOCAFOTS (small dashed line) and 4 times of SAMOCAFOTS (large dashed line). **A)** Data from the different cruises excluding Bedford Basin (see legend). The SeaBAM empirical relationship (O'Reilly et al., 1998) is plotted for comparison. **B)** Bedford Basin data only.

in $F_{<p>}$ and $a_{\text{cdom+det}}(\lambda)$ on the inflection ratio $R_r(443)R_r(555)/R_r(490)^2$ as a function of C , which in principle is relatively insensitive to backscattering (Zaneveld *et al.*, 1998, See also section 4.3).

The same simple sensitivity analysis for influences of $F_{<p>}$ and $a_{\text{cdom+det}}(\lambda)$ on $R_r(490)/R_r(555)$ as a function of C (Figures 4.4 and 4.5) can be repeated for the relationship between $R_r(443)R_r(555)/R_r(490)^2$ and C (Figure 4.6). These analyses suggest that inflection ratios have relatively low sensitivity to $a_{\text{cdom+det}}(\lambda)$, which when varied by a factor of 16 from that expected by the model, yield deviations of less than 20% around the central trend of reflectance ratios as a function of C (Figure 4.6B) in environments with low to moderate inputs of CDOM and detritus. Changes in dominant cell size (Figure 4.6A), on the other hand, are the major cause of variability in the relationship between $R_r(443)R_r(555)/R_r(490)^2$ and C , accounting for deviations of more than 50% in the ratio when C is higher than 2 mg m^{-3} . The simulations with SAMOCAFOTS high CDOM, which is representative of average conditions in Bedford Basin, show the same tendencies, although deviations produced by $a_{\text{cdom+det}}(\lambda)$ can be on the order of 30%, at a given C (Figures 4.6C and 4.6D). Comparisons with data (Figure 4.7) show that, similarly to what was found for the relationship between $R_r(490)/R_r(555)$ and C , the envelopes created by the model simulations included most of the data points. The tendencies in the cruises are also repeated, that is, the presence of small cell sizes during BS97 and a good agreement between the general model and the BS96 data.

4.5.3.1 Comparing effects of size and $a_{\text{cdom+det}}(\lambda)$

Using forward modeling exercises, one can estimate the degree of influence that either changes in phytoplankton cell size range ($F_{<p>}$) or changes in CDOM plus detrital absorption ($a_{\text{cdom+det}}(\lambda)$) have on total absorption at a given C . In turn, ratios of surface reflectance associated with this variability can be estimated, thereby computing the extent

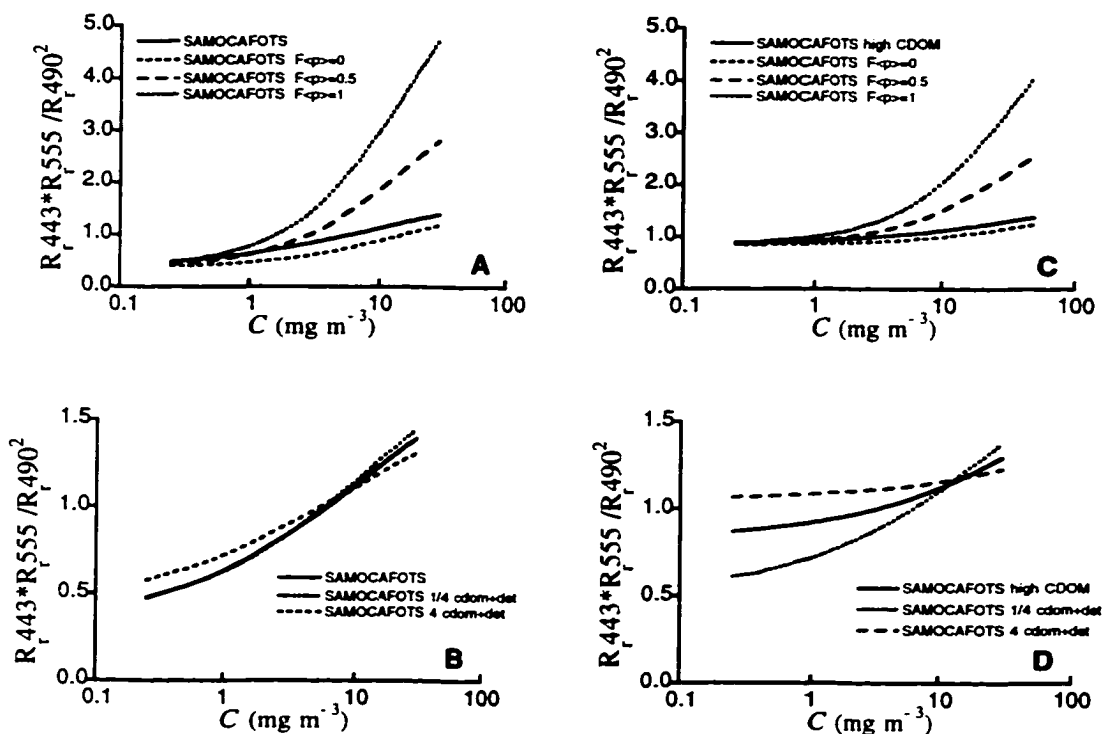


Figure 4.6 Sensitivity analysis of the influence of changes in dominant cell size and $a_{\text{cdom+det}}(\lambda)$ on relationships between $R_r(443)R_r(555)/R_r(490)^2$ versus C . **A)** Solid lines are results of the semi-analytical model SAMOCAFOTS with its general formulation. Dashed lines represent SAMOCAFOTS run with fixed values of $F_{\langle p \rangle}$ (see legend). **B)** Same as **A** but the model runs refer to changes in the total value of absorption by CDOM plus detritus of 1/4 (small dashed line) and 4 times (large dashed line) of that predicted by SAMOCAFOTS. **C and D)** Same as **A** and **B**, but for SAMOCAFOTS high CDOM.

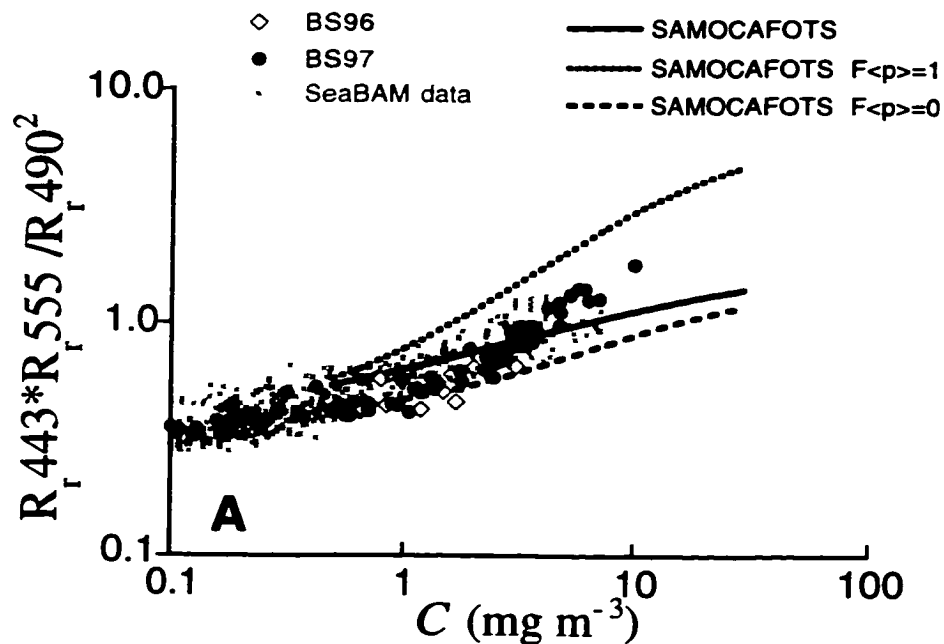


Figure 4.7 Relationships between $R_r(443)R_r(555)/R_r(490)^2$ versus C from cruises excluding the ones in Bedford Basin (see legend). Solid line are result of the semi-analytical model SAMOCAFOTS, showing the central trend of the decrease in $F_{<p>}$ with C , in which small cells dominate at low C and large cells dominate at high C . Small dashed line represents SAMOCAFOTS with $F_{<p>}=1$ (dominance of small cells). Large dashed line represents SAMOCAFOTS with $F_{<p>}=0$ (dominance of large cells).

to which both $F_{<p>}$ and $a_{\text{cdom+det}}(\lambda)$ can influence the retrieval of C from ratios of surface reflectance (Figure 4.8A). The reflectance ratio modeled in Figure 4.8A is sensitive to the ratio of backscattering at 490 vs 555 nm. Because the analyses presented here did not include changes in backscattering, extreme ranges of variability were also computed for the relationship between inflection ratios of surface reflectance and C (Figure 4.8B) which in principle, is affected almost exclusively by total absorption.

These sensitivity analyses show that differences in $F_{<p>}$, thus in cell size range of the dominant organism, can indeed be an important source of variability in algorithms using simple ratios of remote-sensing reflectance at the surface, especially at C above 1-2 mg m^{-3} . Therefore, these changes should be considered in both regional and global bio-optical models, as they can produce deviations of 30 to 50% in $R_r(490)/R_r(555)$ as a function of C . The consequences for retrieving C from $R_r(490)/R_r(555)$ are even more drastic, as the uncertainties for C at a given value of $R_r(490)/R_r(555)$ suggested by the model can be of the order of approximately 10-fold, suggesting that global algorithms for C above 1 to 2 mg m^{-3} will perform unsatisfactorily when cell size changes remarkably (Figure 4.7).

In waters with C below 1 to 2 mg m^{-3} , however, deviations in reflectance ratio associated with changes in cell size range are about the same magnitude as those imposed by a range of values for $a_{\text{cdom+det}}(\lambda)$, encompassing the variability encountered in our data set (Figure 4.3). Waters with low chlorophyll and this range of CDOM include most oceanic situations. Although the lowest model predictions are at C equals to 0.5 mg m^{-3} , it is not unreasonable to assume that the influence of changes in $a_{\text{cdom+det}}(\lambda)$ below 0.5 mg m^{-3} will be even more pronounced. In addition, at a low values of C it is likely that changes in $F_{<p>}$ are rather small (see Figure 4.2) because dominance of larger cell sizes are generally associated with high phytoplankton standing crops (Yentsch and Phinney, 1989; Chisholm, 1992). Mechanistic approaches for bio-optical models in low-chlorophyll waters should concentrate on establishing the relative proportions between phytoplankton and CDOM plus detrital absorption (Garver and Siegel, 1994). At high C ,

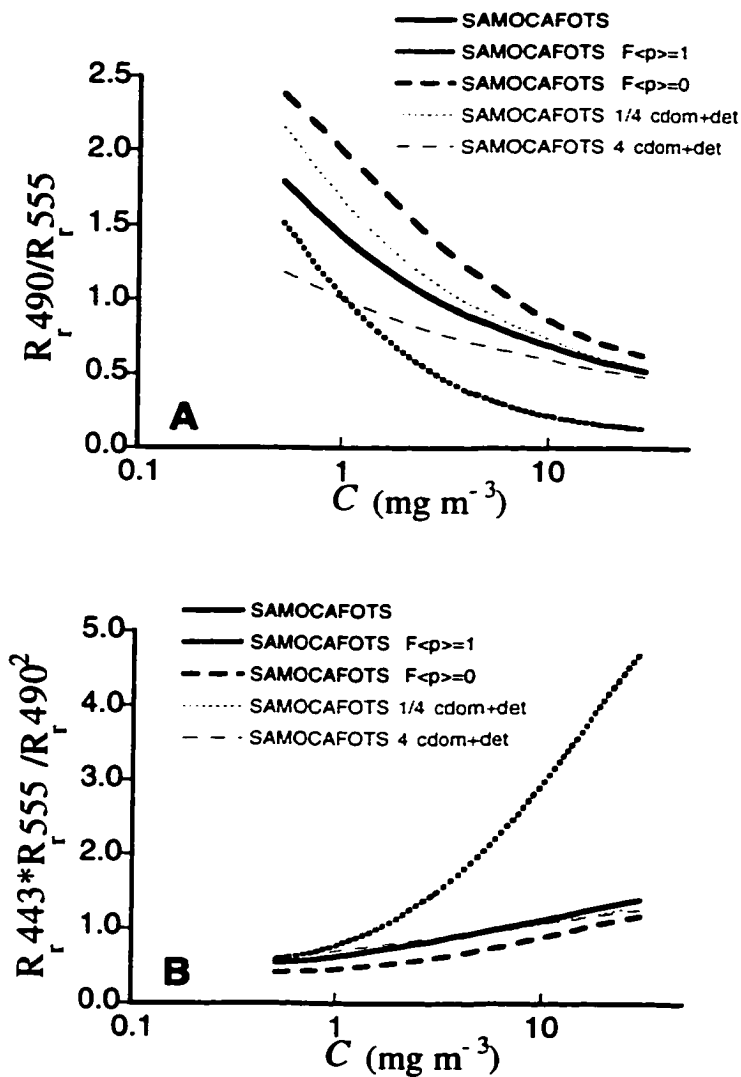


Figure 4.8 Summary of the influence of changes in phytoplankton absorption attributed to changes in cell size range ($F_{<p>}$) and changes in CDOM plus detrital absorption on reflectance ratios. **A)** Relationship between $R_r(490)/R_r(555)$ and C . **B)** Relationship between $R_r(443)R_r(555)/R_r(490)^2$ and C .

hence dominance of phytoplankton absorption, it is clear that changes in dominant cell size have the stronger influence on retrieval of C . On the other hand, it is likely that changes in backscattering play a role on the deviations observed in the data set (Figure 4.4). When the sensitivity to $F_{<p>}$ or to $a_{\text{cdom+det}}(\lambda)$ is quantified in the relationship between $R_r(443)R_r(555)/R_r(490)^2$ (i.e., inflection ratio) and C (Figure 4.8B), one could expect that the use of an inflection ratio for retrieval of C would be reasonable at low C , as both the effects of backscattering and $a_{\text{cdom+det}}(\lambda)$ are minimized. If it is assumed that at low chlorophyll concentrations $F_{<p>}$ can only vary between 1 and 0.5, the uncertainties in C at a given $R_r(443)R_r(555)/R_r(490)^2$ are still around 2-fold. At high C , our model simulations produced variability of more than 50% in $R_r(443)R_r(555)/R_r(490)^2$ at a given C , which suggests that tremendous uncertainties on the retrieval of C in these waters (Figure 4.8B see also Figure 4.7).

4.5.4 Retrieval of the size parameter from relationships between AOPS

4.5.4.1 Model approach

In chapter 2, the results of the sensitivity analyses on relationships between surface vertical attenuation coefficient ($K_d(\lambda)$) and radiance ratios suggested that these relationships are sensitive to changes in the degree of pigment packaging of the entire cell assemblage at medium to high C . It follows that these relationships are also sensitive to changes in $F_{<p>}$ and could be used as a tool for discriminating changes in the cell size ranges using passive optical instruments. The approach was to use a combination of wavebands for both K_d and radiance ratios in which changes in the spectral shape of phytoplankton absorption are the main source of variation.

Relationships between surface diffuse attenuation and surface remote sensing reflectance are examined here. These relationships will be hereafter designated to as AP-type relationships, after the most commonly used empirical formulation of $K_d(490)$ and $L_u(443)/L_u(555)$ by Austin and Petzold (1981). Relationships most responsive to

changes in $F_{<p>}$ can be identified with a simple sensitivity analysis using our semi-analytical model (SAMOCAFOTS).

Similarly to what was done for reflectance ratios in section 4.4.2, the general formulation of the model is presumed to represent “expected” values of total absorption and backscattering, and thus AOPs, for a given range of C . If it is assumed that changes in the behavior of backscattering with C , specifically related to $F_{<p>}$ are small (i.e., keeping the terms describing backscattering exactly as they are in the general formulation of the model), one can compare how sensitive the different AP-type relationships are to changes in cell size range. For the same range in C used in the general formulation of the model, simulations can be created for cases in which small or big cells dominate by fixing $F_{<p>}$ to one and zero, respectively. Because CDOM and detrital absorption modify the spectral shape of total absorption, it is also possible to evaluate how sensitive these relationships are to $a_{\text{cdom+det}}(\lambda)$ in comparison to $F_{<p>}$. The sensitivity analyses for changes in $a_{\text{cdom+det}}(\lambda)$ were made by running the model with $a_{\text{cdom+det}}(\lambda)$ at each C modified to be 1/4 or 4 times the value used in its general formulation. It is important to remember that in all different formulations of the model, the spectral shape of $a_{\text{cdom+det}}$ was kept constant and that our relationships refer to $K_d(\lambda)$ versus $R_r(\lambda_1)/R_r(\lambda_2)$, rather than versus $L_u(\lambda_1)/L_u(\lambda_2)$. The analyses were made for six combinations of diffuse attenuation and reflectance ratios using 490, 510 and 555 nm. These are the wavebands available in our data set that are least influenced by $a_{\text{cdom+det}}(\lambda)$.

Comparing the deviations produced by changes in $F_{<p>}$ and $a_{\text{cdom+det}}(\lambda)$ with C for the 6 different AP-type relationships (Figure 4.9), it becomes clear that changes in $F_{<p>}$ tend to produce a large variation in the shape of the curves, while changes in $a_{\text{cdom+det}}(\lambda)$ tend to modify the absolute value of $K_d(\lambda)$ relative to $R_r(\lambda)/R_r(\lambda)$, and do not affect much the shape of the relationship (see chapter 2). It follows that the AP-type relationship showing the highest degree of “spreading” of the lines due to changes in $F_{<p>}$ could be a potential tool to observe changes in the phytoplankton size structure from measurements of AOPs. In our model simulations, effective AP-type relationships are

those between $K_d(555)$ and either $R_r(510)/R_r(555)$ or $R_r(490)/R_r(555)$ (Figures 4.9C and 4.9E).

The spreading of the lines describing $K_d(555)$ versus $R_r(490)/R_r(555)$ for a given value of $F_{<p>}$ (Figure 4.10 A) occurs mainly because phytoplankton absorption at 555 nm varies just slightly with $F_{<p>}$ (see Figure 4.1A). As $a_{\text{cdom+det}}(550)$ also has little effect over $K_d(555)$, at a given C $K_d(555)$ tends to remain approximately constant. On the other hand, $F_{<p>}$ becomes important for defining phytoplankton absorption at 490 nm, and thus the shape of the curves is governed by $R_r(490)/R_r(555)$. Consequently, a pair of $K_d(555)$ and $R_r(490)/R_r(555)$ values at a given C , will fall on a single possible AP-type curve simulated by $F_{<p>}$.

These analyses suggest that $F_{<p>}$ could be retrieved from $R_r(490)/R_r(555)$ and $K_d(555)$ data pairs collected simultaneously in surface waters, by comparing the observations to the expected relationships from model simulations. The comparison between model and observations could be done, for example, with a nomogram (Figure 4.10) in which observations of $K_d(555)$ and $R_r(490)/R_r(555)$ are plotted, and $F_{<p>}$ is read from it. Alternatively, the curves defining $K_d(555)$ versus $R_r(490)/R_r(555)$ for a fixed value of $F_{<p>}$ could be described with curve fits and the distance of the observed point from the lines computed statistically. The use of such an approach in waters with a high influence of CDOM and detrital absorption is limited as both $K_d(555)$ and $R_r(490)/R_r(555)$ will be affected not only by the proportion of CDOM plus detrital absorption in relation to phytoplankton absorption, but also by the spectral shape of $a_{\text{cdom+det}}$ (see chapter 2) which will vary according to the source of these component (Carder *et al.*, 1991; Green and Blough, 1994), or possibly some degree of photochemical fading (Vodacek *et al.*, 1997). Nomograms can be created to be used for Bedford Basin data, because the parameter values describing $a_{\text{cdom+det}}(\lambda)$ were adjusted to represent the average conditions in the Basin (see Figure 4.3B).

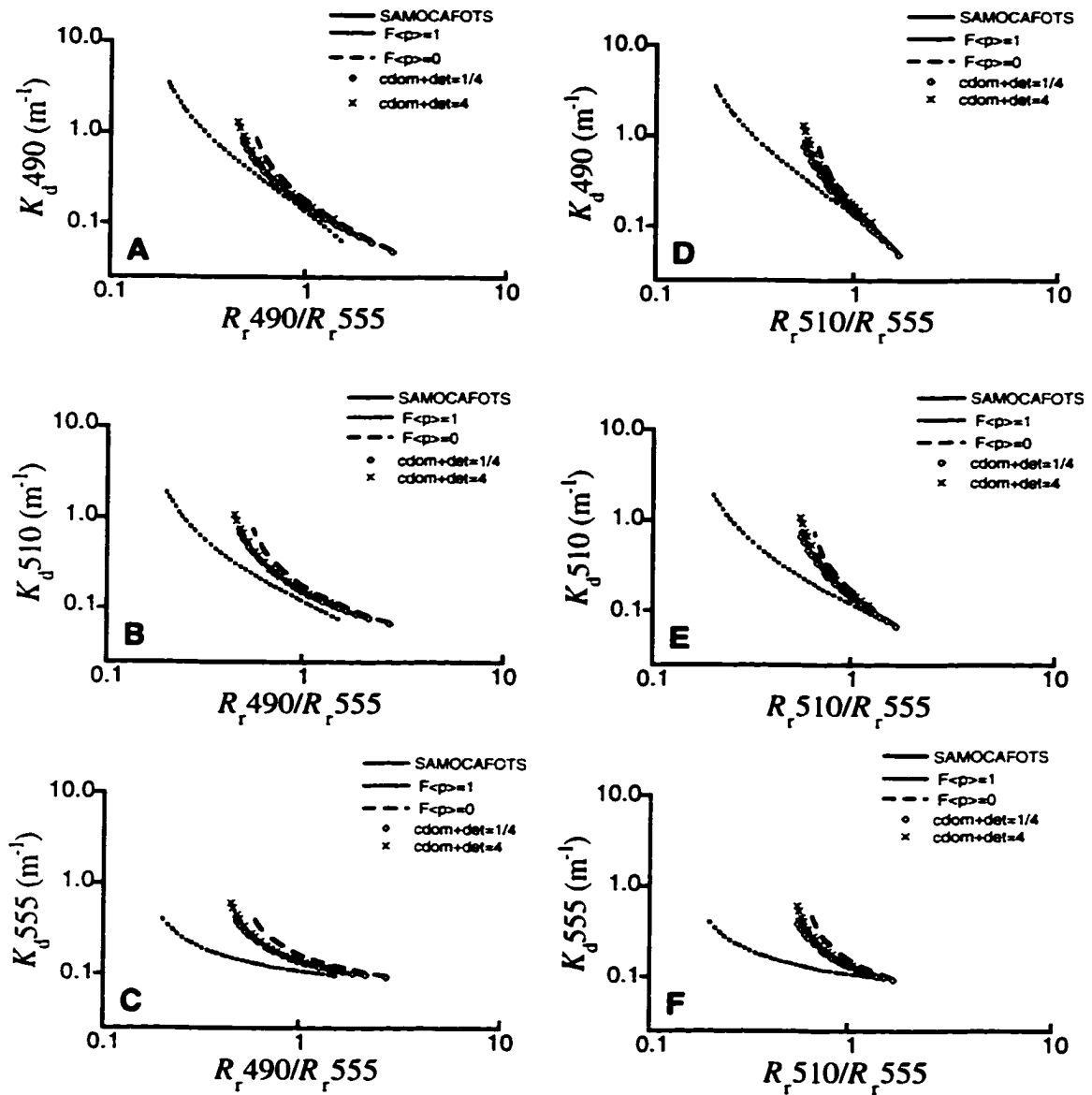


Figure 4.9 Relationships between vertical attenuation coefficient and remote sensing reflectance ratios. Solid lines are results of the general formulation of the semi-analytical model; dotted lines represent model results with dominance of small cells; large-dashed lines represent model results with dominance of big cells; model results are presented for values of absorption CDOM plus detritus of 1/4 (diamonds) and 4 times (x) of that predicted by SAMOCAFOTS.

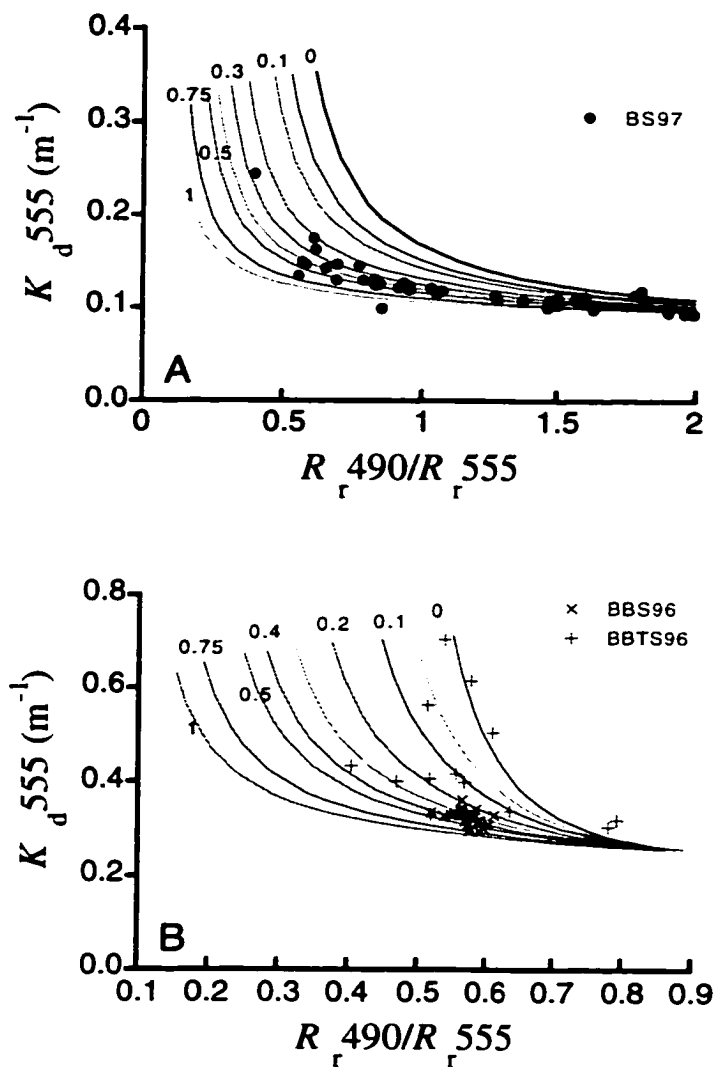


Figure 4.10 Nomograms for retrieving F_{cp} from relationships between vertical attenuation coefficient at 555 nm and remote sensing reflectance ratio of 490 to 555 nm. Lines represent model runs of SAMOCAFOTS (A) and SAMOCAFOTS high CDOM (B) with fixed values of F_{cp} as designated in the lines. Data are plotted for comparison (see legend for cruises). Note scale changes.

4.5.4.1 Comparison of the model approach with independent data

Three data sets will be used to analyze the performance of this approach because they have an appropriate range of conditions and measurements: Bering Sea in 1997, the time series in Bedford Basin in 1996, and the summer intensive sampling in Bedford Basin in 1996. Visual inspection of the data points in the respective nomograms somewhat confirm the expectations. Data from Bering Sea in 1997 followed the model results of dominant small cells (Figure 4.10A). Small cells also dominated during the summer of 1996 in Bedford Basin, (Figure 4.10B) and during the time series a wide range of $F_{<p>}$ values was observed (see also Figure 4.2). Note that some data points fall outside the possible range described by $F_{<p>}$ in Figure 4.10B. The model can be run with negative values of $F_{<p>}$ to expand the range of the nomogram. When those nomograms are used, however, the results are not very encouraging (Figure 4.11). There is a clear bias underestimating $F_{<p>}$ and the dispersion of the points is high (r^2 is around 0.15 for Bering Sea data and around 0.67 for the Bedford Basin data).

Both the bias and dispersion of the points can be related to many factors. The model estimates intrinsically assume that there are no errors in the measurements of AOPs and IOPs. In our data set, one can expect some errors in both, although care was taken to minimize the known factors that produced variability. Measurements of phytoplankton absorption using the filter pad method (Mitchell, 1990) are subject to uncertainties related to the path length correction (beta factor); however, care was taken to have enough material on the filter to avoid this problem. In addition, the samples were duplicated. Measurements of surface reflectance can be affected by errors in the instrument calibrations. All instruments were calibrated prior to the cruise, following rigorous protocols. Both surface reflectance and diffuse attenuation measurements can be affected by the sea state during the sampling. This problem was minimized by averaging the data from the radiometer buoys (Cullen *et al.*, 1994), eliminating data points of the profiler (used for $K_d(\lambda)$ computations) above a threshold of instrument vertical tilt (see

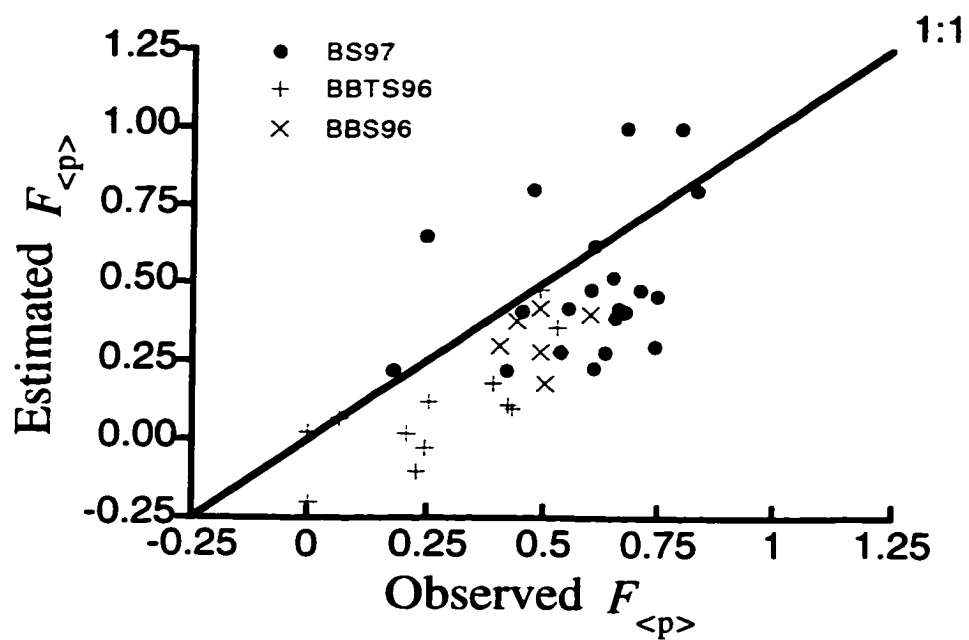


Figure 4.11 Retrieved $F_{<p>}$ from the nomogram of Figure 4.11 versus observed $F_{<p>}$ computed from surface samples of phytoplankton absorption (see legend for cruises).

methods) and by performing multiple casts. Small errors in $K_d(\lambda)$ could also be introduced by changes in cloudiness which can affect the spectral downwelling irradiance. However, the portions of the casts used (i.e., uppermost layer) were collected quickly, and the average of multiple casts also minimized this problem. Thus, although the individual sources of errors are expected to be small, when combined they may add to produce deviations on the relationships that are independent of $F_{<p>}$.

The use of the nomogram also assumed that there are no errors in the parameterization of the model. Although SAMOCAFOTS reproduces well empirical relationships between AOPs within the range of C for which it was parameterized, the simulations for the dominance of different cell sizes were done by only changing the parameter values controlling phytoplankton absorption. All the other terms, such as backscattering and CDOM plus detrital absorption, were kept as they were in the general formulation of the model. Deviations will be produced, especially in the Bedford Basin data, by episodic and high CDOM inputs which will significantly affect $K_d(555)$, invalidating the nomogram. In addition, the terms related to the geometrical distribution of the light field (i.e., $f(\lambda)$, $Q(\lambda)$ and $\bar{\mu}_d$) were kept constant in all simulations, and perhaps there are some intrinsic relationships between them and $F_{<p>}$; at least in conditions with high C , there is evidence that changes in phytoplankton can have an effect on the geometrical distribution of the light field (Morel and Gentili, 1996).

Because the spreading of the different lines in the nomogram is mainly controlled by $R_r(490)/R_r(555)$, uncertainties will always be associated with the backscattering term (see equation 4.4 and Table 4.2). As mentioned in section 4.3, a way to minimize both the uncertainties in $b_b(\lambda)$ and the effects of the geometrical distribution of the light field (Zaneveld *et al.*, 1998), is the use of an inflection ratio algorithm. The same approach was tried for retrieving $F_{<p>}$ with a nomogram relating $K_d(555)$ and $(R_r(443)R_r(555))/R_r(490)^2$ for the Bering Sea data only (Figure 4.12A). The use of such a nomogram for the Bedford Basin data (not shown) yielded extremely poor results, as many of the points fell outside the range defined by the model. This is probably a result

of the inclusion of the 443 nm channel in the analysis, which increases the effects of CDOM and detritus absorption, and perhaps CDOM fluorescence.

Comparing the retrieval of $F_{<p>}$ in the Bering Sea data using the two nomograms (Figures 4.11 and 4.12B), one observe that although the dispersion of the points was somewhat reduced when the inflection ratio nomogram was used (r^2 is around 0.56 versus 0.15) there is still a bias which results in an underestimate of $F_{<p>}$ (Figure 4.12B). This suggests that the uncertainties in the model are probably related to the parameterization of total absorption. Nonetheless, this cruise represents only one set of observations and more data are still necessary to confirm this assumption. It is important to note, however, that the parameterization of phytoplankton absorption in the model is limited at C below 0.5 mg m^{-3} (see chapter 2 and also Figures 4.4 and 4.7).

When all uncertainties are taken into account, the retrieval of $F_{<p>}$ in the Bedford Basin data set using the nomogram derived from of $K_d(555)$, and $R_r(490)/R_r(555)$ is fairly significant. Because much of the variability in Bedford Basin can be related to increases in CDOM and detritus input, it is reasonable to assume that in environments such as the Basin, the approach would work better if measurements of CDOM and detrital absorption were made concurrently to reflectance ratios and attenuation.

4.6 Summary and conclusions

In this chapter, the influence of phytoplankton absorption associated with different size ranges of phytoplankton on apparent optical properties was investigated. Using forward modeling, one is able to simulate AOPs for dominance of small and large phytoplankton cells for a given trophic gradient, thereby describing the maximum variability forced by cell size range (represented by $F_{<p>}$). A wide range of field data was used to confirm the model predictions. It was verified that the degree of variability imposed by extreme changes in cell size on remote sensing reflectance ratios of 490 to 555 nm as functions of C can be on the order of 30 to 50%, especially at C above 1-2

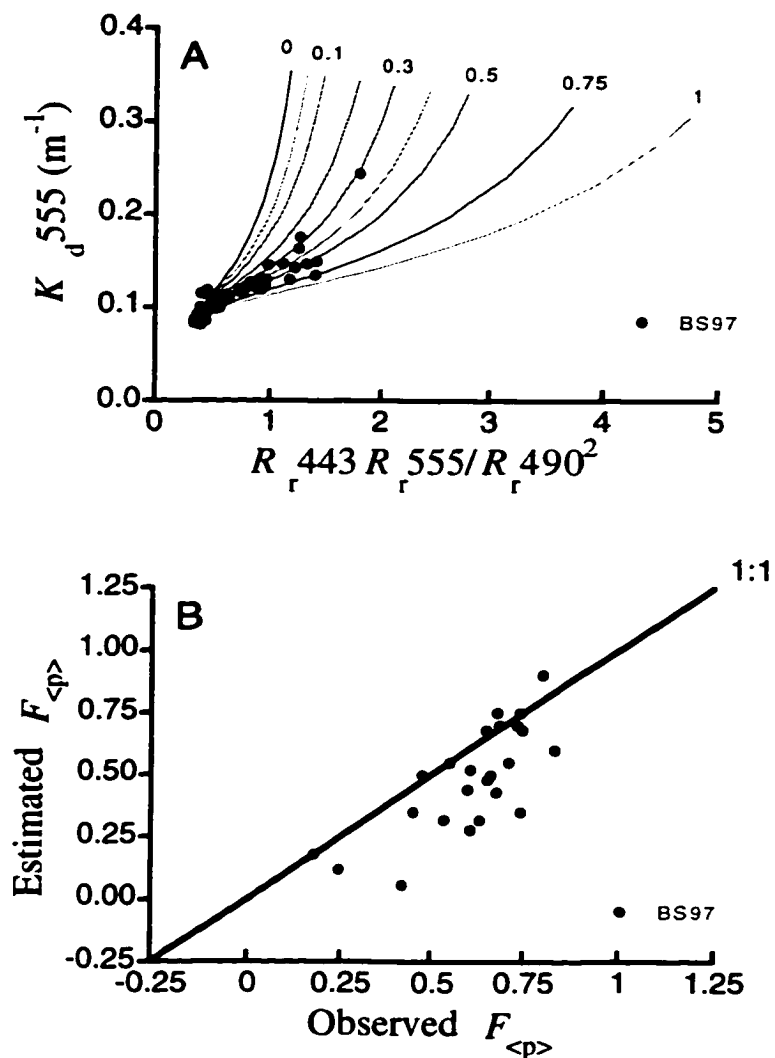


Figure 4.12 A) Nomogram for retrieving $F_{<p>}$ from relationships between vertical attenuation coefficient at 555 nm and remote sensing inflection reflectance ratio using 443, 490 and 555 nm (equation 4.5). Lines represent model runs of SAMOCAFOTS with fixed values of $F_{<p>}$ as designated in the lines. Data from BS97 is plotted for comparison. B) Retrieved $F_{<p>}$ from the nomogram in A versus observed $F_{<p>}$ computed from surface samples of phytoplankton absorption during BS97.

mg m⁻³, and as a consequence, the analyses suggest that uncertainties in C derived from reflectance ratios algorithms can be on the order of 2 to 8-fold due to changes in cell size. At lower C , the effects of size are less than or equal to the variability imposed by changes in CDOM plus detrital absorption. These results are valid for environments in which total absorption is the major factor controlling AOPs.

Approaches to observing bio-optical variability of phytoplankton minimizing the influence of CDOM and detritus, as well as minimizing the influence of backscattering, were also investigated. The goal was to establishing a combination of measurements that would allow the retrieval of $F_{<p>}$ from measurements of AOPs only. Model simulations of relationships between vertical attenuation coefficient and remote sensing reflectances in a combination of wavebands in which influences of CDOM and detritus are minimized indicated that these relationships can be sensitive to the dominant cell size of phytoplankton. The analysis suggested that nomograms can be used for the retrieval of $F_{<p>}$. Tests with our data, however, indicated that the retrieval is complicated by the simplifications made in the model, possibly related to the parameterization of backscattering and of the terms governing the geometrical distribution of light, as a bias in the retrieval of $F_{<p>}$ was still observed when the parameter values for absorption in the model were adjusted to represent the region of study (Bedford Basin).

In summary, although $F_{<p>}$ is a good estimator of the spectral shape of bulk phytoplankton absorption (chapter 3), and can be shown to produce consistent deviations in AOPs and C with a simple model and data, its retrieval from ocean color alone or from measurements of a combination of AOPs will depend on more accurate retrieval of properties such as backscattering and perhaps factors controlling the geometrical distribution of the light field. A possible path would be through inversion models (e.g., Garver and Siegel, 1997) in which the optical properties of all relevant component are explicitly incorporated in the model through their spectral shapes for both backscattering and absorption, with two spectral shapes to accommodate the contributions of small versus large cells to the absorption of light by phytoplankton.

Chapter 5

Summary, conclusions and future directions

5.1 Introduction

The goal of this thesis was to describe how different communities of phytoplankton affect apparent optical properties of surface waters of the coastal ocean. In particular, the research was intended to provide a context for developing ecological interpretations of relationships between apparent optical properties (AOPs), such as surface reflectance (i.e., ocean color) and diffuse attenuation coefficient. One important step in this process was to parameterize changes in the optical properties of phytoplankton assemblages in coastal waters as functions of trophic status. By describing central trends in AOPs with trophic status as functions of ecological characteristics of phytoplankton communities, it becomes possible to interpret quantitatively the deviations from the central trends in relationships between AOPs as functions of the same ecological characteristics, provided that all the other optically active components besides phytoplankton are taken into consideration.

Because most phytoplankton groups show unimportant backscattering, changes in absorption spectra are the main characteristics which can be used to discriminate the influence of different groups on ocean color and on the attenuation of light. Therefore, in order to quantify the effects of different communities of phytoplankton on apparent

optical properties, it is necessary to quantify not only how spectral absorption varies and how this relates to changes in phytoplankton communities, but also the relative importance of phytoplankton absorption in determining AOPs, compared to the other absorbing and refractive components in the ocean.

In general, the nature of phytoplankton communities can be related to the local trophic status: along a gradient from oligotrophic to eutrophic waters, different communities are formed by the addition of distinct groups of larger cells to a relatively constant background of smaller cells. The consequences of the overall increase in cell size with trophic status are reflected in well known, and extensively reported, empirical relationships between specific absorption coefficient and C , defined in this thesis as the concentration of fluorometrically measured chlorophyll plus pheopigments. These empirical relationships encompass the increase in intracellular shading (packaging) with C , which flattens the absorption spectra, and the decrease of the importance of accessory pigments in relation to the ubiquitous chlorophyll a . A central trend in absorption spectra influenced by pigment packaging and accessory pigments is thus expected in a given trophic range. This thesis proposes a parameterization of phytoplankton absorption as a function of pigment packaging and accessory pigments (both as functions of C) consistent with measurements and theory, thereby allowing mechanistic approaches to interpreting the general trends in phytoplankton optical properties as a function of trophic status.

When large data sets of specific absorption coefficients and C are pooled together, however, considerable variation is observed around the central trend. The variability is due to changes in the degree of pigment packaging (i.e., cell sizes and intracellular pigment concentration), and in the relative contribution of accessory pigments, different from the central trend. In order to interpret deviations in an ecological context, this thesis proposes a parameterization of the spectra shape of phytoplankton absorption in terms of phytoplankton community structure, relating these spectral shapes to the dominant cell size range. Once this new parameterization is incorporated in the semi-analytical

formulations describing AOPs, one can use forward modeling to quantify the consequences of varying cell size on relationships between AOPs.

5.2. General conclusions and future work

Reconciling relationships between inherent and apparent optical properties, as well as theoretical, laboratory and field observations, semi-analytical expressions were constructed to explore the effects of diverse optically active components (water, phytoplankton, detritus and CDOM) on the relationship between upwelling radiance ratios and diffuse attenuation as functions of C . The degree to which changes in pigment packaging and pigment composition alter the absorption of idealized phytoplankton cells was investigated in detail, using a parameterization that allowed a sensitivity analysis of the prominent factors affecting their optical properties. The general model, describing absorption and backscattering of the different optical components as functions of C , explained more than 80% of the variability in published relationships between radiance ratios and diffuse attenuation coefficients. Independent bio-optical data from a variety of environments, combined with the results of the sensitivity analysis, indicated that observed variability around the central tendencies of relationships between diffuse attenuation and upwelling radiance ratios could be substantially reproduced by: 1) changes in the degree of pigment packaging at high accessory pigment concentration; 2) variability in the spectral shape of the scattering coefficient (implying changes in the size distribution of the particles and also different types of particles) in environments where CDOM and detrital absorption are important; and 3) variability in non-phytoplanktonic absorption, particularly changes in S , the slope of the decrease in CDOM plus detrital absorption with wavelength, when their contribution is important. In summary, chapter 2 showed that:

- Consistent changes in the degree of packaging and accessory pigment concentration with trophic status can explain in large part the central trend in

relationships between diffuse attenuation and upwelling radiance ratios found in our data set.

- Deviations from the central trend can be attributed to changes in packaging and accessory pigments from different communities of phytoplankton, but their effects cannot be discriminated from the influence of CDOM and detrital absorption.

Two ecologically relevant factors known to affect the spectral shape of the absorption coefficient, that is cell size and taxonomic composition, were used to classify distinct natural communities in chapter 3. Their effects on changes in the spectral shape of absorption coefficient were quantified using 4 fixed size ranges. This approach was extended to a new parameterization of phytoplankton absorption consistent with the cell size range of the dominant organism. In summary, the results of chapter 3 were:

- Despite the differences in taxonomic composition observed in a large variety of marine environments, the shape of the absorption spectra for whole phytoplankton assemblages varied systematically with the cell size range of the dominant organism.
- Comparison of the diverse natural communities observed in our data set indicated that when dominant cell size range is specified (that is, pico-, ultra-, nano- and microplankton), more than 80% of the variability in the shape of absorption spectra between 400 and 700 nm can be explained.
- A linear decomposition of the observed phytoplankton absorption spectra of the different communities into a size parameter, $F_{<p>}$, and two basis vectors representing the two extreme possible spectral shapes (from the smallest and biggest dominant cell size observed), reproduced well ($r^2 > 0.95$) all of observed

spectral shapes when the entire visible range (i.e., 301 wavelengths) was considered. The size parameter describes changes in both packaging and accessory pigments.

In chapter 4, the size parameter $F_{<p>}$ was incorporated in the semi-analytical formulations described in chapter 2. The objective was to compute changes in relationships between apparent optical properties, as a function of trophic status, that could be related to cell size range directly. When apparent optical properties are computed for wavebands not strongly influenced by CDOM plus detrital absorption, deviations in relationships between apparent optical properties can be shown through forward modeling to be forced principally by changes in phytoplankton cell size with trophic status. Approaches to observing bio-optical variability of phytoplankton using measurements that minimize the influence of CDOM and detritus, as well as backscattering, were investigated. The primary findings of chapter 4 were:

- The degree of variability imposed by extreme changes in cell size on the commonly used relationship between C and remote sensing reflectance ratios of 490 to 555 nm can be on the order of 30 to 50% variability in the reflectance ratio at a given C , especially at C above 1-2 mg m⁻³; the uncertainties in C derived from empirical algorithms using reflectance ratios can be thus of the order of 2 to 8-fold due to changes in size range alone. At lower C , the effects of size are smaller than, or similar to the variability imposed by changes in the proportion of phytoplankton absorption compared to CDOM plus detrital absorption.
- Model simulations suggested that relationships between diffuse attenuation at 555 nm and the ratio of surface reflectance of 490 to 555 nm could be used for the retrieval of $F_{<p>}$ through nomograms. Tests with our data, however, indicated that the retrieval is complicated by the simplifications made in the parameterization of

the model (e.g., the assumed spectral shape of the backscattering or the assumed spectrally-invariant factors governing the geometrical distribution of the light field), even when the model is properly adjusted to represent the region of study.

In conclusion, this thesis reconciled well known trends in the behavior of bio-optical properties with trophic status into a quantitative and ecologically relevant context of changes in phytoplankton community structure. Recalling chapter 1, the main objectives of this thesis were:

- 1) to understand how different communities can affect AOPs;
- 2) to quantify these influences; and
- 3) to propose approaches that allow ecological interpretation of optical data (e.g., relationships between AOPs) by the retrieval of parameters that are related to changes in phytoplankton community structure.

The parameterization of pigment packaging and accessory pigments as functions of C (chapter 2), created a very useful, and extremely simple tool to explore the effects of idealized assemblages of phytoplankton on relationships between apparent optical properties, and mainly addressed objective 1. The semi-analytical expressions are simple, with equations for absorption and backscattering by the other optically active components independently parameterized as a function of trophic status. The model is thus easily applied in a diverse range of coastal environments by adjusting the relevant parameter values in the model.

The size parameter, $F_{<p>}$, and the two basis vectors provided a quantitative description of phytoplankton absorption that is strongly related to the cell size range of the dominant organism, independent of any measure of trophic status, thereby addressing objective 2. The implementation of $F_{<p>}$ in the semi-analytical model provided a simple way to characterize the effects of natural communities in the model and concurrently, to explore through forward modeling the influence of different communities of

phytoplankton on relationships between apparent optical properties. Approaches for retrieval of parameters such as $F_{<p>}$ from relationships between AOPs were developed to address objective 3: distinct curves of diffuse attenuation at 555 nm versus the ratio of surface reflectance at 490 to that at 555 nm for different values of $F_{<p>}$ can be constructed with the semi-analytical model. This approach suggested that changes in dominant cell size in coastal waters can be followed using these distinct relationships between AOPs, thereby providing a tool to observe and monitor changes in the nature of phytoplankton community using optical measurements only.

Chapter 4 suggested that the retrieval of parameters such as $F_{<p>}$ from ocean color alone (e.g., using inversion models) or from relationships between AOPs could be refined if the expressions governing backscattering, and perhaps those describing the factors controlling the geometrical distribution of the light field, were improved in the semi-analytical model. Future work should, thus, be focused on obtaining the data and developing the expressions to describe how the different optically active components in sea water quantitatively affect backscattering and factors related to the geometrical distribution of light.

Community structure of phytoplankton is defined as the mosaic of different species present in a body of water. Many biogeochemical processes in the ocean are directly linked to the size structure of phytoplankton assemblages, such as particle fluxes (e.g., sedimentation rates) and the efficiency of transfer of energy between phytoplankton and higher trophic levels (e.g. length of trophic chain and consequences for fisheries). Thus, the knowledge of cell size, along with the knowledge of phytoplankton abundance, can improve estimates of these biogeochemical processes.

No method can replace microscopic analyses to quantify community structure, i.e., the abundance of organisms at species level: pigment analyses can give only a rough idea of the different classes present, and the description of different cell sizes alone gives no taxonomic information. The parameter $F_{<p>}$ is likewise imperfect, but because it describes the covariation between cell size and concentration of accessory pigments, and

the consequences of these changes for the absorption spectra of natural phytoplankton, it can be a useful bio-optical tool. It is also reasonable to assume that physiological and ecological characteristics directly related to absorption of light by phytoplankton or cell size structure are also strongly related to $F_{<p>}$. An interesting subject for future work is, therefore, the establishment of relationships between $F_{<p>}$, obtained from bio-optical measurements, and both physiological characteristics such as primary production parameters, and ecologically important processes such as particle fluxes and trophic transfer to fisheries.

This thesis shows that mechanistic approaches to interpreting bio-optical data are feasible by the use of simple parameters, combined with semi-analytical models, that relate optical signatures to ecological features of phytoplankton.

References

- Aarup, T., N. Holt and N.K. Højerslev. (1996). Optical measurements in the North Sea-Baltic transition zone, III, Statistical analysis of bio-optical data from the Eastern North Sea, the Skaterrak and the Kattegat. *Cont. Shelf Res.* **16**(10): 1355-1377.
- Ackleson, S.G., J.J. Cullen, J. Brown and M.P. Lesser. (1990). Some changes in the optical properties of marine phytoplankton in response to high light intensity. *SPIE Ocean Optics X* **1302**:238-249.
- Agusti, S. (1991). Allometric scaling of light absorption and scattering by phytoplankton cells. *Can. J. Fish. Aquat. Sci.* **48**:763-768.
- Ahn, Y.H., A. Bricaud and A. Morel. (1992). Light backscattering efficiency and related properties of some phytoplankters. *Deep-Sea Res.* **39**(11-12A): 1835-1855.
- Aiken, J., G.F. Moore, C.C. Trees, S.B. Hooker and D.K. Clark. (1995). The SeaWiFS CZCS-type pigment algorithm. *In*: S. B. Hooker and E. R. Firestone (ed.). NASA Goddard Space Flight Center, Greenbelt, p. 34.
- Austin, R.W. and T.J. Petzold. (1981). Remote sensing of the diffuse attenuation coefficient of sea water using the Coastal Zone Color Scanner. *In*: J. R. F. Gower (ed.). *Oceanography from Space*. Plenum, New York, p. 239-256.
- Austin, R.W. and T.J. Petzold. (1986). Spectral dependence of the diffuse attenuation coefficient of light in ocean waters. *Opt. Eng.* **25**:471-479.
- Babin, M., J.C. Therriault, L. Legendre and A. Condal. (1993). Variations in the specific absorption coefficient for natural phytoplankton assemblages: Impact on estimates of primary production. *Limnol. Oceanogr.* **38**(1): 154-177.

- Balch, W.M. and F.T. Haxo. (1984). Spectral properties of *Noctliuca miliaris* Suriray, a heterotrophic dinoflagellate. *J. Plankton Res.* 6(3): 515-525.
- Balch, W.M., K.A. Kilpatrick and C.C. Trees. (1996). The 1991 coccolithophore bloom in the central North Atlantic. 1. Optical properties and factors affecting their distribution. *Limnol. Oceanogr.* 41(8): 1669-1683.
- Banse, K. (1982). Cell volumes, maximal growth rates of unicellular algae and ciliates, and the role of ciliates in the marine pelagial. *Limnol. Oceanogr.* 27(6): 1059-1071.
- Bartlett, J.S. (1996). The influence of Raman scattering by seawater and fluorescence by phytoplankton on ocean colour. Department of Oceanography. 134
- Bartlett, J.S., A.M. Ciotti, R.F. Davis and J.J. Cullen. (1998). The spectral effects of clouds on solar irradiance. *J. Geophys. Res.* 103(C13): 31,017-31,031.
- Bidigare, R.R., J.H. Morrow and D.A.Kiefer. (1988). Derivative analysis of spectral absorption by phytoplankton pigments. *Ocean Opt. 9 Proc., SPIE, Int. Soc. Opt. Eng.* 925:101-108.
- Bidigare, R.R., M.E. Ondrusek, J.H. Morrow and D.A. Kiefer. (1990). *In vivo* absorption properties of algal pigments. *Opt. Eng.* 1302:290-302.
- Bishop, Y.M.M., S.E. Fienberg and P.W. Holland. (1975). *Discrete Multivariate Analysis: Theory and Practice.*, MIT Press, Cambridge, Mass, 557 pp.
- Bohren, C.F. and D.R. Hoffman. (1983). *Absorption and Scattering of Light by Small Particles.*, J. Wiley and Sons, New York, 530 pp.
- Bricaud, A., M. Babin, A. Morel and H. Claustre. (1995). Variability in the chlorophyll-specific absorption coefficients of natural phytoplankton: Analysis and parameterization. *J. Geophys. Res.* 100(C7): 13,321-13,332.

- Bricaud, A. and A. Morel. (1986). Light attenuation and scattering by phytoplankton cells: a theoretical modeling. *Appl. Opt.* **25**(4): 571-580.
- Bricaud, A. and A. Morel. (1988). Optical properties of diverse phytoplankton species: experimental results and theoretical interpretation. *J. Plankton Res.* **10**(5): 851-873.
- Bricaud, A., A. Morel and L. Prieur. (1981). Absorption by dissolved organic matter of the sea (yellow substance) in the UV and visible domains. *Limnol. Oceanogr.* **26**(1): 43-53.
- Bricaud, A., A. Morel and L. Prieur. (1983). Optical efficiency factors of some phytoplankters. *Limnol. Oceanogr.* **28**(5): 816-832.
- Bricaud, A. and D. Stramski. (1990). Spectral absorption coefficients of living phytoplankton and nonalgal biogenous matter: A comparison between the Peru upwelling area and the Sargasso Sea. *Limnol. Oceanogr.* **35**(3): 562-582.
- Brown, C.W., W.E. Esaias and A.M. Thompson. (1995). Predicting phytoplankton composition from space -- using the ratio of euphotic depth to mixed-layer depth: An evaluation. *Remote Sens. Environ.* **53**(3): 172-176.
- Buiteveld, H., J.H.M. Hakvoort and M. Donze. (1994). The optical properties of pure water. *SPIE Ocean Optics XII* **2258**:
- Bukata, R.P., J.H. Jerome and J.E. Bruton. (1988). Particulate concentrations in Lake St. Clair as recorded by a shipborne multispectral optical monitoring system. *Remote Sens. Environ.* **25**:201-229.
- Bukata, R.P., J.H. Jerome, K.Y. Kondratyev and D.V. Pozdnyakov. (1995). *Optical Properties and Remote Sensing of Inland and Coastal Waters.*, CRC Press, Boca Raton, 362 pp.

- Campbell, J.W. (1995). The lognormal distribution as a model for bio-optical variability in the sea. *J. Geophys. Res.* **100**(c7): 13,237-13,254.
- Campbell, J.W. and W.E. Esaias. (1983). Basis for spectral curvature algorithms in remote sensing of chlorophyll. *Appl. Opt.* **22**(7): 1084-1093.
- Carder, K.L., S.K. Hawes, K.A. Baker, R.C. Smith, R.G. Steward and B.G. Mitchell. (1991). Reflectance model for quantifying chlorophyll a in the presence of productivity degradation products. *J. Geophys. Res.* **96**(C11): 599-611.
- Carder, K.L., C. Hu and A. Strub. (1999). Application of a semi-analytical SeaWiFS algorithm for chlorophyll-a and gelbstoff. American Society of Limnology and Oceanography Meeting.
- Carder, K.L., R.G. Steward, G.R. Harvey and P.B. Ortner. (1989). Marine humic and fulvic acids: Their effects on remote sensing of ocean chlorophyll. *Limnol. Oceanogr.* **34**(1): 68-81.
- Carr, M.E. (1998). A numerical study of the effect of periodic nutrient supply on pathways of carbon in a coastal upwelling regime. *J. Plankton Res.* **20**(3): 491-516.
- Chavez, F.P., K.R. Buck, R.R. Bidigare, D.M. Karl, D. Hebel, M. Latasa, L. Campbell and J. Newton. (1995). On the chlorophyll a retention properties of glass-fiber GF/F filters. *Limnol. Oceanogr.* **40**(2): 428-433.
- Chisholm, S.W. (1992). Phytoplankton size. *In*: P. G. Falkowski and A. Woodhead (ed.). Primary Productivity and Biogeochemical Cycles in the Sea. Plenum Press, New York, p. 213-238.
- Chisholm, S.W., R.J. Olson, E.R. Zettler, R. Goericke, J.B. Waterbury and N.A. Welschmeyer. (1988). A novel free-living prochlorophyte abundant in the oceanic euphotic zone. *Nature* **334**:340-343.

- Ciotti, A.M., J.J. Cullen, C.S. Roesler and M.R. Lewis. (1996). The influence of phytoplankton size structure on the spectral attenuation coefficient in the upper ocean. *Ocean Opt. 13 Proc., SPIE, Int. Soc. Opt. Eng.* **2963**:380-385.
- Clarke, G.L., G.C. Ewing and C.J. Lorenzen. (1970). Spectra of backscattered light from the sea obtained from aircraft as a measure of chlorophyll concentration. *Science* **167**:1119-1121.
- Claustre, H. (1994). The trophic status of various oceanic provinces as revealed by phytoplankton pigment signatures. *Limnol. Oceanogr.* **39**(5): 1206-1210.
- Cleveland, J.S. (1995). Regional models for phytoplankton absorption as a function of chlorophyll a concentration. *J. Geophys. Res.* **100**(c7): 13,333-13,344.
- Coachman, L.K. (1986). Circulation, water masses, and fluxes on the southeastern Bering Sea shelf. *Cont. Shelf Res.* **5**:23-108.
- Cowles, T.J., R.A. Desiderio and S. Neuer. (1993). In situ characterization of phytoplankton from vertical profiles of fluorescence emission spectra. *Mar. Biol.* **115**:217-222.
- Cullen, J.J. (1982). The deep chlorophyll maximum: comparing vertical profiles of chlorophyll a. *Can. J. Fish. Aquat. Sci.* **39**(5): 791-803.
- Cullen, J.J., A.M. Ciotti, R.F. Davis, S.C. Johannessen, B. Nieke, J.P. Parkhill and P.J. Staben. (1998). Bio-optical variability in the Bering Sea as influenced by a mesoscale eddy and shelf processes. Ocean Sciences Meeting, San Diego, California
- Cullen, J.J., A.M. Ciotti, R.F. Davis and M.R. Lewis. (1997). Optical detection and assessment of algal blooms. *Limnol. Oceanogr.* **42**(5): 1223-1239.

- Cullen, J.J., A.M. Ciotti and M.R. Lewis. (1994). Observing biologically induced optical variability in coastal waters. *Ocean Opt. 12 Proc., SPIE, Int. Soc. Opt. Eng.* **2258**:105-115.
- Delgado, M., M. Latasa and M. Estrada. (1992). Variability in the size-fractionated distribution of the phytoplankton across the Catalan Front of the North-West Mediterranean. *J. Plankton Res.* **14**(5): 753-771.
- Dickson, M.L. and P.A. Wheeler. (1993). Chlorophyll *a* concentrations in the North Pacific: Does a latitudinal gradient exist? *Limnol. Oceanogr.* **38**:1813-1818.
- Doerffer, R. and J. Fischer. (1994). Concentrations of chlorophyll, suspended matter and gelbstoff in case II waters derived from satellite coastal zone color scanner data with inverse modeling methods. *J. Geophys. Res.* **99**(C4): 7457-7466.
- Duysens, L.N.M. (1956). The flattening of the absorption spectrum of suspensions as compared to that of solutions. *Biochim. Biophys. Acta* **19**:1-12.
- Eppley, R.W., W.G. Harrison, S.W. Chisholm and E. Stewart. (1977). Particulate organic matter in surface waters off southern California and its relationship to phytoplankton. *J. Mar. Res.* **35**(4): 671-696.
- Eppley, R.W. and C.S. Weiler. (1979). The dominance of nanoplankton as an indicator of marine pollution: A critique. *Oceanol. Acta* **2**(2): 241-245.
- Estrada, M. and E. Berdalet. (1997). Phytoplankton in a turbulent world. *Sci. Mar.* **61**(Supl. 1): 125-140.
- Graham, A. (1981). *Kronecker products and matrix calculus: with applications*. Wiley, New York, 130 pp.

- Garver, S.A. and D.A. Siegel. (1994). Variability in near-surface particulate absorption spectra: What can a satellite ocean color imager see? *Limnol. Oceanogr.* **39**(6): 1349-1367.
- Garver, S.A. and D.A. Siegel. (1997). Inherent optical property inversion of ocean color spectra and its biogeochemical interpretation 1. Time Series from the Sargasso Sea. *J. Geophys. Res.* **102**(C8): 18,607-18,625.
- Geider, R.J., J. La Roche, R.M. Greene and M. Olaizola. (1993). Response of the photosynthetic apparatus of *Phaeodactylum tricornutum* (Bacillariophyceae) to nitrate, phosphate, or iron starvation. *J. Phycol.* **29**(6): 755-766.
- Geider, R.J. and B.A. Osborne. (1986). Light absorption, photosynthesis and growth of *Nannochloris atomus* in nutrient-saturated cultures. *Mar. Biol.* **93**(3): 351-360.
- Gieskes, W.W.C., G.W. Kraay, A. Nontji, D. Setiapermana and A.B. Sutomo. (1988). Monsoonal alternation of a mixed and a layered structure in the phytoplankton of the euphotic zone of the Banda Sea (Indonesia): A mathematical analysis of algal pigment fingerprints. *Neth. J. Sea Res.* **22**(2): 123-137.
- Goericke, R. and D.J. Repeta. (1992). The pigments of *Prochlorococcus marinus* : The presence of divinyl chlorophyll a and b in a marine procaryote. *Limnol. Oceanogr.* **37**(2): 425-433.
- Gordon, H. (1979). Diffuse reflectance of the ocean: the theory of its augmentation by chlorophyll *a* fluorescence. *Appl. Opt.* **21**:2489-2492.
- Gordon, H.R., O.B. Brown, R.H. Evans, J.W. Brown, R.C. Smith, K.S. Baker and D.K. Clark. (1988). A semianalytic radiance model of ocean color. *J. Geophys. Res.* **93**:10909-10924.

- Gordon, H.R., O.B. Brown and M.M. Jacobs. (1975). Computed relationships between the inherent and apparent optical properties of a flat homogeneous ocean. *Appl. Opt.* **14**:417-427.
- Gordon, H.R., D.K. Clark, J.W. Brown, O.B. Brown, R.H. Evans and W.W. Broenkow. (1983). Phytoplankton pigment concentrations in the Middle Atlantic Bight: comparison between ship determinations and Coastal Zone Color Scanner estimates. *Appl. Opt.* **22**:20-36.
- Gordon, H.R. and A.Y. Morel. (1983). *Remote Assessment of Ocean Color for Interpretation of Visible Satellite Imagery: A Review.*, Springer-Verlag, New York, 114 pp.
- Gower, J.F.R. and G. Borstad. (1981). Use of the *in-vivo* fluorescence line at 685 nm for remote sensing surveys of surface chlorophyll *a*. *In*: J. F. R. Gower (ed.). *Oceanography from Space*. Plenum Press, New York, p. 281-294.
- Green, S.A. and N.V. Blough. (1994). Optical absorption and fluorescence properties of chromophoric dissolved organic matter in natural waters. *Limnol. Oceanogr.* **39**(8): 1903-1916.
- Gregg, W.W. and K.L. Carder. (1990). A simple spectral solar irradiance model for cloudless maritime atmospheres. *Limnol. Oceanogr.* **35**(8): 1657-1675.
- Hallegraeff, G.M. (1993). A review of harmful algal blooms and their apparent global increase. *Phycol.* **32**:79-99.
- Harris, G.P. (1986). *Phytoplankton Ecology: Structure, function and fluctuation.*, Univ. Press, Cambridge, 393 pp.
- Hill, P.S. (1992). Reconciling aggregation theory with observed vertical fluxes following phytoplankton blooms. *J. Geophys. Res.* **C97**:2295-2308.

- Hochman, H.T., J.J. Walsh and K.L. Carder. (1995). Analysis of ocean color components within stratified and well-mixed waters of the western English Channel. *J. Geophys. Res.* **100**(C6): 10,777-10,787.
- Hoepffner, N. and S. Sathyendranath. (1991). Effect of pigment composition on absorption properties of phytoplankton. *Mar. Ecol. Prog. Ser.* **73**:11-23.
- Hoepffner, N. and S. Sathyendranath. (1992). Bio-optical characteristics of coastal waters: absorption spectra of phytoplankton and pigment distribution in the western North Atlantic. *Limnol. Oceanogr.* **37**(8): 1660-1679.
- Hoge, F.E. and R.N. Swift. (1990). Photosynthetic accessory pigments: Evidence for the influence of phycoerythrin on the submarine light field. *Remote Sens. Environ.* **34**(1): 19-35.
- Hovis, W.A., D.K. Clark, F. Anderson, R.W. Austin, W.H. Wilson, E.T. Baker, D. Ball, H.R. Gordon, J.L. Mueller, S.Z. El-Sayed, B. Sturm, R.C. Wrigley and C.S. Yentsch. (1980). Nimbus-7 Coastal Zone Color Scanner: System Description and Initial Imagery. *Science* **210**:
- Jeffrey, S.W. and G.M. Hallegraeff. (1987). Chlorophyllase distribution in ten classes of phytoplankton: A problem for chlorophyll analysis. *Mar. Ecol. Prog. Ser.* **35**(3): 293-304.
- Jeffrey, S.W. and G.F. Humphrey. (1975). New spectrophotometric equations for determining chlorophylls *a*, *b*, *c1* and *c2* in higher plants, algae and natural phytoplankton. *Biochem. Physiol. Pflanzen* **167**:191-194.
- Jeffrey, S.W., R.F.C. Mantoura and S.W. Wright. (1997). *Phytoplankton pigments in oceanography: guidelines to modern methods.*, UNESCO Publishing, Paris, 661 pp.

- Jeffrey, S.W. and M. Vesk. (1997). Introduction to marine phytoplankton and their pigment signatures. *In*: S. W. Jeffrey, R. F. C. Mantoura and S. W. Wright (ed.). *Phytoplankton pigments in oceanography: guidelines to modern methods*. UNESCO, Paris, p. 37-84.
- Jeffrey, S.W. and S.W. Wright. (1994). Photosynthetic pigments in the haptophyta. *In*: J. C. Green and B. S. C. Leadbeater (ed.). *The Haptophyte Algae*. Clarendon Press, Oxford, p. 111-132.
- Johnsen, G., N.B. Nelson, R.V.M. Jovine and B.B. Prézelin. (1994a). Chromoprotein- and pigment-dependent modelling of spectral light absorption in two dinoflagellates, *Prorocentrum minimum* and *Heterocapsa pygmaea*. *Mar. Ecol. Prog. Ser.* **114**(3): 245-258.
- Johnsen, G. and E. Sakshaug. (1993). Bio-optical characteristics and photoadaptive responses in the toxic and bloom-forming dinoflagellates *Gyrodinium aureolum*, *Gymnodinium galatheanum*, and two strains of *Prorocentrum minimum*. *J. Phycol.* **29**(5): 627-642.
- Johnsen, G., O. Samset, L. Granskog and E. Sakshaug. (1994b). *In vivo* absorption characteristics in 10 classes of bloom-forming phytoplankton: Taxonomic characteristics and responses to photoadaptation by means of discriminant and HPLC analysis. *Mar. Ecol. Prog. Ser.* **105**:149-157.
- Joint, I. (1991). The allometric determination of pelagic production rates. *J. Plankton Res* **13**(suppl): 69-81.
- Karentz, D., F.S. McKuen, M.C. Land and W.C. Dunlap. (1991). Survey of mycosporine-like amino acid compounds in Antarctic marine organisms: potential protection from ultraviolet exposure. *Mar. Biol.* **108**(1): 157-166.

- Kjørboe, T. (1993). Turbulence, phytoplankton cell size, and the structure of pelagic food webs. *Adv. Mar. Biol.* **29**:1-61.
- Kirk, J.T.O. (1976). Yellow substance (gelbstoff) and its contribution to the attenuation of photosynthetically active radiation in some inland and coastal south-eastern australian waters. *Aust. J. Mar. Freshwater Res.* **27**:61-71.
- Kirk, J.T.O. (1994a). Characteristics of the light field in highly turbid waters: A Monte Carlo study. *Limnol. Oceanogr.* **39**(3): 702-706.
- Kirk, J.T.O. (1994b). *Light and Photosynthesis in Aquatic Ecosystems.*, Cambridge Univ. Press, New York, 509 pp.
- Klein-Breteler, W.C.M. (1985). Fixation artefacts of phytoplankton in zooplankton grazing experiments. *In*: C. Bakker (ed.). The measurement of ingestion of phytoplankton by zooplankton: techniques, problems and recommendations. p. 13-19.
- Kocur, C. (1982). Phytoplankton distribution in Southeastern Bering Sea shelf waters during Spring. College of Arts and Sciences. 48
- Kyewalyanga, M.N., T. Platt and S. Sathyendranath. (1997). Estimation of the photosynthetic action spectrum: Implication for primary production models. *Mar. Ecol. Prog. Ser.* **146**:1-3.
- Lazinsky, D. and L. Sicko Goad. (1979). Paraformaldehyde-glutaraldehyde as a routine phytoplankton fixative. *Micron* **10**(1): 49-50.
- Lee, Z., K.L. Carder, R.G. Steward, T.G. Peacock and C.O. Davis. (1998). An empirical algorithm for light absorption by ocean water. *J. Geophys. Res.* **103**(C12): 27,967-27,978.

- Legendre, L. and J.L. Fèvre. (1989). Hydrodynamic singularities as controls of recycled versus export production in oceans. *In: W. H. Berger, V. S. Smetacek and G. Wefer (ed.). Productivity of the Ocean: Present and Past. John Wiley, New York, p. 49-63.*
- Letelier, R.M., R.R. Bidigare, D.V. Hebel, M. Ondrusek, C.D. Winn and D.M. Karl. (1993). Temporal variability of phytoplankton community structure based on pigment analysis. *Limnol. Oceanogr.* **38**(7): 1420-1437.
- Lewis, M.R., M.E. Carr, G.C. Feldman, W. Esais and C. McClain. (1990). Influence of penetrating solar radiation on the heat budget of the equatorial Pacific Ocean. *Nature* **347**:543-545.
- Lewis, M.R. and J.J. Cullen. (1991). From cells to the ocean: Satellite ocean color. *In: S. Demers (ed.). Particle Analysis in Oceanography. Springer-Verlag, New York, p. 325-337.*
- Li, W.K.W. (1995). Composition of ultraphytoplankton in the Central North Atlantic. *Mar. Ecol. Prog. Ser.* **122**(1-3): 1-8.
- Li, W.K.W., P.M. Dickie and J.A. Spry. (1998). Plankton monitoring program in Bedford Basin, 1991-1997. *Can. Data Rep. Fish. Aquat. Sci.* **1036**:vii+342.
- Loisel, H. and A. Morel. (1998). Light scattering and chlorophyll concentration in case I waters: a re-examination. *Limnol. Oceanogr.* **43**(5): 847-858.
- Longhurst, A., S. Sathyendranath, T. Platt and C. Caverhill. (1995). An estimate of global primary production in the ocean from satellite radiometer data. *J. Plankton Res.* **17**(6): 1245-1271.
- Lutz, V.A., S. Sathyendranath and E.J.H. Head. (1996). Absorption coefficient of phytoplankton: regional variations in the North Atlantic. *Mar. Ecol. Prog. Ser.* **135**(1-3): 197-213.

- MacIntyre, J.G., J.J. Cullen and A.D. Cembella. (1997). Vertical migration, nutrition and toxicity in the dinoflagellate *Alexandrium tamarense*. *Mar. Ecol. Progr. Ser.* **148**(1): 201-216.
- Maffione, R.A. and D.R. Dana. (1997). Instruments and methods for measuring the backward-scattering coefficient of ocean waters. *App. Opt.* **36**(24): 6057-6068.
- Malone, T.C. (1980). Algal size. *In*: I. Morris (ed.). *The Physiological Ecology of Phytoplankton*. Univ. of Calif. Press, Berkeley, p. 433-463.
- Mantoura, R.F.C., S.W. Jeffrey, C.A. Llewellyn, H. Claustre and C.E. Morales. (1997). Comparison between spectrophotometric, fluorometric and HPLC methods for chlorophyll analysis. *In*: S. W. Jeffrey, R. F. C. Mantoura and S. W. Wright (ed.). *Phytoplankton pigments in oceanography: guidelines to modern methods*. UNESCO, Paris, p. 361-380.
- Margalef, R. (1978). Life forms of phytoplankton as survival alternatives in an unstable environment. *Oceanol. Acta* **1**:493-509.
- Michaels, A.F. and M.W. Silver. (1988). Primary production, sinking fluxes and the microbial food web. *Deep-Sea Res.* **35**:473-490.
- Mie, G. (1908). Beiträge zur optik trüber medien, speziell kolloidaler metallosungen. *Ann. Phys.* **25**:377-445.
- Miller, W.L. (1994). Recent advances in the photochemistry of natural dissolved organic matter. *In*: G. R. Heltz (ed.). *Aquatic and Surface Photochemistry*. A.F. Lewis, New York, p. 111-127.
- Millie, D.F., H.W. Paerl and J.P. Hurley. (1993). Microalgal pigment assessments using high-performance liquid chromatography: A synopsis of organismal and ecological applications. **50**(11): 2,513-2,528.

- Millie, D.F., O.M. Schofield and G.J. Kirkpatrick. (1997). Detection of harmful algal blooms using photopigments and absorption signatures: A case study of the Florida red tide dinoflagellate, *Gymnodinium breve*. *Limnol. Oceanogr.* **42**(5 pt.2): 1240-1252.
- Mitchell, B.G. (1990). Algorithms for determining the absorption coefficient of aquatic particulates using the quantitative filter technique (QFT). *SPIE, Ocean Optics X* **1302**:137-148.
- Mitchell, B.G. (1992). Predictive bio-optical relationships for polar oceans and marginal ice zones. *J. Mar. Syst.* **3**:1-2.
- Mitchell, B.G. and O. Holm-Hansen. (1991). Bio-optical properties of Antarctic Peninsula waters: Differentiation from temperate ocean models. *Deep Sea Res. A Oceanogr. Res. Pap.* **38**(8): 1009-1028.
- Mitchell, B.G. and D.A. Kiefer. (1983). Determination of absorption and fluorescence excitation spectra for phytoplankton. 5th Conference of the European society for comparative physiology and biochemistry, Taormina, Sicily, Italy
- Mobley, C.D. (1994). *Light and Water: Radiative transfer in natural waters.*, Academic, San Diego, Calif., 592 pp.
- Mobley, C.D. and D. Stramski. (1997). Effects of microbial particles on oceanic optics: Methodology for radiative transfer modeling and example simulations. *Limnol. Oceanogr.* **42**(3): 550-560.
- Moore, L.R., R. Goericke and S.W. Chisholm. (1995). Comparative physiology of *Synechococcus* and *Prochlorococcus*: influence of light and temperature on growth, pigments, fluorescence and absorptive properties. *Mar. Ecol. Prog. Ser.* **116**(1-3): 259-275.

- Morel, A. (1987). Chlorophyll-specific scattering coefficient of phytoplankton. A simplified theoretical approach. *Deep Sea Res* **34**(7A): 1093-1105.
- Morel, A. (1988). Optical modeling of the upper ocean in relation to its biogenous matter content (Case I waters). *J. Geophys. Res.* **93**:10749-10768.
- Morel, A. (1991). Optics of marine particles and marine optics. *In*: S. Demers (ed.). Particle analysis in oceanography. Springer-Verlag, Berlin, p. 141-188.
- Morel, A. (1994). Optics from the single cell to the mesoscale. *In*: R. W. Spinrad, K. L. Carder and M. J. Perry (ed.). Ocean Optics. Oxford Univ. Press, New York, p. 93-106.
- Morel, A. (1997). Consequences of a *Synechococcus* bloom upon the optical properties of oceanic (case 1) waters. *Limnol. Oceanogr.* **42**(8): 1746-1754.
- Morel, A. and Y.-H. Ahn. (1990). Optical efficiency factors of free-living marine bacteria: Influence of bacterioplankton upon the optical properties and particulate organic carbon in oceanic waters. *J. Mar. Res.* **48**:145-175.
- Morel, A. and Y.H. Ahn. (1991). Optics of heterotrophic nanoflagellates and ciliates: A tentative assessment of their scattering role in oceanic waters compared to those of bacterial and algal cells. *J. Mar. Res.* **49**(1): 177-202.
- Morel, A. and A. Bricaud. (1981). Theoretical results concerning light absorption in a discrete medium, and application to specific absorption of phytoplankton. *Deep-Sea Res.* **28A**(11): 1375-1393.
- Morel, A. and A. Bricaud. (1986). Inherent properties of algal cells including picoplankton: Theoretical and experimental results. *In*: T. Platt and W. K. W. Li (ed.). Photosynthetic Picoplankton. p. 521-559.

- Morel, A. and B. Gentili. (1993). Diffuse reflectance of oceanic waters, 2, Bidirectional aspects. *Appl. Opt.* **32**(33): 6864-6872.
- Morel, A. and B. Gentili. (1996). Diffuse reflectance of oceanic waters, 3, Implication of bidirectionality for the remote-sensing problem. *Appl. Opt.* **35**(24): 4850-4862.
- Morel, A. and L. Prieur. (1977). Analysis of variations in ocean color. *Limnol. Oceanogr.* **22**(4): 709-722.
- Morel, A. and R.C. Smith. (1974). Optical properties of pure water and pure sea water. *In: N. G. Jerlov and E. S. Nielsen (ed.). Optical Aspects of Oceanography.* Academic Press, San Diego, CA, p. 1-24.
- Morel, A., Y. Ahn, F. Partensky, D. Vaultot and H. Claustre. (1993). Prochlorococcus and Synechococcus: A comparative study of their optical properties in relation to their size and pigmentation. *J. Mar. Res.* **5**(3): 617-649.
- Mueller, J.L. (1976). Ocean color spectra measured off the Oregon coast. *Appl. Opt.* **15**:394-402.
- Mueller, J.L. and C.C. Trees. (1997). Revised SeaWiFS prelaunch algorithm for the diffuse attenuation coefficient K(490). *In: E. Yeh, R. A. Barnes, M. Darzi, L. Kumar, E. A. Early, B. C. Johnson, J. J. Mueller and C. C. Trees (ed.). Case Studies for SeaWiFS Calibration and Validation, Part 4.* NASA Tech. Memo. 104566, p. 18-21.
- Nelson, J.R. and C.Y. Robertson. (1993). Detrital spectral absorption: Laboratory studies of visible light effects on phytodetritus absorption, bacterial spectral signal, and comparison to field measurements. *J. Mar. Res.* **51**(1): 181-207.
- Nelson, N.B. and B.B. Prézelin. (1990). Chromatic light effects and physiological modeling of absorption properties of *Heterocapsa pygmaea* (= *Glenodinium sp.*). *Mar. Ecol. Prog. Ser.* **63**(1): 37-40.

- Neville, R.A. and J.F.R. Gower. (1977). Passive remote sensing of phytoplankton via chlorophyll fluorescence. *J. Geophys. Res.* **82**:3487-3493.
- O'Reilly, J.E., S. Maritorena, B.G. Mitchell, D.A. Siegel, K.L. Carder, S.A. Garver and C.R. McClain. (1998). Ocean color chlorophyll algorithms for SeaWiFS. *J. Geophys. Res.* **103**(C11): 24,937-24,953.
- Olson, R.J., S.W. Chisholm, E.R. Zettler and E.V. Armbrust. (1990). Pigments, size, and distributions of *Synechococcus* in the North Atlantic and Pacific Oceans. *Limnol. Oceanogr.* **35**:45-58.
- Platt, T. and K. Denman. (1977). Organisation in the pelagic ecosystem. *Helgol. Wiss. Meeresunters, ISSN 30*(1-4): 575-581.
- Platt, T. and B. Irwin. (1971). Variability and its effect on the 24h chlorophyll budget of a small marine basin. *Mar. Biol.* **62**:52-65.
- Platt, T., S. Sathyendranath, C.M. Caverhill and M.R. Lewis. (1988). Oceanic primary production and available light: further algorithms for remote sensing. *Deep-Sea Res.* **35**:855-879.
- Pope, R.M. and E.S. Fry. (1997). Absorption spectrum (380-700 nm) of pure water: II. Integrating cavity measurements. *Appl. Opt.* **36**:8710-8723.
- Preisendorfer, R.W. (1961). Application of radiative transfer theory to light measurements in the sea. *Monogr.* 10: 11-30
- Prézelin, B.B. and H.A. Matlick. (1983). Nutrient-dependent low-light adaptation in the dinoflagellate *Gonayaulax polyedra*. *Mar. Biol.* **74**(2): 141-150.
- Richards, T.A. and T.G. Thompson. (1952). The estimation and characterization of plankton populations by pigment analysis. II. A spectrophotometric method for the estimation of plankton pigments. *J. Mar. Res.* **11**:156-172.

- Richardson, T.L., Á.M. Ciotti, J.J. Cullen and T. Villareal. (1996). Physiological and optical properties of *Rhizosolenia formosa* (Bacillariophyceae) in the context of open-ocean vertical migration. *J. Phycol.* **32**:741-757.
- Riegman, R. (1998). Species composition of harmful algal blooms in relation to macronutrient dynamics. *In*: D. M. Anderson, A. D. Cembella and G. M. Hallegraeff (ed.). Physiological ecology of harmful algal blooms. Springer-Verlag, Berlin, p. 475-488.
- Riegman, R., B.R. Kuipers, A.A.M. Noordeloos and H.J. Witte. (1993). Size-differential control of phytoplankton and the structure of plankton communities. *Neth. J. Sea Res.* **31**(3): 255-265.
- Roesler, C.S. (1992). Modeling *in situ* phytoplankton absorption from total absorption spectra in productive inland waters.
- Roesler, C.S. and M.J. Perry. (1995). *In situ* phytoplankton absorption, fluorescence emission, and particulate backscattering spectra determined from reflectance. *J. Geophys. Res.* **100**(C7): 13,279-13,294.
- Roesler, C.S., M.J. Perry and K.L. Carder. (1989). Modeling *in situ* phytoplankton absorption from total absorption spectra in productive inland waters. *Limnol. Oceanogr.* **34**(8): 1510-1523.
- Rowan, K.S. (1989). *Photosynthetic pigments of algae.*, Univ. Press, Cambridge, 334 pp.
- Sathyendranath, S., F.E. Hoge, T. Platt and R.N. Swift. (1994). Detection of phytoplankton pigments from ocean color: Improved algorithms. *Appl. Opt.* **33**(6): 1081-1089.
- Sathyendranath, S., L. Lazzara and L. Prieur. (1987). Variations in the spectral values of specific absorption of phytoplankton. *Limnol. Oceanogr.* **32**(2): 403-415.

- Sathyendranath, S. and T. Platt. (1988). The spectral irradiance field at the surface and in the interior of the ocean: A model for applications in oceanography and remote sensing. *J. Geophys. Res.* **93**(C8): 9270-9280.
- Sathyendranath, S., L. Prieur and A. Morel. (1989). A three-component model of ocean colour and its application to remote sensing of phytoplankton pigments in coastal waters. *Int. J. Remote Sens.* **10**(8): 1373-1394.
- Schumacher, J.D. and P.J. Stabeno. (1994). Ubiquitous eddies of the eastern Bering Sea and their coincidence with concentrations of larval pollock. *Fish. Oceanogr.* **3**(3): 182-190.
- Shoaf, W.T. and B.W. Lium. (1976). Improved extraction of chlorophyll *a* and *b* from algae using dimethyl sulfoxide. *Limnol. Oceanogr.* **21**:926-928.
- Sieburth, J.M., V. Smetacek and J. Lentz. (1978). Pelagic ecosystem structure: Heterotrophic compartments of the plankton and their relationship to plankton size fractions. *Limnol. Oceanogr.* **23**(6): 1256-1263.
- SooHoo, J.B. and D.A. Kiefer. (1982). Vertical distribution of phaeopigments, 2, Rates of production and kinetics of photooxidation. *Deep-Sea Res.* **29**(12A): 1553-1563.
- Sosik, H.M. and B.G. Mitchell. (1991). Absorption, fluorescence, and quantum yield for growth in nitrogen-limited *Dunaliella tertiolecta*. *Limnol. Oceanogr.* **36**(3): 910-921.
- Sosik, H.M. and B.G. Mitchell. (1994). Effects of temperature on growth, light absorption, and quantum yield in *Dunaliella tertiolecta* (Chlorophyceae). *J. Phycol.* **30**(5): 833-840.
- Sosik, H.M. and B.G. Mitchell. (1995). Light absorption by phytoplankton, photosynthetic pigments and detritus in the California Current System. *Deep-Sea Res.* **42**(10): 1717-1748.

- Sournia, A., M.J. Chretiennot-Dinet and M. Ricard. (1991). Marine phytoplankton: how many species in the world ocean? *J. Plankton Res.* **13**(5): 1093-1099.
- Springer, A.M., C.P. McRoy and M.V. Flint. (1996). The Bering Sea Green Belt: Shelf-edge processes and ecosystem production. *Fish. Oceanogr.* **5**:3-4.
- Stavn, R.H. (1993). Effects of Raman scattering across the visible spectrum in clear ocean water: A Monte Carlo study. *Appl. Opt.* **32**:6853-6863.
- Stavn, R.H. and A.D. Weidemann. (1992). Raman scattering in ocean optics. In: R. W. Spinrad (ed.). *Ocean Optics X. Proc. SPIE*, p. 94-100.
- Stramski, D. (1994). Gas microbubbles: An assessment of their significance to light scattering in quiescent sea. *Ocean Opt. 12 Proc., SPIE, Int. Soc. Opt. Eng.* **2258**: 704-710.
- Stramski, D. and D.A. Kiefer. (1991). Light scattering by microorganisms in the open ocean. *Prog. Oceanogr.* **28**:343-383.
- Stramski, D. and C.D. Mobley. (1997). Effects of microbial particles on oceanic optics: A database of single-particle optical properties. *Limnol. Oceanogr.* **42**(3): 538-549.
- Stramski, D. and R.A. Reynolds. (1993). Diel variations on the optical properties of a marine diatom. *Limnol. Oceanogr.* **38**(7): 1347-1364.
- Stramski, D., G. Rosenberg and L. Legendre. (1993). Photosynthetic and optical properties of the marine chlorophyte *Dunaliella tertiolecta* grown under fluctuating light caused by surface-wave focusing. *Mar. Ecol. Prog. Ser.* **115**(3): 363-372.

- Stramski, D., A. Shalapyonok and R.R. Reynolds. (1995). Optical characterization of the oceanic unicellular cyanobacteria *Synechococcus* grown under a day-night cycle in natural irradiance. *J. Geoph. Res.* **100**(c7): 13,295-13,307.
- Stuart, V., S. Sathyendranath, T. Platt, H. Maass and B.D. Irwin. (1998). Pigments and species composition of natural phytoplankton populations: Effects on the absorption spectra. *J. Plankton Res.* **20**(2): 187-217.
- Subramaniam, A. and E.J. Carpenter. (1994). An empirically derived protocol for the detection of blooms of the marine cyanobacterium *Trichodesmium* using CZCS imagery. *Int. J. Remote Sens.* **15**(8): 1559-1569.
- Taylor, A.H., R.J. Geider and F.J.H. Gilbert. (1997). Seasonal and latitudinal dependencies of phytoplankton carbon-to-chlorophyll a ratios: Results of a modelling study. *Mar. Ecol. Prog. Ser.* **152**:1-3.
- Thingstad, T.F. and E. Sakshaug. (1990). Control of phytoplankton growth in nutrient recycling systems. Theory and terminology. *Mar. Ecol. Prog. Ser.* **63**(2-3): 261-272.
- Thomas, A.C. and P.T. Strub. (1989). Interannual variability in phytoplankton pigment distribution during the spring transition along the west coast of North America. *J. Geophys. Res. C Oceans* **94**(12): 18095-18117.
- Tomas, C.R. (1997). *Identifying Marine Phytoplankton.*, Academic, San Diego, California, 858 pp.
- Ulloa, O., S. Sathyendranath and T. Platt. (1994). Effect of the particle size distribution on the backscattering ratio in seawater. *Appl. Opt.* **33**:7070-7077.
- Ulloa, O., S. Sathyendranath, T. Platt and R.A. Quiñones. (1992). Light scattering by marine heterotrophic bacteria. *J. Geophys. Res.* **C97**(6): 9619-9629.

- Utermöhl, H. (1958). Zur Vervollkommung der quantitativen Phytoplankton Methodik. *Mitt. int. Verein. theor. angew. Limnologie* **9**(1-38):
- van de Hulst, H.C. (1957). *Light Scattering by Small Particles.*, John Willey, New York, pp.
- Verkhunov, A.V. and Y.Y. Tkachenko. (1992). Recent observations of variability in the western Bering Sea current system. *J. Geophys. Res. C Oceans* **97**(C9): 14369-14376.
- Vodacek, A., N.V. Blough, M.D. DeGrandpre, E.T. Peltzer and R.K. Nelson. (1997). Seasonal variation of CDOM and DOC in the Middle Atlantic Bight: Terrestrial inputs and photooxidation. *Limnol. Oceanogr.* **42**(4): 674-686.
- Vodacek, A., S.A. Green and N.V. Blough. (1994). An experimental model of the solar-stimulated fluorescence of chromophoric dissolved organic matter. *Limnol. Oceanogr.* **39**(1): 1-11.
- Waters, K.J. (1995). Effects of Raman scattering on the water-leaving radiance. *J. Geophys. Res.* **100**(c7): 13,151-13,161.
- Wozniak, B., W.v. Smekot-Wensierksi, R. Doerffer and H. Gräbgrl. (1994). On the relationship between spectral reflected irradiance at the sea surface and optical properties of marine phytoplankton. *Ocean Opt. 12 Proc., SPIE, Int. Soc. Opt. Eng.* **2258**: 976-993.
- Yentsch, C.M., P.K. Horan, K. Muirhead, Q. Dortch, E. Hauggen, L. Legendre, L.S. Murphy, M.J. Perry, D.A. Phinney, S.A. Pomponi, R.W. Spinrad, M. Wood, C.S. Yentsch and B.J. Zahuranec. (1983). Flow cytometry and cell sorting: A Technique for analysis and sorting of aquatic particles. *Limnol. Oceanogr.* **28**(6): 1275-1280.

- Yentsch, C.S. (1962). Measurement of visible light absorption by particulate matter in the ocean. *Limnol. Oceanogr.* **7**(2): 207-217.
- Yentsch, C.S. and D.A. Phinney. (1985). Spectral fluorescence: an ataxonomic tool for studying the structure of phytoplankton populations. *Journal of Plankton Research* **7**(5): 617-632.
- Yentsch, C.S. and D.A. Phinney. (1989). A bridge between ocean optics and microbial ecology. *Limnol. Oceanogr.* **34**(8): 1694-1705.
- Yentsch, C.S. and C.M. Yentsch. (1982). The attenuation of light by marine phytoplankton with specific reference to the absorption of near-UV radiation. *In: D. Karentz, F. S. McKuen, M. C. Land and W. C. Dunlap (ed.). The role of solar ultraviolet radiation in marine ecosystems. Plenum, New York, p. 691-700.*
- Zaneveld, J.R.V., A.H. Barnard and W.S. Pegau. (1998). A nearly backscattering independent algorithm for the retrieval of spectral absorption from remote sensing reflectance. Ocean Sciences Meeting, San Diego, California
- Zhang, X., M.R. Lewis and B. Johnson. (1998). The influence of bubbles on scattering of light in the ocean. *Appl. Opt.* **37**(27): 6525-6536.